CHARACTERIZING CANCER CELLS USING GEDI DEVICES: CAPTURE, IN-SITU ANALYSIS, AND ELUTION FOR EX-SITU ANALYSIS AND CULTURE

A Dissertation

Presented to the Faculty of the Graduate School

of Cornell University

in Partial Fulfillment of the Requirements for the Degree of

Doctor of Philosophy

by

Erica Delores Pratt

May 2015

© 2015 Erica Delores Pratt
ALL RIGHTS RESERVED

CHARACTERIZING CANCER CELLS USING GEDI DEVICES: CAPTURE, IN-SITU ANALYSIS, AND ELUTION FOR EX-SITU ANALYSIS AND CULTURE

Erica Delores Pratt, Ph.D.

Cornell University 2015

Several methodologies exist for the isolation of circulating tumor cells (CTCs) from cancer patient blood samples. However, there are few straightforward functional analyses for these cells, either downstream or *in-situ*, particularly in immunocapture-based systems. My thesis work has focused on two methods of cell extraction, and one *in-situ* assay, that can enable single-cell CTC interrogation using Geometrically Enhanced Differential Immunocapture (GEDI) microdevices. I will also present a non-mechanical, non-enzymatic, method of whole-cell release by substituting standard biotin-avidin immunochemistry with reversible biotin analogues. These data are one of the first demonstration of linker chemistry substitution for release of cancer cells, and can be combined with various biomechanical assays (e.g. traction force microscopy) to quantify an individual cells properties. Together, these methods provide a toolbox for straightforward extraction of cancer cells from CTC-capture devices, which can enable characterization of individual cell genotype and phenotype. I will also outline experiments which combine high-efficiency, high-purity GEDI cell capture with single-nucleus sequencing (SNS) for single-cell copy-number variation analyses (GEDI-SNS). I will show that GEDI-SNS is comparable to standard methods, can be used to identify key cancer-related genetic variations, and can differentiate between different cancer cell populations of the same tissue ori-

gin. Finally, I will present the development of an on-chip assay to monitor Ca^{2+} homeostasis, which has been shown to be critical in taxane chemoresistance, as well as acquisition of a hormonally-independent phenotype. Using real-time, time-lapse, microscopy, I will monitor Ca^{2+} flux in cancer cells as a functional assay to inform drug treatment.

BIOGRAPHICAL SKETCH

Erica Delores Pratt earned her Bachelor of Science degree in Mechanical Engineering and Biomedical Engineering from Carnegie Mellon University in 2008. She joined the doctoral program in Biomedical Engineering at Cornell University that same year. In 2012, she was awarded her Master of Science degree in Biomedical Engineering. Her dissertation, *"Characterizing cancer cells using GEDI devices: Capture, in-situ analysis, and elution for ex-situ analysis and culture"* has been supervised by Prof. Brian J. Kirby.

Erica has been the recipient of numerous awards and honors, including a Sloan PhD Fellowship and National Science Foundation Graduate Research Fellowship. Erica has also received competitive grant funding from Cornell's Center on the Microenvironment and Metastasis based on the strength of her research. In 2015, she was selected as an Edward A. Bouchet Graduate Honor Society Fellow.

Erica has presented her research at numerous workshops at meetings, including the World Circulating Tumor Cell Summit and the Biomedical Engineering Society Meeting. Her work has been published in *Analytical Chemistry* and *Chemical Engineering Science*. After completing her doctorate, Erica will begin her postdoctoral research in cancer biology at the University of Michigan.

ACKNOWLEDGEMENTS

I thank my mother, Betty Pratt, for her passion to ensure I had the best education possible. She always encouraged me to pursue my interests to the best of my ability. I hope my achievements validate the sacrifices she made.

I am grateful to my advisor, Prof. Brian Kirby, for his guidance during my time at Cornell. I would not be the researcher that I am today without his passion for mentorship and dedication to his students' personal and professional development.

I also thank my thesis committee members through the years. I appreciate the expertise and guidance professors Lance Collins, Paraskevi Giannakakou, Jan Lammerding, and Ankur Singh have contributed during my time at Cornell. Their assistance was critical to the completion of my degree.

My time at Cornell has been enriched by my friendships with Patti Wojcik and Laura Houghton. Their investment in my happiness and success has truly been a blessing. Similarly, thank you to Carissa (plus Hannah and Noura), Laura, Bo Ri, Erika, Fai, Grace, Mo, Natalie, and my fellow SLers.

Finally, I would like to thank all members, past and present, that I have worked with during my time in Prof. Kirby's research group. In particular, I would like to thank Jason Gleghorn for his mentorship and the example he set for me. I also value the friendship and assistance I received from Ben Hawkins, Alex Barbati, Charlie Huang, Steven Santana, Fredrik Thege, and Jack Hartman.

TABLE OF CONTENTS

Biographical Sketch . . . iii
Acknowledgements . . . iv
Table of Contents . . . v
List of Tables . . . vii
List of Figures . . . viii

1 Introduction **1**

2 Rare Cell Capture in Microfluidic Devices **4**
2.1 Abstract . . . 4
2.2 Introduction . . . 5
2.3 Non-electrokinetic Methods . . . 6
2.3.1 Immobilization via Antibody or Aptamer Chemistry . . . 7
2.3.2 Size-based Sorting . . . 11
2.3.3 Sheath Flow & Streamline Sorting . . . 14
2.4 Electrokinetic methods . . . 16
2.4.1 Electrode-based DEP . . . 18
2.4.2 Insulative DEP . . . 27
2.4.3 Prospects for DEP rare cell capture . . . 30
2.5 Performance Criteria . . . 32
2.6 Discussion & Conclusion . . . 34

3 Capture and Elusion of Cancer Cells from Geometrically Enhanced Differential Immunocapture Microdevices using Reversible Biotin Analogues **40**
3.1 Abstract . . . 40
3.2 Introduction . . . 40
3.3 Materials & Methods . . . 43
3.3.1 Device Fabrication . . . 43
3.3.2 Surface Biofunctionalization . . . 44
3.3.3 Cancer Cell Capture & Release . . . 45
3.4 Results & Discussion . . . 47
3.4.1 Linker Performance on Planar Surfaces. . . . 47
3.4.2 Linker implementation in GEDI μdevices . . . 50
3.4.3 Summary . . . 53

4 Single-Cell Copy Number Analysis of Prostate Cancer Cells Captured with GEDI Microdevices **55**
4.1 Abstract . . . 55
4.2 Introduction . . . 56
4.3 Materials and Methods . . . 58
4.3.1 Device fabrication and functionalization . . . 58

4.3.2 Cell line preparation . . . 58
4.3.3 Isolation and nuclei extraction for single-cell SNS . . . 59
4.4 Results and discussion . . . 60
4.4.1 Repeatability and robustness of GEDI-SNS . . . 60
4.4.2 CNV-based differentiation of prostate cells . . . 62
4.5 Summary . . . 63
4.6 Acknowledgment . . . 64
4.7 Supplementary Information . . . 65
4.7.1 Single Nucleus Sequencing (SNS) experimental details . . . 65
4.7.2 LNCaP preparation via serial dilution . . . 65

5 *In-situ* Measurement of Ca^{2+}-flux to Assess Taxane Treatment Efficacy 69
5.1 Abstract . . . 69
5.2 Introduction . . . 70
5.3 Materials & Methods . . . 72
5.3.1 Cell Culture . . . 72
5.3.2 Cell Preparation and Labeling . . . 72
5.3.3 Intracellular Ca^{2+} Imaging . . . 73
5.4 Results & Discussion . . . 74
5.4.1 LNCaP response to ER-stress via Thapsigargin . . . 74
5.4.2 Summary . . . 75
5.4.3 Future Work . . . 76

6 Conclusion 78
6.1 Summary of Accomplishments . . . 78
6.2 Future Work . . . 80

Bibliography 82

LIST OF TABLES

2.1 Non-electrokinetic cell fractionation and isolation studies 37
2.2 Electrokinetic cell fractionation and isolation studies 39

3.1 List of biofunctionalization chemistries and substrates used. Si=Silicon, PS=Polystyrene 46
3.2 LNCaP cell capture and release efficiencies in GEDI microdevices as a function of various surface chemistry parameters. . . . 54

4.1 Number of successfully amplified cell nuclei as compared to predicated values using Poissons distribution. 66

LIST OF FIGURES

2.1 (A) Schematic of an micro-pillar device's architecture. Adapted from [46] (B) Schematic of a Weir microfilter's operation. Adapted from [67] (C) Example of a Hele-Shaw flow cell where the dotted line is the region of linearly increasing shear (D) Schematic of a sheath-flow based separation system. Adapted from [172] 9

2.2 (A) Interdigitated array (IDA) electrodes. (B) Electrosmear slide showing fractionation tumor cells and blood components. Reproduced from [28]. (C) Castellated IDA electrodes. (D) DEP field-flow fractionation operates by levitating cells against gravity to different heights in the channel via negative DEP, allowing separation to be achieved based on their differing flow velocities. (E) Configuration and forces in a twDEP electrode array. (F) Summation of forces near an angled electrode. 20

2.3 (A) Schematic of curved constriction in channel depth. Inset: top view of device fabricated in Zeonor 1020R polymer substrate. Reproduced from [52]. (B) Trapping of live (green) and dead (red) *E. coli* with separation of populations using insulative post array. Reproduced from [88]. 29

3.1 Diagram of GEDI device fabrication using silicon and polystyrene substrates. A) Si wafers were patterned using photolightography and underwent DRIE to form pillar arrays in the bed of the device. B) Etched Si wafers were fluorinated, and PDMS was cast to form a negative GEDI mold. The PDMS mold was used to hot emboss thermoplastic polystyrene at high temperatures (155 °C). 44

3.2 Characterization of biotin and biotin analogue capture performance in 2D microfluidic flow chambers. A) Schematic of Hele-Shaw flow cell showing that unique device geometry following iso-pressure lines results in a linearly decreasing shear stress along the centerline of the device. B) Calculation of shear stress around a post in a GEDI microarray at two operational flow rates: 1 mL/hr and 0.75 mL/hr. Hele-Shaw flow cells are designed to match this shear stress range. C) J591-conjugated biotin and biotin evaluation and mAb surface saturation (10 μg/mL). PCBJ591 performance is indistinguishable from BJ591; however DBJ591 captures cells at a rate only slightly above control (NeutrAvidin alone). 49

3.3 Assessment of PSMA+ LNCaP and PSMA- BXPC3 cell line capture on J591-immobilized polystyrene surfaces using various biofunctionalization protocols. PSMA+ cell lines are captured on PS surfaces at rates comparable to glass in using A) standard silanization chemistry and B) simple NeutrAvidin physabsorption. PSMA- cells are captured at negligible rates, indicating low non-specific adhesion. C) Cells are captured at lower rates on surfaces treated with O_2 plasma and D) very low rates on NeutrAvidin control surfaces. 50
3.4 A) Capture efficiencies of PSMA+ prostate cancer cells in Biotin-J591, Desthiobiotin-J591, and Photocleavable-biotin-J591 functionalized GEDI microdevices. Recapitulating Hele-Shaw data, BJ591 and PCBJ591 performance is nearly indistinguishable, while DBJ591 exhibits a markedly lower rate of capture. B) Release efficiencies for DBJ591 and PCBJ591 compared to trypsin control in GEDI microdevices. Cells were exposed to trypsin for up to 30 min before being flushed with PBS buffer solution. DBJ591 enables high efficiency cell release, while PCBJ591 is much more variable. 51
3.5 A) Capture and B) Release efficiency of prostate cancer cells as a function of: PCB:J591 biotinylation molar ratio, PCBJ591 surface density, and thermal oxidation of the Si surface. PCBJ591 capture remains relatively robust to all parameters. Lower molar ratios, and oxidized surfaces result in greater cell release. 52

4.1 A)LNCaP nuclei were sorted via three methods 1) FACS only. 2) capture in GEDI microdevices, followed by serial dilution. 3) serial dilution only. VCaP controls underwent FACS. B) On-chip lysis of LNCaP cells in a GEDI microdevice via NST-DAPI buffer. Digestion of labeled cell membrane (green), and simultaneous nucleus labeling (red) is easily observed. Scale bars are 100 μm. . 59
4.2 A) Copy-number profiles of individual LNCaP and VCaP nuclei after undergoing amplification followed by single-nucleus sequencing. B) By comparing copy-number profiles of the two different prostate cancer cell lines, one can contrast unique genetic amplifications and deletions across their respective genomes. CNVs of interest are marked by solid gray line. 62
4.3 A) Simple linear regression was used to determine r^2 values for copy-number profile comparisons. B) Dendrogram showing level of genetic relationship between cell populations. (2) indicates profiles averaged over two nuclei, all others are from single cells. 64

4.4 Simple linear regression for a bulk LNCaP sample from cell culture (150 cells). The averaged genetic profile agrees very well with copy-number profile generated form a single nuclei from a GEDI microdevice (r^2 = 0.904). 67
4.5 Pairwise comparisons of various SNS samples. 68

5.1 Imaging setup for continuous superperfusion of LNCaP cells with Ca^{2+} agonists. 73
5.2 A) Fluorescent intensity images of cells loaded with Ca^{2+}-sensitive dye Fluo-4AM. Fluorescent intensity does not increase upon application of thapsigargin, but does when exposed to 2 mM Ca^{2+}, and also upon exposure to 5 μM of Ca^{2+} ionophore Ionomycin (Iono) in 10 mM Ca^{2+}-HBSS. Scale bar 50 μm. B) Traces of cell response to TG and ionomycin exposure. White bars indicate 0 mM [Ca^{2+}]. Data average of 23 cells across two experiments. 77

CHAPTER 1

INTRODUCTION

The primary goal of this work is the development of techniques to characterize and chemically release circulating tumor cells (CTCs) from microfluidic devices. CTCs provide the capacity for real-time genetic characterization of a disseminating tumor cell population. Allard et al. and Danila et al. have shown that enumeration is positively correlated with metastasis and tumor load [3, 31]. As tumor genetic heterogeneity emerges as an effective biomarker of malignant processes, more research has focused on characterizing CTC heterogeneity. Early research from Maheswaran et al. and others relied on bulk averages of CTC properties [101, 179]. In contrast, Powell et al. used single-cell analyses and reported high intra- and inter-patient CTC genetic heterogeneity [127]. Ozkumur et al. also reported variety in surface marker expression in CTCs isolated from the same patient [121]. Ex-vivo culture also showed that CTC morphology and invasion potential are equally diverse [78, 178]. Magbanua et al. and Yu et al. found that these properties are dynamic, and are directly affected by changes in therapy [100, 180]. This points to a need for straightforward single-cell analyses for CTCs once isolated from blood samples.

Microfluidic technology has emerged to the forefront of CTC isolation, due to the ability to manipulate and isolate CTCs in a highly controlled fashion, as well as for its high-throughput capabilities. We have developed a high efficiency, high purity CTC capture technology called geometrically enhanced differential immunocapture (GEDI) [46]. In this thesis, I will develop *in-situ* and *ex-situ* assays that allow for single-cell characterization post-isolation from GEDI microdevices.

Most morphological and biomechanical measurements of cells require whole cell manipulation that is largely incompatible with rigid microdevices, which are often made of silicon or glass. In chapter 3, I present work characterizing a toolbox of reversible biotin analogues to release intact cancer cells from GEDI microdevices for off-chip biological analysis. I have focused on two reversible analogues A) Desthio-biotin, a low-affinity linker which can be competitively displaced by biotin, and B) Photocleavable-biotin, a reversible linker which photolyses upon exposure to UVA (365 nm) light. Once developed, these reversible immunocapture chemistries are generalizable across microfluidic platforms.

In chapter 4, I outline my work, in collaboration with Cold Spring Harbor Laboratory, designing an *ex-situ* single-cell copy-number profile assay using captured in GEDI microdevices. Although researchers have measured copy-number variation (CNV) in resected tumor tissue and pooled CTC samples, no reported microfluidic technology has shown reproducible CNV analysis at the single-cell level. I demonstrate a method for repeatable nuclei extraction and CNV analysis. In particular, we analyze the robustness and resolution of our method in identifying cancer- and cell line-specific CNVs, which is a first step building accurate phylogenetic trees of cancer evolution.

There are few functional measurements of CTCs that indicate drug efficacy. In chapter 5, I conclude with the development of an *in-situ* assay of cell chemoresistance. Vanoverberghe et al., Capiod et al. and others have shown that disregulation of Ca^{2+} homeostasis has been associated with taxane resistance, and acquisition of hormonally-independent phenotypes [160, 12, 122], and is easily visualized via live-cell time-lapse microscopy. We have shown previously the ability to monitor taxane efficacy on the genomic pathway using CTCs as tu-

mor surrogates. Development of an assay targeting non-genomic pathways of chemoresistance could be critical for informing treatment options and avoiding drug cross-resistance.

CHAPTER 2

RARE CELL CAPTURE IN MICROFLUIDIC DEVICES[1]

2.1 Abstract

This chapter reviews existing methods for the isolation, fractionation, or capture of rare cells in microfluidic devices. Rare cell capture devices face the challenge of maintaining the efficiency standard of traditional bulk separation methods such as flow cytometers and immunomagnetic separators while requiring very high purity of the target cell population, which is typically already at very low starting concentrations. Two major classifications of rare cell capture approaches are covered: (1) non-electrokinetic methods (e.g. immobilization via antibody or aptamer chemistry, size-based sorting, and sheath flow and streamline sorting) are discussed for applications using blood cells, cancer cells, and other mammalian cells, and (2) electrokinetic (primarily dielectrophoretic) methods using both electrode-based and insulative geometries are presented with a view towards pathogen detection, blood fractionation, and cancer cell isolation. The included methods were evaluated based on performance criteria including cell type modeled and used, number of steps/stages, cell viability, and enrichment, efficiency, and/or purity. Major areas for improvement are increasing viability and capture efficiency/purity of directly processed biological samples, as a majority current studies only process spiked cell lines or pre-

[1]Erica D. Pratt*, Chao Huang*, Benjamin G. Hawkins, Jason P. Gleghorn, Brian J. Kirby. "Rare cell capture in microfluidic devices," *Chemical Engineering Science*, 66(7): 1508-1522, 2011 [129]. *Authors contributed equally to this work.

EDP independently wrote the non-electrokinetics section and respective table, and CH independently wrote the electrokinetics section and respective table; the remaining sections were written in collaboration. BGH, JPG, and BJK provided technical expertise and guidance on formatting and organization.

diluted/lysed samples. Despite these current challenges, multiple strides have been made in the development of devices for rare cell capture and the subsequent elucidation of new biological phenomena; this article serves to highlight this progress as well as the electrokinetic and non-electrokinetic methods that can potentially be combined to improve performance in future studies.

2.2 Introduction

The isolation, fractionation, and capture of cells from suspensions has a wide range of applications, from the detection of bacteria [94, 172] to the enumeration of cancer cells [44, 15, 115]. The benefits and limitations of flow cytometers, immunomagnetic separators and other macro-sized sorting equipment have been studied extensively in experimentation and in review [123, 17, 84] when compared to the abilities of microdevices. This article focuses on devices and techniques with potential to analyze cells that are typically found at low concentrations in suspension; such devices are currently used, or have the potential to be used, for applications in environmental pathogen detection [87, 177] and cancer cell isolation from patient blood samples [46]. The discussion is divided into sections that detail two major classifications of microfluidic approaches, non-electrokinetic and electrokinetic, followed by a summary of performance criteria by which these methods are evaluated; studies that focused on quantifying these performance specifications are highlighted in tables at the end of the article. While rare cell capture is the ultimate motivation of this paper, many of the described methods exist only as proof-of-concept studies. Thus, this article serves to highlight both the progress made in using microfluidic devices for rare cell capture and the techniques that may contribute to rare cell capture in

the near future.

2.3 Non-electrokinetic Methods

This chapter focuses upon non-electrokinetic methods of cell isolation, capture, or fractionation from a suspension. As such, it lends itself naturally to organization by sorting technique. Each sorting methodology is further subdivided into cell separations of interest: blood cell fractionation, cancer cells, other mammalian cells, and prokaryotes and viruses.

Blood cell fractionation, as defined here, focuses on isolation of cell types native to circulation. Most of the studies described here revolve around the capture or elimination of white blood cells (WBCs). WBCs are of value in many diagnostic assays and studies of disease progression, but they must first be separated from the bulk blood suspension. However, WBC concentrations are low as compared to red blood cells (RBCs), roughly 1 to 1000 [114, 159]. Conversely, for the purpose of leukemia treatments, blood transfusions, etc, it is vital to eliminate WBCs as a source of contamination [138].

Studies for the isolation of cancer cells focus upon approximating, or capturing, circulating tumor cells(CTCs), which can be found in the circulation of cancer patients [115, 46, 146]. CTCs have been used as prognostic indicators of patient survival[31] as well as representative tissue for genetic analyses [146]. CTCs are 10^6 rarer than WBCs, making their capture particularly challenging [115, 1, 46].

Non-electokinetic microfluidic techniques have also been applied to study

other mammalian cells. Applications are quite disparate, ranging from sorting of cells based on stages of cell cycle [24] to isolation of fetal nucleated red blood cells (nRBCs) from maternal blood [63, 109, 110].

2.3.1 Immobilization via Antibody or Aptamer Chemistry

The microfluidic devices discussed in this section take advantage of biochemical interactions to enhance rare cell capture or fractionation. Immunocapture is a technique frequently used in the extraction of cells, viruses, and proteins from suspension. It employs anti-sera to target biological agents of interest. In rare cell isolation, immunocapture presents an opportunity to separate cells with extremely high specificity from a suspension, in a viable state. In practice, this technique is analogous to microscale affinity chromatography for cells possessing unique markers or characteristics [124].

Blood Cell Fractionation

Chang et al. studied the effect of microfluidic structures on white blood cell (WBC) adhesion using different pillar geometries and orientations. They compared square and rhombic arrays with square and ellipsoidal micropillars, respectively. The micropillars were physisorbed with E-selectin to identify different leukocyte model cell lines (in cell media) via adhesive rolling speeds. Cell rolling velocities were two times as high in rhombic arrays, resulting in 130- to 160-fold enrichment, as opposed to 200-fold enrichment in square arrays. By comparing microarray geometries under identical flow and immunocapture conditions, Chang et al. demonstrated that the type of pillar geometry alone

influenced cell adhesion mechanics and, by extension, isolation [14].

In contrast, Murthy et al. focused upon the effects of shear stress on leukocyte adhesion mechanics. They studied the effects of shear stress using a Hele-Shaw flow cell with a device geometry that created a linear variation in shear stress along its axis(see Figure 2.1C). The researchers used anti-CD5, anti-CD19, and PEG to isolate T- and B-lymphocytes from a heterogeneous PBS suspension. Non-target cells were depleted from heterogeneous mixtures, resulting in suspensions that were 97% pure [114]. Sin et al. extended this work to blood, and studied the effects of suspension density on cell binding and the time-scale of cell-antibody kinetics. Within three minutes they obtained 100% and 75% pure suspensions of T-lymphocytes and B-lymphocytes, respectively [142]. Wang et al. also captured T-lymphocytes using anti-CD3-coated micropillars. They surrounded their pillars with segmented curved walls to increase the range of shear stresses experienced by the cells. Using this technique, they were able to isolate T-lymphocytes spiked in blood with 80% efficiency [168]. These studies, in combination, demonstrated that the fluid mechanics of microfluidic devices influence efficient immobilization in addition to antibody/aptamer specificity.

Cancer Cells

Many microfludic devices take advantage of the 3D structure of channels to increase the surface area available to be coated with the antibody or aptamer of choice. Du et al. demonstrated the efficacy of this technique in straight microchannels by differentially capturing human mammary epithelial cells and breast cancer cells by use of epithelial membrane antigen (EMA) and epithelial growth factor receptor (EGFR) [39]. The sensitivity of capture to antibody

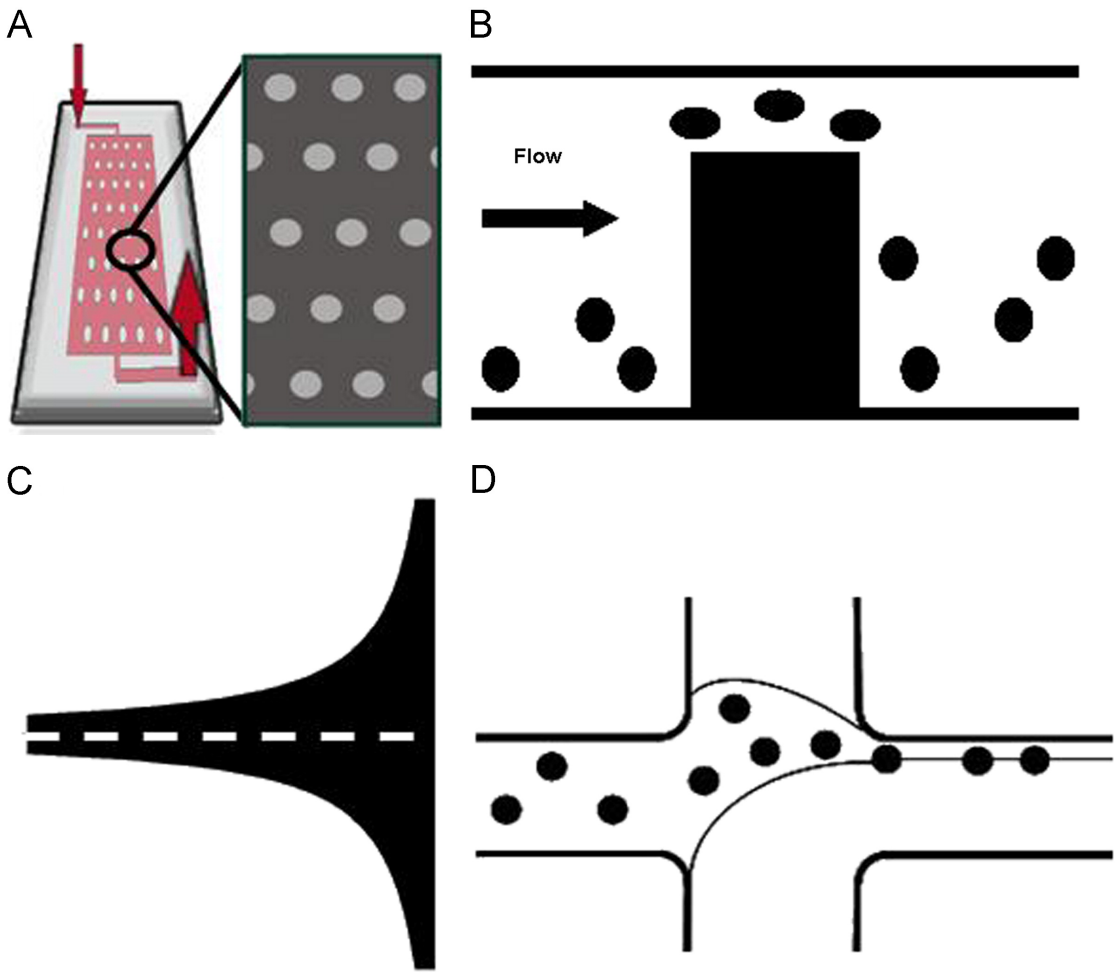

Figure 2.1: (A) Schematic of an micro-pillar device's architecture. Adapted from [46] (B) Schematic of a Weir microfilter's operation. Adapted from [67] (C) Example of a Hele-Shaw flow cell where the dotted line is the region of linearly increasing shear (D) Schematic of a sheath-flow based separation system. Adapted from [172]

dilution alone was also demonstrated using the same device geometry. Using this isolation technique, their capture rates from a PBS suspension ranged up to 30%. Xu et al. used DNA aptamers within an S-shaped microfluidic device [173] to capture cancer cells from PBS. Using aptamers targeted to various leukemia and lymphoma cell lines lines, their device efficiencies ranged from 50-83% with

88-97% purity. Recent work by Wang, et al. on silicon nanopillars (SiNPs) indicated that the topology of the microdevice itself may contribute greatly to the efficiency of rare cell capture. Comparing EpCAM functionalized SiNPs and flat surfaces, there was approximately 6-fold increase in capture efficiency, from 4-14% to 45-65% [165].

Cancer cells have also been captured from blood-based systems. Liu et al. used nickel micro-pillars to immobilize functionalized superparamagnetic beads to create a capture zone within their microfludic devices. Using magnetic fields, they then immobilized and released an immortalized lung cancer cell line mixed with human RBCs. This method produced 133-fold enrichment with 62-74% capture efficiency [94]. Adams et al. observed cell margination along the walls of linear channels when working with whole rabbit blood. They hypothesized that this reduced the rate of cell-antibody interactions in their devices [1]. This phenomenon was no longer seen when straight-walled channels were exchanged for sinusoidally varying ones. In combination with anti-epithelial growth factor receptor (EpCAM) antibodies, Adams et al. achieved immortalized breast cancer cell capture efficiencs of 97%. The device was translated to the capture of model prostate cancer cells spiked in PBS, using anti-prostate specific membrane antigen(PSMA) aptamers with an efficiency of 90% [36].

While the prior studies worked with model cell lines spiked in buffer solution [39, 173, 36, 165] or blood systems [94, 1, 115, 46], this method has also been used for cancer patient blood samples [115, 46]. Nagrath et al. used a dense array of micro-pillars coated in EpCAM to increase the number of cell-antibody interactions for a given suspension volume. Using this approach, they isolated lung, prostate, pancreatic and other cell lines from blood samples with average

efficiency and purity of 65% and 50% respectively [115]. Recently, Gleghorn et al. used computational modeling to design micro-pillar arrays such that cell-antibody interactions were size-dependent. Using microdevices functionalized with anti-PSMA antibodies, prostate cancer cells were captured at efficiences of 85-97% with purities of 68% [46] (see Figure 2.1A).

Other Mammalian Cells

Plouffe et al. used previously discussed microfluidic devices [114, 142] to selectively isolate endothelial cells (ECs) and smooth muscle cells (SMCs) from suspension. They coated their devices with peptides (REDV and VAPG) targeted to ECs and SMCs, and investigated binding to target cells as a function of shear stress. Using these peptide sequences, they differentially isolated ECs and SMCs from homogenous and heterogenous suspensions with purities of 86% and 83%, respectively [124]. Plouffe et al. further demonstrated the feasibility of peptide-based capture systems by using a 3-stage isolation system to deplete heterogenous suspensions of ECs, SMCs and fibroblasts [125]. Using this system, they were able to achieve 96% to 99% depletion of the three different cell types with over 97% viability of non-immobilized cells. Their work agreed with results on shear-dependent cell capture discussed previously [114, 142], showing this relationship to be true regardless of cell type.

2.3.2 Size-based Sorting

Size-based sorting affords the ability to capture target cells without knowledge of the target cell's biochemical characteristics. This is an attractive option

if the target cell's size is extreme in relation to its medium and also if the cell's properties are not well understood. Many approaches have been used to attempt size-sensitive isolation, ranging from size-dependent transport through small geometries to size-dependent particle pathlines in open obstacle arrays [65, 158, 159, 138, 142, 33, 67].

Blood Cell Fractionation

Much research has been done to develop microfluidic platforms to fractionate blood components, particuarly WBCs, based on size. Sethu et al. developed a microfluidic diffusive filter for WBC depletion from whole human blood. The system allowed biconcave red blood cells (RBCs) egress from the main device while larger WBCs were retained. The filtration elements were placed on the sides of the main channel, to minimize clogging by distributing RBC egress points along the length of the channel rather than focusing it in one area. To maintain equivalent volumetric flow rates in each segment, they used a flared geometry designed using Hele-Shaw analysis.Using this diffusive filter technique, over 97% WBC depletion was achieved [138].

Ji et al. reviewed various other microfludic filtration techniques for the application of WBC depletion. They found that pillar filters and cross-flow filters had high WBC depletion rates and could be used to process large sample volumes [67]. VanDelinder et al. also investigated cross-flow filters for WBC depletion, but also observed that RBC clogging hindered performance. They subsequently attempted WBC isolation using repeated microfluidic array geometries, achieving 98% WBC retention from human blood with no RBC lysis [158, 159].

Davis et al. and Inglis et al. used microfluidic devices featuring pillars. Rather than using the pillars to create microfludic slits to obstruct larger cell flow, they used the micropillars to create particle-size-dependent pathlines such that target cells were sorted into predetermined outlet ports based on size alone [33, 65]. Using this technique, Davis et al. depleted lymphocytes and monocytes from blood with 100% efficiency and Inglis et al. were able to separate lymphocytes from diluted blood suspensions with 73% efficiency.

Cancer Cells

Zheng et al. developed paralyene microfilters for the isolation of immortalized prostate cancer cell lines. Using pressure-driven flow to force cell suspensions through the filter, their cell recoveries ranged from 87% to 89% [183]. Cells retained on the microfilters were lysed for genomic analysis. Chen et al. used a combination of experimental results and physical modeling to develop a weir filter to selectively isolate cancer cells based upon their deformability [18](see Figure 2.1B). Using a filter fabricated specifically for their model lung adenocarcinoma cells, they were able to achieve over 99.9% capture efficiency from diluted human blood samples.

Other Mammalian Cells

Mohamed et al. also used pillar filters for the goal of isolating fetal nucleated red blood cells (fNRBCs) from maternal blood [110]. The pillars were placed to create succesively narrower channels in the device such that cell capture between pillars was a function of size and deformability. RBCs and fNRBCs were

isolated from goose blood and cord blood samples, respectively. Mohamed et al. reported no significant clogging using this staged pillar technique; however, blood samples were diluted pre-isolation. Huang et al. separated NRBCs based on size-dependent pathlines as described previously [33, 65]. Their device successfully eliminated over 99% of RBCs; NRBCs were further purified from contaminating WBCs by use of magnetic separation. Huang et al. successfully enriched NRBCs by a factor of 10- to 20 more than previously reported techniques [63].

2.3.3 Sheath Flow & Streamline Sorting

These devices take advantage of the fluid flow associated with the imposition of certain geometries or parallel fluid flows of different flow rates to passively sort or segregate target cells (see Figure 2.1D). This is another label-free and chemistry-free method of cell isolation that is most commonly used when size differences between cells is significant.

Blood Cell Fractionation

SooHoo et al. used a microfluidics-based aqueous two-phase system (ATPS) to enrich leukocytes from blood suspension. Using one stream of polyethylene glycol (PEG) and one of dextran (DEX), with Zap-oglobin as the lysing agent, they achieved 100% RBC depletion from human blood samples [144]. Zheng et al. developed devices based on T-shaped bifurcated channels to separate WBCs from RBCs. By adjusting the length of the T-channel, and the vertical distance between upstream and downstream side walls, cells were directed to different

stream lines based on size alone. They were able to separate WBCs from diluted blood with 97% efficiency. However, they found that RBC orientation heavily influenced the segregation of small WBCs from RBCs [184].

Other Mammalian Cells

Kuntaegowdanahalli et al. used spiral microchannels to segregate cells based on size across the width of their devices. Using a five-loop system, they sorted neuroblastoma cells from glioma cells with 80% efficiency [85]. The cells were then placed in culture and exhibited 90% viability after sorting. Lin et al. used multiple sheath flows in parallel to sort yeast cells from suspension. They used two streams of unequal flow rate to achieve a focusing effect and were able to separate yeast cells with 87.7% efficiency and 94.1% purity [93].

In contrast, Choi et al. used a series of slanted microfluidic channels of periodically varying heights to sort cells by cell-cycle phase. The slanted obstacles generated streamlines that diverted cells transverse to the flow, towards the wall of the device. There, the cell-obstacle interactions diverted larger cells out of the transverse streamlines, keeping them near the wall, while smaller cells diverged from the wall [24]. They achieved lateral separation of G_0/G_1 phase and G_2/M phase monocyte model cells with over 4-fold G_2/M cell enrichment.

Prokaryotes & Viruses

Wu et al. used sheath flows to sort *E. coli* from blood. High concentrations (greater than 10^8cells/ml) of *E. coli* cells were spiked into diluted human RBCs and were enriched 300-fold over the course of separation. They demonstrated a

sorting efficiency of 62% and purity of 99.87%. The bacteria were expanded in culture and exhibited over 95% viability [172].

In summary,the devices described above all use varying non-electrokinetic techniques to successfully isolate a broad range of cell types. However, despite a variety of isolation mechanisms and microfluidic designs, there is no single microfluidic device that can produce pure cell populations with high efficiency. For these devices to be used for rigorous biochemical and genetic assays, it is essential that a method of high purity, high efficiency capture be found. An additional challenge is that many rare cells of interest (e.g. leukocytes, CTCs, yeast, bacteria) are found in the blood, a dense suspension that often hinders characterization of device performance. For micorfludidic devices to reach their full potential as rare cell capture platforms, it is essential that these elements be addressed and improved upon.

2.4 Electrokinetic methods

Electrokinetic methods comprise those methods that use electric fields to actuate cells. In microfluidic devices, the two most widespread electrokinetic techniques for manipulating cells are electrophoresis and dielectrophoresis. Electrophoresis refers to net migration due to the action of an electric field on the net fixed charge of a particle. This technique has been used to study cells at the membrane level [106], and methods such as capillary electrophoresis and microfluidic free-flow electrophoresis have been developed to separate different populations of biomolecules, viruses, bacteria, and eukaryotic cells [82, 156]. However, as the net charge of a cell's electrical phenotype is often not specific

enough to distinguish between a mixture of different cells, electrophoresis has been used minimally as a cell separation technique and is not suited for applications in rare cell capture. Thus, this review will focus primarily on dielectrophoretic techniques.

Dielectrophoresis (DEP) refers to the net migration of polarized particles owing to interactions with an electric field gradient, and depends on cell wall, membrane, and cytoplasmic electrical properties [68, 75]. The DEP force is a direct function of these electrical properties as well as cell size, the electrical properties of the fluid medium, and the magnitude and frequency of the applied electric field; the dependence on this wealth of parameters makes DEP an attractive tool for distinguishing between different cell types [161, 51]. DEP response is classified into two regimes: when particles are more polarizable than the medium, positive DEP results and the particles are attracted to stronger field regions; conversely, when particles are less polarizable than the medium, negative DEP results and the particles are repelled from stronger field regions; the frequency at which the DEP force switches from one regime to the other (i.e. when the force is zero) is termed the "crossover frequency" [68, 112]. The sign and magnitude of the DEP force provides the basis for DEP cell separation techniques, and this review will cover the most common device geometries used for these techniques. The scope of this review on DEP methods will be limited to those used for capture, separation, or concentration of bulk cell populations; DEP methods for single cell capture or manipulation are covered in other reviews [161, 51, 5, 69, 181]. The DEP methods are organized by the type of device geometry used; each section includes a brief description of the physics associated with the technique and a summary of how it is applied to separate different cell types with a view towards pathogen detection, blood fractionation,

or cancer cell isolation. Many DEP experiments have used model systems to characterize geometric performance, or as mockups of rare cell capture experiments. Thus, this section includes many devices that do not capture rare cells, but whose performance informs the potential for rare cell capture with DEP.

2.4.1 Electrode-based DEP

Microfabricated electrodes are the most common and practical method for creating the non-uniform electric fields necessary for DEP. While potential limitations to the use of electrode-based DEP include fouling and electrolysis at low electric field frequencies as well as increased fabrication time and cost required for more complex electrode configurations, a majority of DEP techniques use microfabricated electrodes owing to their simplicity and flexibility in implementation. The following sections will cover the most common and simple device geometries used for cell separation.

Interdigitated array (IDA) electrodes

Interdigitated arrays consist of spatially alternating sets of grounded and energized electrodes that create non-uniform electric field regions and trap particles against a flow via positive DEP (Figure 2.2A). IDA electrodes are one of the most commonly used electrode configurations because their use entails minimal design parameters (electrode length and width, inter-electrode distance, and channel depth) and experimental parameters (flow rate, electric field magnitude and frequency), and yields analytical solutions for electric fields and particle motion [148]. IDA electrodes are typically used for "binary" cell separation; an electric

field is applied to capture the target cells from a mixture of two or more cell types via positive DEP, the non-target cells are minimally affected by the field or repelled via negative DEP and are flushed out of the device, and finally the field is turned off to release the target cells for separate collection. Through DEP characterization, a frequency regime can be selected in which one cell type is attracted to the electrodes (positive DEP) while another cell type is repelled into the regions separating the electrodes (negative DEP). Rare cell capture requires that all non-target cells be repelled, which can be demanding if the suspension is complex.

IDA electrodes have been used to separate or concentrate bacteria for potential applications in pathogen sensing. Typical cell concentrations used for these studies lie in the range of 10^5 to 10^9 cells/mL. Efforts to detect foodborne pathogens such as those in the genus *Literia* include separation of live and heat-treated *L. innocua* with 90% efficiency; as the cell membrane becomes permeable upon death, large changes in conductivity can result in differences in the DEP response of live and dead cells [91]. Researchers have also used positive DEP to attract a mixture of *Listeria* and *Escherichia* species to antibody-coated electrodes and selectively capture only *L. monocytogenes* (i.e. immunocapture) with 87-92% efficiency [177, 79]. To aid efforts in detecting environmental pathogens, researchers have demonstrated concentration of *Bacillus subtilis* spores (a surrogate bacteria used for research on *Bacillus anthracis*, i.e., anthrax) from airborne environmental samples containing diesel particulate matter with up to 60% purity; appropriate frequency ranges for separation were selected based on crossover frequency measurements [41]. Additionally, Gadish et al. concentrated *B. subtilis* by integration of a chaotic mixer to bring the spores into closer proximity with the IDA electrodes and enrich the sample ninefold [42], and Liu

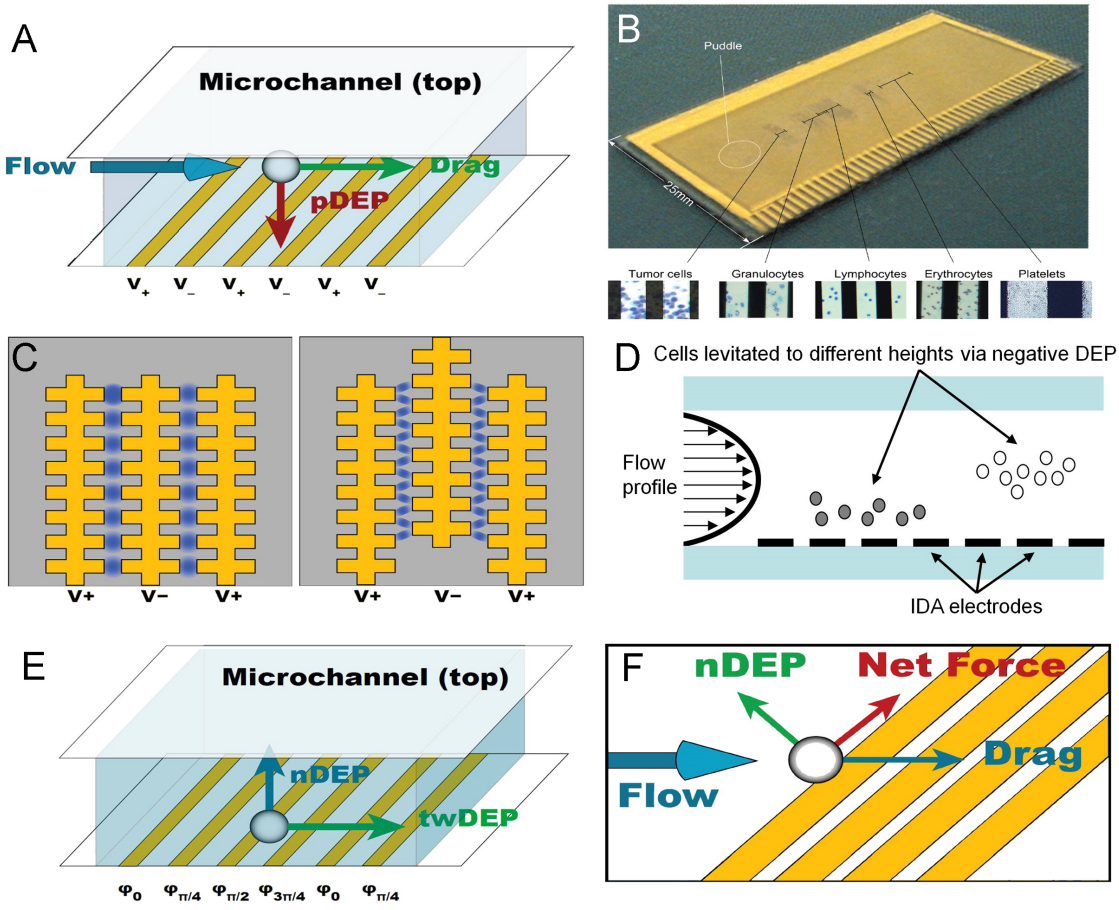

Figure 2.2: (A) Interdigitated array (IDA) electrodes. (B) Electrosmear slide showing fractionation tumor cells and blood components. Reproduced from [28]. (C) Castellated IDA electrodes. (D) DEP field-flow fractionation operates by levitating cells against gravity to different heights in the channel via negative DEP, allowing separation to be achieved based on their differing flow velocities. (E) Configuration and forces in a twDEP electrode array. (F) Summation of forces near an angled electrode.

et al. captured *B. anthracis* with 90% efficiency for impedance measurements in order to detect viable spores electrically by their germination [95].

IDA electrodes have also been used for blood fractionation. Cristofanilli et al. used an "electrosmear" slide that was coated to promote cell adhesion and patterned with IDA electrodes to which different electric field frequencies were

applied along the length of the device [28]. Near the inlet port, a low frequency was applied to levitate all cells via negative DEP to avoid adhesion to the slide, and as the blood sample obtained from a murine aspiration biopsy was flowed further along the device, different constituents of blood as well as biopsied tumor cells from a cancer line grown in nude mice were pulled toward and adhered to the electrodes via positive DEP in different regions of the slide, based on their previously characterized dielectric properties (Figure 2.2B) [28].

Castellated IDA electrodes

Castellated electrode arrays consist of interdigitated electrodes with width variation along their length, which create alternating regions of high and low electric field magnitude at the tips of the electrodes and the regions separating each electrode, respectively (Figure 2.2C). The advantage of castellated electrodes is the localization of high electric field regions, which can be used to trap or concentrate flowing cells in the device effectively. The procedure for cell separation using castellated electrodes is the same as that used with straight IDA electrodes; this procedure has been used for binary separation of a mixture of two bacteria types, including yeast, *E. coli*, and *Micrococcus lysodeikticus* [102], as well as for separation of viable and non-viable yeast cells [103]. Optical absorbance of DEP trapping was measured to calculate the effective conductivity of the cells and predict their DEP response.

Castellated IDA electrodes have been used for cell separation between bacteria and blood cells for applications in pathogen detection, with typical cell concentrations of 10^6 to 10^7 cells/mL; researchers have demonstrated separation of *M. lysodeikticus* from erythrocytes based on their differing dielectric properties

[163]. Isolation of erythrocytes infected with malaria pathogen from healthy erythrocytes was also achieved with 90% efficiency owing to the sharp increase in membrane conductivity of erythrocytes hosting malarial parasites [45]. In addition, Huang et al. demonstrated simultaneous separation of multiple bacteria (*Bacillus cereus, E. coli, L. monocytogenes*) from diluted blood with up to 97% efficiency using size-based DEP separation and post-separation PCR analysis [61].

Castellated IDA electrodes have also been used for applications in cancer cell isolation. Becker et al. characterized the dielectric parameters of cultured breast cancer cells, lymphocytes, and erythrocytes using particle electrorotation techniques, and subsequently trapped the breast cancer cells from a suspension of diluted blood, demonstrating up to 95% purity in captured cancer cells [7]. More recently, Tai et al. developed an automatic platform for separation of viable and non-viable cultured human lung cancer cells based on differing dielectric properties with 81-84% efficiency and nucleus collection for nuclear protein extraction [150]. While castellated IDA electrodes are similar in function and application (e.g. binary sorting) to straight IDA electrodes, their ability to create alternating regions of high and low electric field magnitude makes them better suited for concentrating samples or patterning particles at a specific location than straight IDA electrodes. As is the case for straight IDA electrodes, the challenge associated with castellated IDA electrodes is in finding a frequency or set of frequencies such that only the rare cells are attracted to the electrodes.

IDA electrodes for flow-field fractionation

In DEP flow-field fractionation (DEP-FFF), IDA electrodes are fabricated on the bottom of a device channel, and flowing particles of differing dielectric properties are levitated against gravity via negative DEP. The levitated particles equilibrate to different heights in the channel owing to the distinct DEP force on different types of particles, and these differing heights allow separation to be achieved by sequential collection based on different flow velocities due to the parabolic velocity distribution of low-Reynolds-number Poiseuille flow (Figure 2.2D). The velocities of different cells can be characterized by measuring cell elution fractograms as a function of frequency [60]. The main advantage of DEP-FFF is its ability to achieve continuous-flow separation of bioparticles with size and/or dielectric differences under a constantly applied electric field, therefore avoiding the need for activation and deactivation of the field as required by binary sorting devices.

DEP-FFF has been used often as a technique to separate different cell types in blood, with cell concentrations ranging from 10^5 to 10^7 cells/mL. Researchers have demonstrated separation of erythrocytes from latex beads and characterization of their different levitation heights [135], as well as binary separation of human leukocyte subpopulations (T-, B-lymphocytes, monocytes, and granulocytes) based on differing membrane dielectric properties with 87-98% purity, which can be used for clinical applications in differential analysis of leukocytes [175]. More recently, Hashimoto et al. performed selective capture of neutrophils and eosinophils from a mixed leukocyte suspension with 80% efficiency by deflecting the target cells away from the IDA electrodes and toward an antibody-coated layer on the opposite wall [50]. DEP-FFF also has

been used extensively for the separation and isolation of cancer cells. In particular, the Gascoyne research group has demonstrated separation of cultured human leukemia cells from diluted blood after characterizing the cells by DEP levitation experiments [59], separation of cultured human breast cancer cells from whole blood based on measured differences in cell size and membrane capacitance [176, 44], and separation of cultured human breast cancer cells from normal T-lymphocytes and hematopoietic CD34+ stem cells [60, 167], all with efficiencies and/or purities over 90%.

In more recent years, DEP-FFF has been used for a larger variety of applications as well as in different device geometries. These applications include separation of cells with high and low embryogenic potential in suspension cultures of carrot based on their differences in size and cytoplasm density [40], toxicity testing by dielectric characterization of cultured human leukemia cells with membrane dissimilarities due to exposure to various toxic agents [130], and enrichment of a progenitor cell population in a mixture of cell debris and erythrocytes from freshly harvested adipose tissue [162]. Finally, vertical IDA electrodes have been fabricated on the sidewalls of the device channel (as opposed to horizontal electrodes on the bottom of the channel) to achieve lateral separation through separate outlets. This device geometry has been used to separate mammalian cells of different sizes [165] and viable from non-viable yeast cells [11], as well as to enrich *Babesia bovis*-infected erythrocytes sevenfold [11]. Unlike trapping on straight or castellated IDA electrodes, DEP-FFF allows cells to be separated based on the magnitude of the DEP response rather than just the sign of the response, and rare cell capture can be achieved in theory if the DEP response of a cell can be distinguished within the sensitivity of the device.

IDA electrodes for traveling-wave DEP

IDA electrodes have been used for a technique called traveling-wave DEP (twDEP) to fractionate bioparticles. The electrodes are independently driven with different electric field phases, and particles are levitated against gravity owing to negative DEP (Figure 2.2E). Fractionation is achieved by varying the electric field phases to drive the particles transverse to the direction of flow at different velocities. Cui and Morgan detailed the design and fabrication of a twDEP device and demonstrated particle motion using polystyrene latex particles [29]. The main advantage of twDEP is that fractionation may be achieved based on the particles' differing velocities alone; there is no need to drive fluid flow or to trap or concentrate particles via positive DEP.

Building on the successful implementation of twDEP on polystyrene beads, a number of biological separations have been achieved. Bacteria separation has been demonstrated by use of viable and non-viable yeast cells [151, 83]; as well, blood fractionation has been demonstrated by separating T-lymphocytes and erythrocytes by applying multiple frequencies to direct the cells to move in opposite directions such that they were collected separately through different outlets [98]. twDEP has also been used for applications in pathogen detection; a spiral electrode array was characterized and used for a 1000-fold enrichment of malaria-infected erythrocytes from normal erythrocytes with 90% purity [166, 45]. Application of the traveling field caused normal erythrocytes to be trapped at the electrode edges via positive DEP, while infected cells were levitated via negative DEP and carried to the center of the spiral [45]. More recently, Cheng et al. developed a high-throughput 3D twDEP device used for focusing and sorting particles, and demonstrated its ability to separate bacte-

ria and blood cells based on DEP mobility magnitude as well as direction [20]. Other recent studies used twDEP for characterization of cultured lymphoma and myeloma cells for potential applications in rare cell capture [13] and the development of a DEP pump for blood delivery in microfluidic devices [90].

Angled electrodes

Angled electrodes are most often used for binary separation of bioparticles or to create localized particle pathlines due to the particles' negative DEP mobilities. As the particles approach an electrode, the negative DEP force that acts on them can exceed drag forces, resulting in a net force parallel to the electrodes. Particles then travel along the length of the electrode until drag forces exceed the DEP force, at which point the particles can flow past the electrodes (Figure 2.2F). Displacing particles transverse to the direction of flow allows angled electrodes to preferentially direct particles to different outlets or focus them into concentrated streams.

Angled electrodes have been used to sort and concentrate various bacterial samples. Cheng et al. designed a device with 3D electrode gates to focus and separate yeast and *E. coli* into different outlets, after which surface-enhanced Raman scattering was used to detect bacteria concentration and evaluate efficiency [19]. Kim et al. tagged *E. coli* with different sized microspheres and used angled electrodes to separate the two target cell types into different outlets, after which capture efficiency and purity was evaluated using flow cytometry [72]. More recently, a magnetic separation module was incorporated into the device to capture magnetically-tagged cells and separate them from unlabeled non-target cells, which improved the device's ability to separate multiple cell types

[74]. Vahey and Voldman developed a separation method termed "isodielectric separation," which uses a diffusive mixer to establish an electrical conductivity gradient across the width of a channel containing angled electrodes [157]. DEP forces vary along the length of the electrodes, which direct and separate viable and non-viable yeast cells across the device in the direction of decreasing conductivity until they reach their respective isodielectric points, where there is no net force [157].

Angled electrodes have also been used for binary sorting of mammalian and blood cells. To address the need for a noninvasive method for sorting cell populations according to their cell-cycle phase, Kim et al. separated cultured human breast cancer cells based on their differing sizes due to their cell cycle phase [73]. Angled electrodes were also used to demonstrate a low-stress platelet size-based DEP separation technique by separating platelets from diluted whole blood with 95% purity [126].

2.4.2 Insulative DEP

Insulative DEP techniques rely on constrictions or expansions in channel geometry to generate electric field non-uniformities and deflect or trap bioparticles via negative DEP. While this approach places limits on the frequencies and geometries used, the main advantage of insulative DEP is that no internal electrodes are used. This leads to simpler device fabrication, reduced propensity for fouling, and the possibility of using a DC field for electrokinetic particle transport as well as trapping via DEP [88].

Angled and curved constrictions

The simplest geometry in an insulative DEP device is a perpendicular insulative constriction in the device channel. Kang et al. demonstrated size-based separation of live cells by using rectangular constrictions to deflect larger cells (white blood cells and cultured mammalian breast cancer cells) via negative DEP to a different trajectory than smaller blood components (red blood cells, platelets) [70]. Binary sorting is achieved by fabricating two outlet channels for the separate trajectories.

Extending the basic principles of rectangular constrictions, angled constrictions have also been used to separate and concentrate bioparticles. The DEP force acting perpendicular to the constriction depends on the angle that the constriction forms with the channel. If this DEP force is smaller than the drag force, then particles will flow past the constriction unaffected; if, however, the DEP force exceeds the drag force, then the particles are stopped at and deflected parallel to the constriction. Angled constrictions have been used to demonstrate size-based separation of *B. subtilis* from polystyrene particles [6]. Curved constrictions, in which the angle of constriction varies continuously across the channel, have also been used to separate different sized particles (Figure 2.3A) [52].

Post arrays

DEP trapping using an array of insulating posts was reported by Cummings and Singh, who investigated various geometric variables that affect the electric field, including post shape, distance between posts, and array angle to

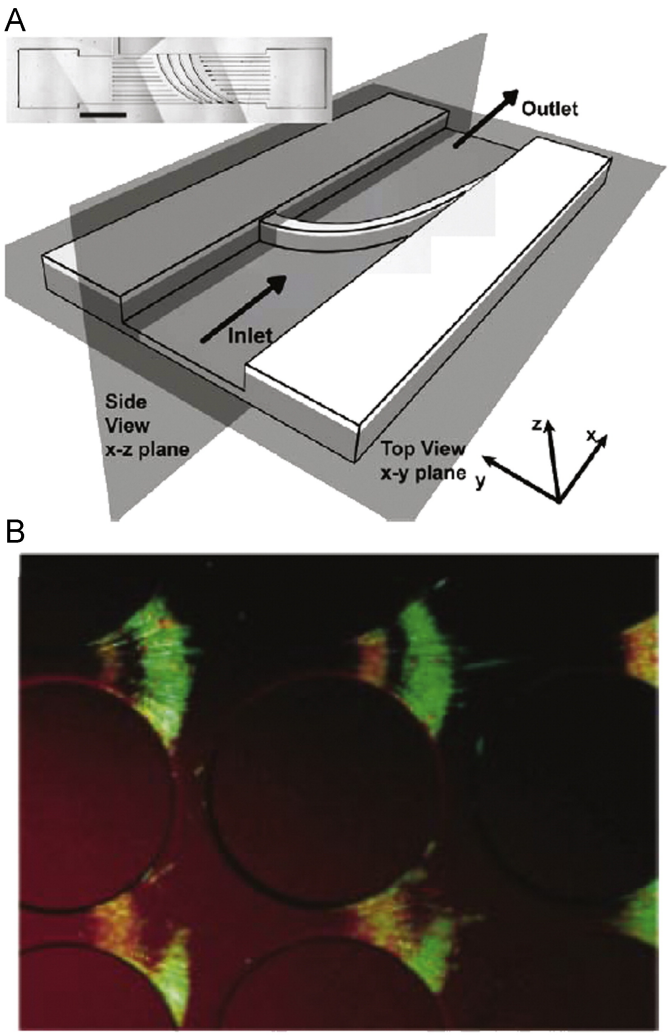

Figure 2.3: (A) Schematic of curved constriction in channel depth. Inset: top view of device fabricated in Zeonor 1020R polymer substrate. Reproduced from [52]. (B) Trapping of live (green) and dead (red) *E. coli* with separation of populations using insulative post array. Reproduced from [88].

the applied field [30]. Using an array of circular posts etched in a glass substrate, researchers at Sandia National Laboratories have demonstrated trapping of polystyrene beads [107] and separation of live and dead *E. coli* based on their differing magnitudes in negative DEP response (Figure 2.3B) [88]. The group later demonstrated separation and concentration of any two pairs of *E. coli*, *B.*

subtilis, *B. cereus*, and *Bacillus megaterium* [89], as well as tobacco mosaic virus [87]. A direct application of this technique is for the detection of microbes in drinking water, which is hindered by current analytical instruments that require significant concentration of microbes in order to detect them [87].

Other geometries

A variety of other device geometries have been designed for bioparticle separation and isolation using insulative DEP. Chou et al. used an array of constrictions to trap and concentrate single- and double-stranded DNA [25]. Pysher et al. designed channel walls with a sawtooth pattern to produce spatially resolved separation of live and dead *E. coli* and *B. subtilis* [132]. More recently, Church et al. fabricated a serpentine channel to filter *E. coli* from yeast cells [26], Cho et al. positioned plastic membranes with honeycomb-shaped pores between electrodes to trap and release *E. coli* in the flow channel [23], and Shafiee et al. developed a "contactless" DEP technique to isolate live/dead cultured human leukemia cells by using thin insulating barriers to separate the electrodes used to apply the electric field from the sample channel, thus preventing potential issues such as contamination and bubble formation [139].

2.4.3 Prospects for DEP rare cell capture

The preceding sections on electrode-based and insulative DEP techniques introduced the most common device geometries that researchers have used to separate different populations of cells. Those studies that focused on quantifying experimental performance criteria such as efficiency, enrichment, and/or purity

are summarized in Table 2.2. Overall, DEP methods are advantageous because they do not require a biochemical labeling step to achieve continuous-flow separation. Additionally, it is possible to achieve DEP cell separation without *a priori* knowledge of the different cells' properties. For binary separation using IDA electrodes, only the frequency range in which the cells experience DEP forces opposite in sign needs to be known; for methods that use angled electrodes or insulative constrictions and techniques such as DEP-FFF and twDEP, only the cells' relative DEP response magnitudes is required to achieve separation of several cell types. As such, DEP offers the ability to isolate single cells (because of its sensitivity to cellular dielectric properties) as well as the possibility for separation of cell populations in which not all cell types have been characterized. In the latter case, DEP potentially can be used to screen for cells with unknown membrane phenotypes, which can facilitate research on bacterial species such as *Mycobacterium tuberculosis*, whose pathogenicity is closely tied to membrane composition [134].

Using only DEP techniques for rare cell capture in pathogen detection or tumor cell isolation, however, is challenging; studies have reported significant decreases in cell capture efficiency or purity as target cell concentrations became more dilute [44, 41, 45, 61]. While numerous DEP methods for cell separation of artificial samples have been reviewed in this article, we are not aware of a study that demonstrates strictly dielectrophoretic capture of pathogens from environmental (air or water) samples or capture of viable tumor cells from whole blood of cancer patients. In the future development of rare cell capture microfluidic devices, it may be beneficial to merge DEP methods with techniques such as magnetic-activated cell sorting [72, 74] or immunocapture [177, 50]. Such hybrid techniques combine the actuation of DEP with the chemical-specificity of

immunocapture techniques; a system could be developed in which the applied electric field is tuned low enough to cause no physiological harm to target cells while inducing a strong enough DEP force to cause or prevent interactions with immunocapture surfaces. These synergistic effects have the potential to minimize problems associated with immunocapture techniques (e.g. nonspecific binding) and yield higher performance in rare cell capture efficiency and purity compared to using DEP techniques alone.

2.5 Performance Criteria

In the previous sections, we have described a variety of different methods to isolate a multitude of rare cell types. In this section, we quantitatively compare these disparate studies with a unified set of performance criteria. Comparing the literature systematically identifies the strengths and weakness of the field as a whole and provides insights into future research directions. In the following paragraphs, we define performance metrics by which the literature will be evaluated (see Tables 2.1 & 2.2) and draw conclusions upon analyzing these criteria. Italics are used to highlight headings in these tables.

When comparing different rare cell capture devices, it is important to distinguish between the *cell type modeled* (e.g. cells obtained from biological samples) and the *cell type used* (often an immortalized cell line). This is imperative when the target cell's biological characteristics are not well understood, e.g. circulating tumor cells. While the use of well-understood model cell lines eases the characterization of device performance, their relations to clinical samples are not always well defined. Likewise, the *carrier media* used for experimentation

is often chosen to simplify device characterization. Many rare cells that are targeted for isolation exist in dense biological suspension when *in vivo*, e.g. blood. However, many such fluids present other cellular material that confound quantification of performance for example, changing viscous or conductivity properties. For this reason, rare cells are often captured from diluted biological solutions or even buffer solutions. For devices that use DEP methods, the conductivity of the media and the cell concentrations used are also important as these parameters affect the DEP force and capture efficiency or purity, respectively.

A number of quantitative metrics can be used to describe device performance. *Efficiency* is the most commonly used measure of performance in rare cell isolation literature. Efficiency is defined as the fraction of successfully isolated/fractionated cells with respect to the total number of target cells introduced into the device. High-efficiency microfluidic cell isolation devices are often operated at higher volumetric flowrates than high-purity ones, resulting in increased throughput [46, 138]. Another common metric is *enrichment*, the multiplicative factor by which the number of rare cells per unit volume is increased. In contrast is depletion, where non-target cells are captured within the device, leaving a more pure subpopulation at the outlet [125, 124]. *Purity* is the number of target cells captured divided by the total captured cell population. Purity is an important metric for measuring the selectivity of a device, but its optimization usually results in lower efficiencies and throughputs. However, high purity samples are desirable for a variety of biomolecular assays and tools. Equally important is the *viability* of cells post-capture. Some devices define viability as the percentage of cells left in a functional state post-capture and others post-culture *ex-vitro*. When comparing results from different methods, it is also important to compare the *number of steps/stages* involved. The possibility

of increased performance with multi-stage processing versus the simplicity of device operation are major concerns for devices designed for clinical applications. However, the number of steps/stages was not included for devices that employ DEP methods, as a majority of those listed in Table 2.2had similar procedures that include dielectric characterization, cell staining, on-chip capture or fractionation, and post-process cell counting. Given the data in Tables 2.1 & 2.2 organized under the headings described in previous paragraphs, we can make a number of observations about rare cell capture in microdevices.

2.6 Discussion & Conclusion

Multiple strides have been made in the enrichment, fractionation, and capture of rare cells. The devices outlined in this review have been successfully used for the enrichment of bacteria to the genetic analyses of cancer cells [172, 146, 147]. Microfluidic devices for rare cell capture have elucidated new biological phenomena and afforded multiple avenues of further scientific investigation. Current devices have been successfully implemented in the enumeration of rare cells ranging from NRBCs to CTCs [58, 115, 46]; however the lack of a single microfluidic device that can isolate pure cell populations with high efficiency limits the number of molecular and genetic tools that can be used on these populations.

Additionally, few cell capture studies directly process biological samples [115, 46, 158, 159]. In contrast, most devices spike cell lines into buffer solution [14, 114, 142, 124, 183, 85, 24, 36, 173, 125], or pre-diluted/lysed blood samples [184, 33, 58, 172]. Importantly, in devices that employ DEP methods,

efficiency and purity performance is low when target cell concentrations are dilute [41, 45, 61, 44], thus making rare cell capture using DEP techniques alone extremely difficult. In addition, many more cell capture devices approximate the *ex vivo* target with a model equivalent [173, 36, 91, 42, 41, 7, 176, 60] rather than capture of the actual *in vivo* target [159, 138, 177, 95]. Most use of undiluted *ex vivo* targets is for WBC fractionation, with few exceptions for other rare cell types [115, 58, 46].

Similarly, the viability of cells after the capture process is not a well-quantified area, but one that is a crucial performance evaluation metric for rare cell capture devices. Mechanical stresses from shear, either from electric- (i.e. DEP forces), contact- (i.e. from pillar filters) or fluid-induced forces (i.e. obstacle-based arrays) can lead to gene upregulation or even induce an apoptotic response [169, 119]. Directly tied to cell viability is cell release and culture post-capture. Some attempts have been made to elute rare cells from devices [173, 1, 36, 94, 182, 183, 172], especially those using affinity-based methods (i.e. immunocapture) [1, 36]. Although a majority of devices that employ DEP methods do not quantify post-process viability, other researchers have established that exposure to electric fields from microfabricated electrodes used for DEP techniques often does not alter cell viability [164, 54]. Electric field magnitudes and frequencies used for these devices are listed in the *Experimental Parameters* column of Table 2.2. Ultimately, in situations where the target cell can be as few as 1 per billion non-target cells (e.g. bacteria, viruses, CTCs), cell expansion in culture will be a critical step in obtaining enough material for further experimentation.

For future studies and biological applications, the major areas for improve-

ment are ability to elute cells in an undamaged state, increased cell survivability, and systems capable of delivering both high capture efficiency and purity. The development of such a platform could be facilitated by incorporating both electrokinetic and non-electrokinetic methods to create hybrid systems, as in recent efforts [177, 50, 72, 74]. Combining the sensitivity of DEP cell manipulation with the robustness of immunocapture has the potential to improve rare cell capture efficiency and purity, and such hybrid systems have scientific value and applicability across a variety of biological fields.

Table 2.1: Non-electrokinetic cell fractionation and isolation studies (abbreviated version from [129]). Acronyms: IC = Immunocapture, SBS = Size-based Sorting, ShF = Sheath Flow, StF = Streamline Focusing, BC = Breast Cancer, CC = Cervical Cancer, LC = Lung Cancer, PC = Prostate Cancer.

Application	Cell modeled	Cell used	Media	Processing	Efficiency	Enrichment	Purity	Analysis	Reference
Blood cell fractionation	B-lymphocytes, T-lymphocytes	Raji, Molt-3	PBS	staining	97%	na	na	anti-CD5, anti-CD19, PEG IC	[114]
	BC, PC, CC, Lymphoblast	MCF7, PC3, HeLa, Daudi	DMEM, Blood	staining, enumeration	80%	na	na	EpCAM IC	[168]
	B-lymphocytes, T-lymphocytes	Raji, Molt-3	PBS	staining, enumeration	na	na	na	anti-CD5, anti-CD19 IC	[142]
	Myeloid cells	HL-60, U-937	RPMI-1600	labeling, enumeration	na	130–200x	na	E-selectin IC	[14]
	Leukocytes	Leukocytes	Whole human blood	enumeration, lysing	na	na	97%	SBS	[138]
	Leukocytes	Leukocytes	Whole human blood	labeling, enumeration	98%	na	na	SBS	[159]
	Leukocytes	Leukocytes	Diluted human blood	enumeration	70–95%	na	na	SBS	[67]
	Leukocytes	Leukocytes	Diluted human blood	flow cytometry, staining, lysing, enumeration	99.6%	na	na	SBS	[33]
	Lymphocytes, monocytes	CD4+ cells, CD14+ cells, J45 lymphocytes	Diluted human blood	labeling, enumeration	73%	na	na	SBS	[65]
	Leukocytes	Leukocytes	Diluted human blood	lysing, enumeration	na	100x	na	ShF	[144]
	Leukocytes	Leukocytes	Diluted human Blood	dilution, enumeration	97%	na	na	StF	[184]
Cancer cells	Normal breast cell, BC	HME, TTU-1	PBS	enumeration, staining	30%	na	na	EMA, EGFR IC	[38]
	Leukemia, lymphoma	CCRF-CEM, Ramos, Toledo	Modified PBS	cytometry, staining, enumeration	50–83%	135x	88-97%	Scg8, TD05, Sgd5 IC	[173]
	BC	MCF7	Whole rabbit blood	check	97%	na	na	EpCAM IC	[1]
	PC	LNCaP	PBS	enumeration, staining	90%	na	na	PSMA, EpCAM IC	[36]
	BC	MCF7	DMEM	staining, enumeration, SEM	45-60%	na	na	EpCAM IC	[165]
	LC	SPC-A-1	Diluted human blood	enumeration	99.9%	na	na	SBS	[16]
	LC	A549	Human RBCs	staining, enumeration	62–74%	133x	na	WGA IC	[94]

Continued on next page

Table 2.1 – continued from previous page

Application	Cell modeled	Cell used	Media	Processing	Efficiency	Enrichment	Purity	Analysis	Reference
	LC, PC, BC, Bladder cancer	NCI-H1650, PC3-9, SKBr-3, T-24	PBS	staining, enumeration	65%	na	na	EpCAM IC	[115]
	LC	NCI-H1650	Whole human blood	staining, enumeration	60%	na	na	EpCAM IC	[115]
	PC	LNCaP	PBS	labeling, enumeration	97%	na	na	PSMA IC	[46]
	PC	LNCaP	Whole human blood	labeling, enumeration	85%	na	68%	PSMA IC	[46]
	PC	PC CTCs	Whole human blood	labeling, enumeration	na	na	62%	PSMA IC	[46]
	LC, PC, Pancreatic cancer, Colon cancer	LC, PC, Pancreatic CTC, Colon CTC	Whole human blood	staining, enumeration	na	na	42–67%	EpCAM IC	[115]
	PC	LNCaP	PBS	labeling, enumeration, electrolysis, PCR	87–89%	na	na	SBS	[183]
	PC	LNCaP	Whole human blood	labeling, enumeration, electrolysis, PCR	89%	na	na	SBS	[183]
Other mammalian cells	Endothelial cells, smooth muscle cells	H5V, A7r5	PBS	labeling, enumeration, staining	na	na	86%; 83%	REDV/VAPG Peptide IC	[124]
	Endothelial cells, smooth muscle cells, fibroblasts	H5V, A7r5, 3T3-6	PBS	labeling, enumeration, staining	na	na	96-99%	REDV/VAPG/ RGDS Peptide IC	[125]
	Neural stem cells	SH-SY5Y, C6	PBS	staining, enumeration, flow cytometry	89%	na	na	SBS	[85]
	G_2/M myeloid cells	U937	10mM sodium borate	flow cytometry	na	4x	na	StF	[24]
	Nucleated RBC	Nucleated RBC	Diluted human blood	filtration, dilution, staining	na	10–20x	na	StF	[58]
Prokaryotes & viruses	*E. coli*	*E. Coli*	Diluted human RBCs	staining, enumeration, SDS page	62%	300x	99.87%	ShF	[172]

Table 2.2: Electrokinetic cell fractionation and isolation studies (abbreviated version from [129]).

Application	Cell modeled	Cell used	Media	Processing	Efficiency	Enrichment	Purity	Technique	Reference
Pathogen detection	*L. monocytogenes*	*L. innocua*	DI water	Cell counting	90%	na	na	IDA	[91]
	L. monocytogenes	*L. monocytogenes*	DI water	Cell counting	87–92%	na	na	IDA + immunocapture	[177]
	B. anthracis	*B. subtilis*	DI water	Measure absorbance	na	9x	na	IDA	[42]
	B. anthracis	*B. subtilis*	DI water	Hemocytometer	na	na	≤60%	IDA	[41]
	B. anthracis	*B. anthracis*	DI water	Cell counting	90%	na	na	IDA	[95]
	Plasmodium falciparum	Malaria-infected erythrocytes	Sucrose buffer	Cell counting	90%	50–200x	na	Castellated	[45]
	na	*B. cereus, E. coli, L. monocytogenes*	Mannitol + PBS	PCR amplification	≤97%	na	na	Castellated	[61]
	na	*E. coli*	DI water	Cell counting	90+%	3000x	na	iDEP	[87]
	na	*E. coli*	PBS	Cell counting	66%	na	na	iDEP	[23]
Cancer cell isolation	Lung cancer	A549-luc-C8	DMEM buffer	Flow cytometry	81–84%	na	na	Castellated	[150]
	Breast cancer	MDA231	Sucrose buffer	Cell counting	na	na	95%	Castellated	[7]
	Breast cancer	MDA-435	Sucrose buffer	Cell counting	na	na	98%	FFF	[176]
	Breast cancer	MDA-435, -468, -231	Sucrose buffer	Cell counting	≤92%	na	na	FFF	[44]
	Breast cancer	MDA-435, CD34+ stem cells	Sucrose buffer	Flow cytometry	na	na	96–99%	FFF	[60]
	Breast cancer	MDA-231	PBS	Flow cytometry	na	4.4x	96%	Angled electrodes	[73]
	Leukemia	THP-1	Sucrose buffer	Cell counting	90+%	na	na	Contactless DEP	[139]
Blood fractionation or enrichment	Leukocytes	Leukocytes	Sucrose buffer	Flow cytometry	na	na	87–98%	FFF	[175]
	Leukocytes	Leukocytes	GIT medium	Cell counting	80%	na	na	FFF + immunocapture	[50]
	Leukocytes	Leukocytes	Sucrose buffer	Flow cytometry	55–75%	na	92–99%	FFF	[167]
	Malaria	Erythrocytes infected with *B. bovis*	PBS	Cell counting	na	7x	na	FFF	[11]
	Malaria	Erythrocytes infected with *P. falciparum*	Sucrose buffer	Cell counting	na	1000x	90%	twDEP	[45]
	Platelets	Concentrated platelets + whole blood	Sucrose buffer	Flow cytometry	na	5.3x	95%	Angled electrodes	[126]

CHAPTER 3

CAPTURE AND ELUSION OF CANCER CELLS FROM GEOMETRICALLY ENHANCED DIFFERENTIAL IMMUNOCAPTURE MICRODEVICES USING REVERSIBLE BIOTIN ANALOGUES[2]

3.1 Abstract

We present a framework for controllable non-mechanical, non-enzymatic whole-cell release from Geometrically Enhanced Differential Immunocapture (GEDI) devices. We previously reported high capture yield, high purity circulating tumor cell (CTC) isolation using targeted anti-sera chemistry [46, 77]. By altering the underlying linker chemistry, we retain high capture rates while also enabling substantial cancer cell elution. These data are one of the first demonstrations of linker chemistry substitution for immunocapture and release of cancer cells.

3.2 Introduction

Circulating tumor cells (CTCs) are cells that are shed from an originating tumor and undergo hematogenous dissemination. CTC extraction from peripheral blood samples enables study during all stages of cancer diagnosis and treatment. However, CTCs are an extremely rare cell population—as few as one per billion blood cells—and require specialized technology capable of high efficiency and high purity CTC isolation. Despite being largely uncharacter-

[2]Steven Santana measured reversible biotin linker performance in 2D Hele-Shaw flow cells. Erica Pratt performed all other experiments and data interpretation.

ized, CTC phenotype and behavior has been studied as potential biomarkers for disease progression. CTCs counts have been correlated with patient progression [3, 31], genome structural variation accurately predicts patient relapse [100, 180], changes in surface protein marker expression correlate with chemoresistant phenotypes [108], and functional assays have sown changes in CTC dimension, morphology, and cytoskeletal structure are related to disease state [77, 78, 178].

Microfluidic devices enable highly controlled CTC isolation through a combination of device geometry and fluid flow. Devices can be multiplexed for high-throughput cell capture[71], contain multi-stage systems to enrich CTCs from blood samples [37, 152, 111], and be combined with high-resolution imaging to characterize of CTC morphology [115, 46, 146, 147, 77]. Microfluidic isolation has been used for passive CTC collection via inertial focusing [121, 56, 143] and microfiltration [92, 153], as well as active capture using anti-sera (e.g. antibodies and aptamers) to target differentially expressed cell membrane surface proteins [115, 46, 64]. Immunocapture-based devices offer the advantage of processing whole blood samples [146, 147, 108], and can be combined with size-based methods to improve capture specificity [46, 77, 154]. However, most use biotin-avidin surface chemistry, one of the strongest non-covalent bonds in nature [113], which is irreversible under physiological conditions. As compared to passive CTC sorting and filtration, eluting intact and viable CTCs from immunocapture-based systems is challenging.

To date, most release methods are not generalizable across microfluidic systems. Multiple devices elute CTCs through manipulation of the underlying substrate, using thermally- or electrically-sensitive materials [49, 57, 66, 133]. CTCs

have also been removed using external shear force from fluid flow or microbubbles [21, 86], though prolonged mechanical stress has been shown to induce gene expression profiles [169, 119]. Chemical disassociation methods, such as trypsin, can be used with varying success in most microfluidic systems. However, recent proteomic analysis has demonstrated that trypsin can disregulate metabolism- and growth-related protein expression, even after extended (24 hr) recovery time [62]. Researchers have also shown that trypsin can have a deleterious effect on cell viability when eluting from microfluidic devices [57]. Other, enzyme-free, chemical methods are relatively ineffective for strongly adherent cells.

To take advantage of the system integration that lab-on-a-chip devices offer, a simple release method useable across microfluidic platforms platforms, without effecting cell integrity or viability, is needed. Reversible biotin analogues are straightforward and general release methods that require a simple linker substitution in standardized surface functionalization protocols. Two commercially available biotin analogues are compatible with physiological conditions, desthiobiotin and photocleavable-biotin. Desthiobiotin is a weak-affinity biotin analogue [113, 53] that has been used to competitively displace biotin-bound cancer cells in immunocapture-based devices [174]. Photocleavable-biotin uses near-UV irradiation to induce photolysis and subsequent linker cleaving from the substrate surface [120]. Similar photolabile-RGD systems released mammalian cells from planar glass surfaces [170], and photocleavable ssDNA-encoded antibody conjugates have been used to release CTCs for single-cell secretion profiling [34]. We present work characterizing these reversible biotin analogues as potential methods of CTC isolation and elution in geometrically enhanced differential immunocapture (GEDI) microdevices.

3.3 Materials & Methods

3.3.1 Device Fabrication

Silicon GEDI devices were fabricated using standard photolithography. Briefly, a contact-photoaligner as used to pattern photoresist-coated silicon wafers with the GEDI design. Wafers were then anisotropically etched to achieve a pillar height of 100 μm using deep silicon Bosch etcher (Unaxis SLR 770). Photoresist and organics were stripped using an oxygen plasma asher (Figure 3.1A).

Polystyrene devices were fabricated using a previously described PDMS hot embossing method. 10:1 PDMS (Dow Corning) was cast onto a fluorinated etched Si wafer and cured at 60 °C overnight. The PDMS negative mold was peeled away, and brought into conformal contact with NuncTM polystyrene microscope slides (Thermo Fisher Scientific). The two were sandwiched together using glass slides and held in place by binder clips. A thinner PDMS layer was placed between the binder clips and glass slides to more evenly distribute the stress. The mold + PS were placed in a 155 °C preheated oven for 14min, and devices were allowed to cool for 30 min before removing them from the PDMS mold (Figure 3.1B). Devices were flooded with a fluorescein solution and imaged on a confocal microscope. Z-stacks of pillar arrays were used to approximate post height at various points of the device, which averaged to 93 ± 9 μm (data not shown).

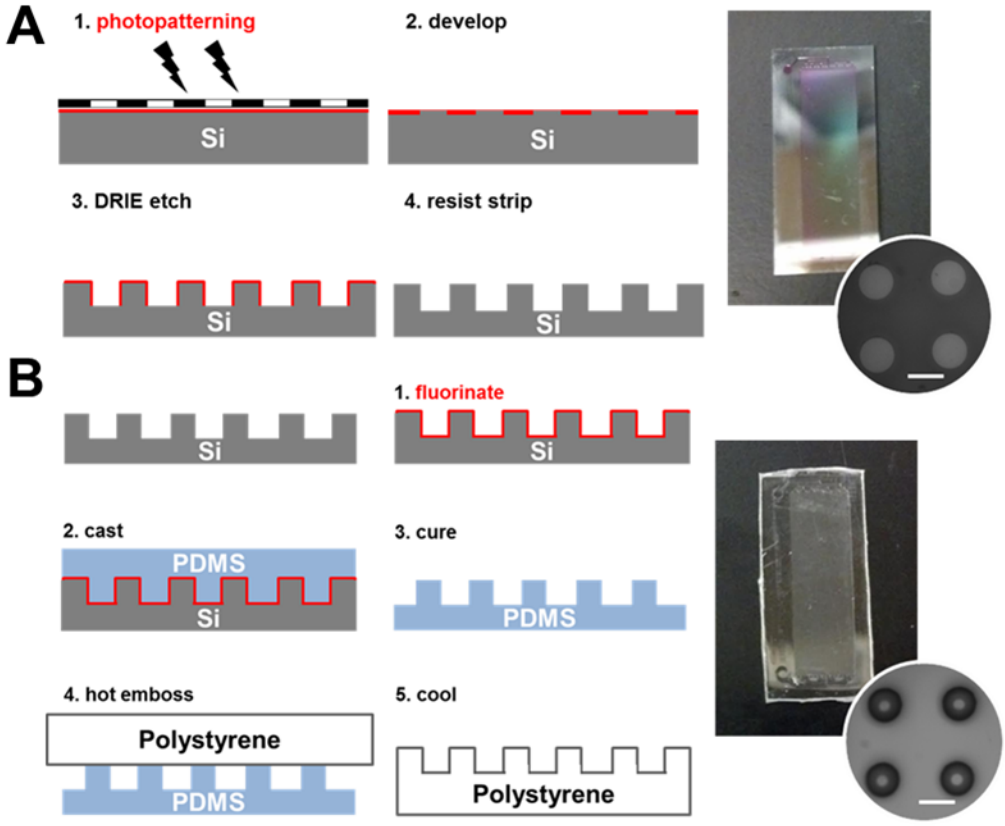

Figure 3.1: Diagram of GEDI device fabrication using silicon and polystyrene substrates. A) Si wafers were patterned using photolightography and underwent DRIE to form pillar arrays in the bed of the device. B) Etched Si wafers were fluorinated, and PDMS was cast to form a negative GEDI mold. The PDMS mold was used to hot emboss thermoplastic polystyrene at high temperatures (155 °C).

3.3.2 Surface Biofunctionalization

Standard Biotin-Avidin chemistry was used to immobilize J591 (courtesy Weill Cornell) on both silicon and polystyrene surfaces. Silicon surfaces were incubated with 4% v/v (3-mercaptopropyl)-trimethoxysilane in 200-proof EtOH(Sigma) for 45 minutes. Surfaces were cross-linked with 0.28% v/v GMBS

(N-[γ-maleimidobutyryloxy]succinimide) in 200-proof EtOH for 20 min, followed by a 45 min incubation with 0.5% v/v NeutrAvidin(Fisher Scientific) in PBS. Polystyrene surfaces were functionalized with both a similar protocol and simple NeutrAvidin physiabsorption. All evaluated chemistries were terminated with a 45 min incubation with PCBJ591 antibody in 1 % BSA PBS.

A subset of silicon surfaces underwent thermal oxidation to increase UVA light penetration, resulting in oxide layers ranging from 500nm to 1μm. A subset of polystyrene surfaces underwent surface hydroxlation via O_2 plasma treatment for 3 min (Table 3.1). Polystyrene capture performance was evaluated on planar surfaces before implementation in GEDI microdevices.

Anti-PSMA monoclonal antibody J591 was labeled using either photocleavable-biotin (NHS-PC-LC_{ws}-Biotin, Ambergen) or desthiobiotin (d-Desthiobiotin, Sigma). Desthiobiotin was resuspended in DMSO at 0.5 M. Photocleavable-biotin ampules were reconstituted in anyhydrous DMF at 50 nM concentration. 10- or 20-fold molar excess of biotin and J591 were mixed and incubated at RT for 30min. The solution was then injected into a hydrated dialysis cassette (Slide-A-Lyzer, Life Technologies) and dialyzed in PBS for 24 hrs, with PBS exchanges at 2 hrs and 4 hrs. The resulting suspensions (PCBJ591,DBJ591) were stored at 4 °C.

3.3.3 Cancer Cell Capture & Release

LNCaP cells were labeled in suspension or adherent with 2μm CalceinAM for 1 hr at 37 °C. Cells were spun down at 1000 rpm for 5 min, and resuspended in PBS. 2 μL of cell suspension was enumerated optically with aid of a hemocy-

Sample	Substrate	Surface Treatment
Si-Mercapto	Silicon	Native Oxide
Si-Oxide-Mercapto	Silicon	$500nm-1\mu m$ thermally grown oxide
PS-Mercapto	Polystyrene	None
PS-Plasma-Mercapto	Polystyrene	O_2 Plasma Treatment
PS-NA	Polystyrene	None
PS-Plasma-NA	Polystyrene	O_2 Plasma Treatment

Table 3.1: List of biofunctionalization chemistries and substrates used. Si=Silicon, PS=Polystyrene

tometer.

Planar surfaces. LNCaP cells were processed in functionalized Hele-Shaw flow cells as previously described[137]. Briefly, cell suspensions in PBS were processed at 0.2 mL/hr, then rinsed with a 1% (m/v) BSA in PBS for 15 min to remove non-adherent cells. Cell counts were taken at 14 unique shear stress values matching those found in GEDI μdevices. Devices were then either exposed to 100μg/mL exogenous biotin in DMSO for 20 min, or exposed to UVA (365nm) light for 15 to 35 min. Cell counts were taken again at the same shear values to calculate release efficiency, defined as Release efficiency was defined as $\frac{\#cells_{captured}-\#cells_{post-treatment}}{\#cells_{captured}}$. A LIVE/DEAD Viability/Cytotoxicity kit(Life Technologies) was used to quantify cell viability of eluted suspensions.

To measure capture on polystyrene surfaces, LNCaPs were incubated on various surface chemistries for 1 min (Table 3.1). The slides were then rinsed three times with PBS for 30s, and imaged at 10x magnification. Cell density per mm^2 was compared to functionalized glass controls.

GEDI μdevices. LNCaPs were diluted to a final density of 200-400 cells/mL in 1% (m/v) BSA + 1mM EDTA in PBS. Samples were processed at 1mL/hr, and then the chip was flushed again with PBS for 15 min. Cells were enumer-

ated manually under the microscope to calculate capture efficiency, defined as $\frac{\#cells_{captured}}{\#cells_{spiked}}$.

DBJ591-GEDI devices were flushed with 100μg/mL exogenous biotin (NHS-LC-LC-Biotin, Life Technologies) at 1mL/hr and allowed to incubate for 20min. Devices were rinsed again with biotin solution, and the effluent collected in 1.5mL Eppendorf tubes.

In PCBJ591-GEDI experiments, devices and tubing were primed with 5% BSA in PBS to minimize nonspecific cell adhesion during release. GEDI devices were placed in chilled water on ice blocks and received pulsed UVA (365nm) exposure. Chips were continually perfused with 5% BSA in PBS at 2 mL/hr while exposed to light to 1 minute, followed by 4 min of non-exposure for a total dosage of 200 kJ/m^2. Effluent was collected in a 1.5 mL Eppendorf tube, and aliquoted into 96-well plates. Cells were placed at 37 °C overnight to settle and adhere to the bottom of the well-plates, and were manually enumerated using a microscope (Nikon TE2000U). In both cases, release efficiency was calculated as defined in the 2D case.

3.4 Results & Discussion

3.4.1 Linker Performance on Planar Surfaces.

Prior to implementation in a complex 3D microdevice, we conducted 2D experiments to determine capture and release performance of desthiobiotin and photocleavable-biotin (Figure 3.2A). Desthiobiotin-conjugated surfaces released

94% of immobilized cells, with no measurable effect on cell viability. However, cell capture was approximately 25% that of biotin-J591 in shear ranges matching GEDI device flow conditions (Figure 3.2B). In contrast, PCBJ591 capture was indistinguishable from standard biotin across the entire shear range (Figure 3.2C). Approximately 55% of cells were released within 15 min of UVA exposure, with minimal change with increased duration(data not shown). These data suggest that Desthiobiotin-NeutrAvidin bonds are easily broken by fluid shear forces. This is consistent with AFM tapping-mode experiments showing desthiobiotin bond strength is almost half that of biotin, measured as 90 pN and 160 pN, respectively [113]. Therefore, for the rest of this study, we will focus on characterizing photocleavable-biotin performance.

We also determined if standard silanization chemistry protocols were effective for PCBJ591 immobilization on polystyrene surfaces. LNCaP cells were captured on planar PS-Mercapto (0.120 ± 0.068 cells/m^2, n=3) and PS-Plasma-Mercapto (0.084 ± 0.042 cells/m^2, n=3) surfaces at similar rates to standard biofunctionalized glass (0.112 ± 0.039 cells/m^2, n=3) (Figure 3.3A). Simple physabsorption of NA to the polystyrene surface was also effective, capturing 0.108 ± 0.002 cells/m^2 (n=3) and 0.062 ± 0.025 cells/m^2 (n=3) for PS-NA and PS-Plasma-NA, respectively (Figure 3.3B). However, this protocol was not effective on glass, capturing 0.046 ± 0.008 cells/m^2 (n=3). Nonspecific adhesion was minimal, the capture rate for NA-terminated polystyrene was 0.0047 ± 0.004 cells/m^2 (n=4) (Figure 3.3C). Plasma cleaned surfaces isolated 0.031 ± 0.011 cells/m^2 (polystyrene, n=4) and 0.067 ± 0.040 cells/m^2 (glass, n=5), showing capture was also antibody-specific (Figure 3.3D). These data show that mercapto silanes are an effective coupling agent for biofunctionalization of both silicon and polystyrene substrates. NeutrAvidin physabsorption is also an effective

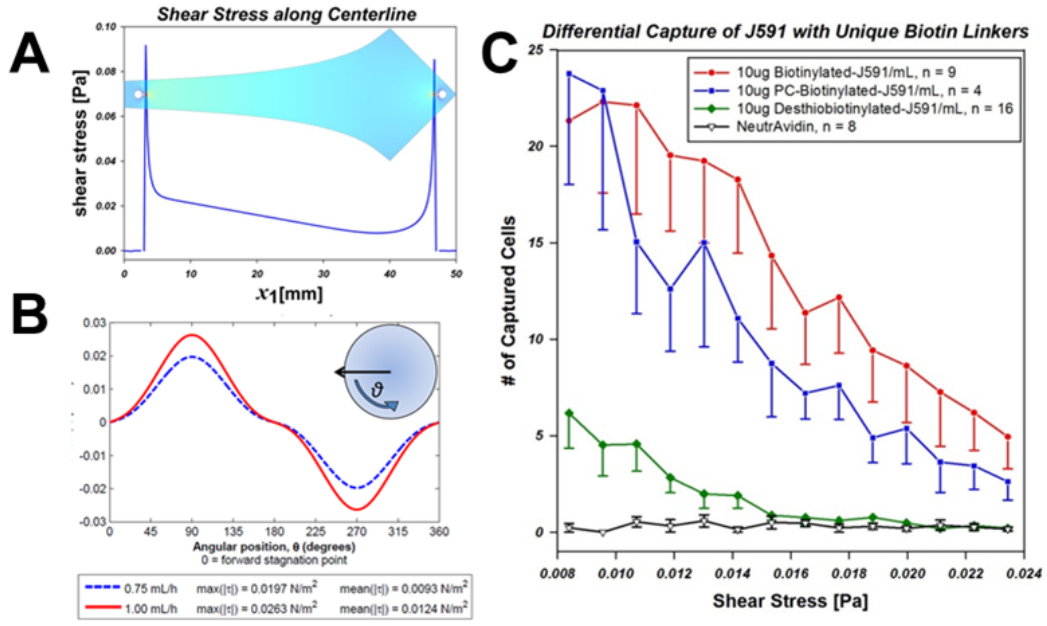

Figure 3.2: Characterization of biotin and biotin analogue capture performance in 2D microfluidic flow chambers. A) Schematic of Hele-Shaw flow cell showing that unique device geometry following iso-pressure lines results in a linearly decreasing shear stress along the centerline of the device. B) Calculation of shear stress around a post in a GEDI microarray at two operational flow rates: 1 mL/hr and 0.75 mL/hr. Hele-Shaw flow cells are designed to match this shear stress range. C) J591-conjugated biotin and biotin evaluation and mAb surface saturation (10 μg/mL). PCBJ591 performance is indistinguishable from BJ591; however DBJ591 captures cells at a rate only slightly above control (NeutrAvidin alone).

method of PCBJ591 immobilization on planar polystyrene surfaces.

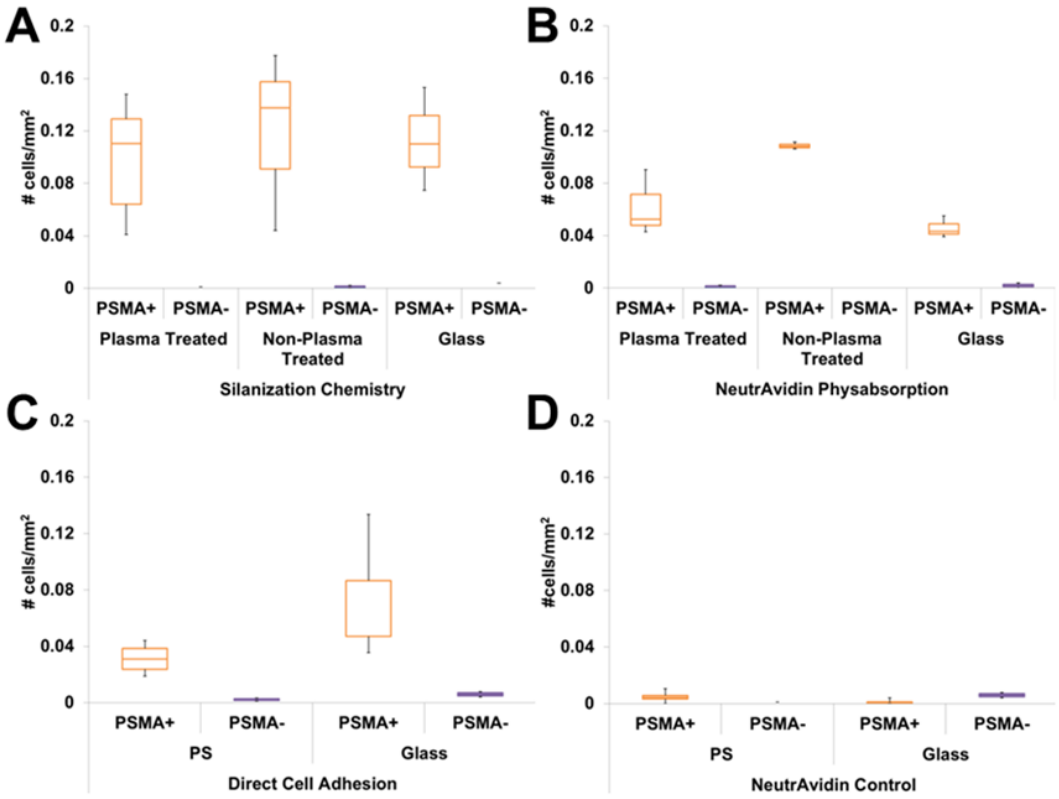

Figure 3.3: Assessment of PSMA+ LNCaP and PSMA- BXPC3 cell line capture on J591-immobilized polystyrene surfaces using various biofunctionalization protocols. PSMA+ cell lines are captured on PS surfaces at rates comparable to glass in using A) standard silanization chemistry and B) simple NeutrAvidin physabsorption. PSMA- cells are captured at negligible rates, indicating low non-specific adhesion. C) Cells are captured at lower rates on surfaces treated with O_2 plasma and D) very low rates on NeutrAvidin control surfaces.

3.4.2 Linker implementation in GEDI μdevices

PCBJ591 capture performance (66.2% ± 24.8%, n=28) was statistically indistinguishable from BJ591 in Si microdevices (63% ± 18.4%, n=14) (Figure 3.4A). We measured capture efficiency at full (10μg/mL) and half PCBJ591 surface satura-

tion (5μg/mL)[137] (Figure 3.5). Reducing antibody surface density resulted in a moderate drop in capture efficiency (61.01% ± 17.81%, n=5) as compared to the saturated case (71.55% ± 28.18%, n=38). We also measured the effect of biotin-avidin bond strength on cell capture via altering the PCBiotin:J591 molar ratio during biotinylation. There was no reduction in antibody functionality, isolating 65.4% ± 21.7% of LNCaP cells at 10:1 molar ratio (n=11) and 66.8% ± 27.2% at 20:1 (n=17)) (Figure 3.5A). These data show cell capture is robust to chemistry alterations that may be conducive to release, such as lowering the biotin-avidin bond strength or reducing the number of PCBJ591 links available for cell binding.

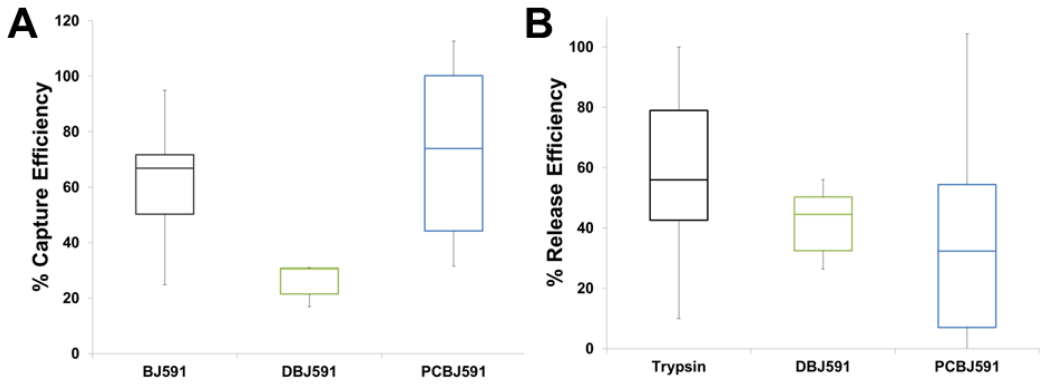

Figure 3.4: A) Capture efficiencies of PSMA+ prostate cancer cells in Biotin-J591, Desthiobiotin-J591, and Photocleavable-biotin-J591 functionalized GEDI microdevices. Recapitulating Hele-Shaw data, BJ591 and PCBJ591 performance is nearly indistinguishable, while DBJ591 exhibits a markedly lower rate of capture. B) Release efficiencies for DBJ591 and PCBJ591 compared to trypsin control in GEDI microdevices. Cells were exposed to trypsin for up to 30 min before being flushed with PBS buffer solution. DBJ591 enables high efficiency cell release, while PCBJ591 is much more variable.

However, despite exploration of a variety of parameters, there was no

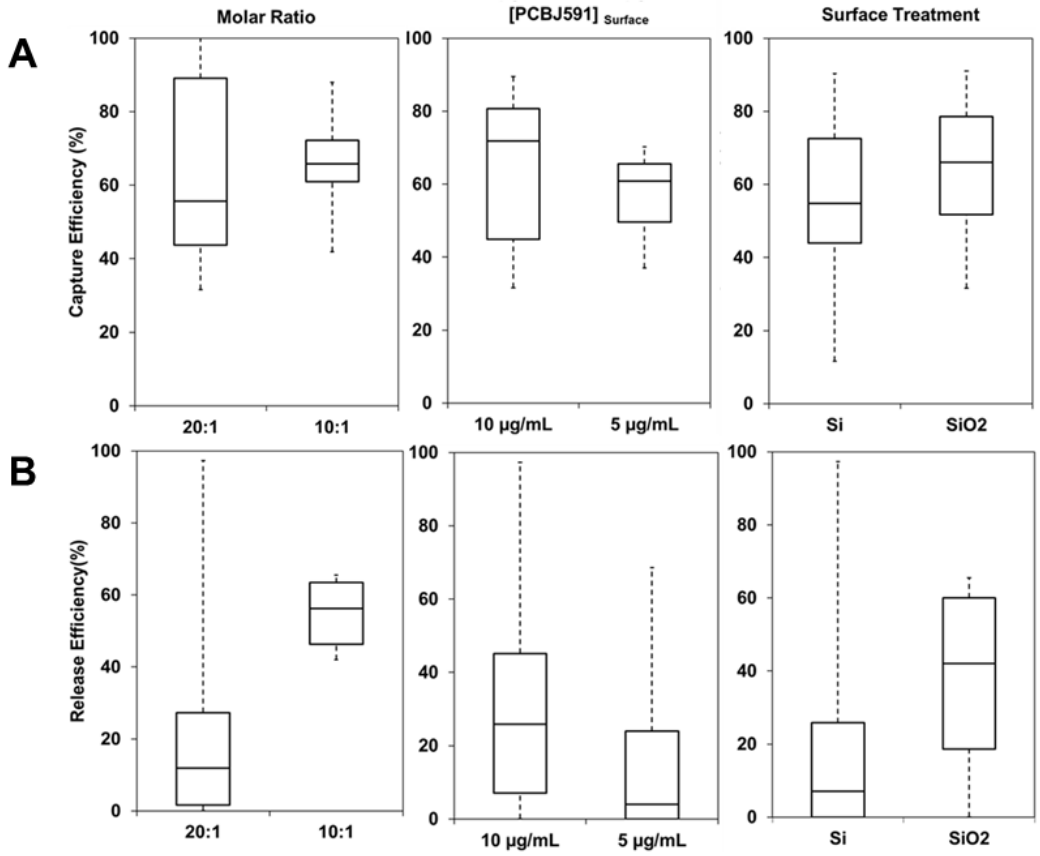

Figure 3.5: A) Capture and B) Release efficiency of prostate cancer cells as a function of: PCB:J591 biotinylation molar ratio, PCBJ591 surface density, and thermal oxidation of the Si surface. PCBJ591 capture remains relatively robust to all parameters. Lower molar ratios, and oxidized surfaces result in greater cell release.

guiding method or approach for reliable cell release (Figure 3.4B). Reduced molar ratio during antibody biotinylation did result in improved cell release (54.8% ± 10.3%, n=6), but had high variability based on antibody lot. Contrary to expectation, cell release decreased when $[PCBJ591]_{surface}$ was reduced to half-saturation (Figure 3.5B). Oxidized Si microdevices appeared to better facilitate UVA penetration, eluting 37.03% ± 23.25% (n=13) of cells as compared to 18.85% ± 25.24% (n=32) for native Si surfaces. These data suggest there are

unaccounted parameters efficient cell release that have yet to be fully explored. These data are summarized in Table 3.2.

3.4.3 Summary

This body of work is an important study of the operational parameters of reversible biotin linkers in microfluidic microdevices. Critical next steps involve further exploration of the photolysis chemistry of photocleavable-biotin, and use of desthiobiotin/photocleavable-biotin cocktails to strike the balance between efficient cell capture and release. Development of a straightforward replacement to standard biotin-avidin chemistry would enable easy combination of lab-on-a-chip devices for multi-stage enrichment and analysis.

Viable whole cell release enables researchers to use assays to characterizing CTC morphology and biomechanics that cannot be supported *in-situ*, or are senstive to chemical or mechanical perturbations. Biomechanical indicators of malignancy, such as increased traction force [81], could be validated in a physiologically-relevant cell population and further explored as potential biomarkers. UV-induced cell release also has potential as a targeted release method to remove small clusters, or individual, CTCs from microdevices using a focused laser. Combined, these features make reversible biotin linkers an attractive release method to facilitate various single-cell CTC analyses.

Fabricating GEDI devices from optically transmissive substrates could enable more efficient cell elution using UVA light, as well as easier high-resolution imaging. In an opaque system, UVA light must be scattered around pillars, or penetrate the cell directly, to effectively photolysis the linker chemistry and in-

		Capture Efficiency	Release Efficiency
Molar ratio	20:1	66.8% ± 27.2%	22.3% ± 26.6%
	10:1	65.4% ± 21.7%	54.8% ± 10.3%
Surface density	10μg/mL	71.55% ± 28.18%	27.62% ± 25.18%
	5μg/mL	60.01% ± 17.81%	19.31 ± 29.23%
Release buffer	PBS	-	33.3% ± 21.2%
	5% BSA	-	18.9 ± 26%

Table 3.2: LNCaP cell capture and release efficiencies in GEDI microdevices as a function of various surface chemistry parameters.

duce mAb cleavage. Transparent systems would minimize this issue, and possibly lower the total dosage required for substantive cell release. This would make photocleavable-biotin an easily generalizable release method that could used across many different microfluidic rare cell processing systems.

Acknowledgement

This work was supported in part by the Cornell Center on the Microenvironment and Metastasis Young Investigator's Award. I would like to thank Steven Santana for his work generating the Hele-Shaw data shown here.

CHAPTER 4

SINGLE-CELL COPY NUMBER ANALYSIS OF PROSTATE CANCER CELLS CAPTURED WITH GEDI MICRODEVICES[3]

4.1 Abstract

Limited access to tumor tissue makes repeated sampling and real-time tracking of cancer progression infeasible. Circulating tumor cells (CTCs) provide the capacity for real-time genetic characterization of a disseminating tumor cell population via simple blood draw. However, there is no straightforward method to analyze broadscale genetic rearrangements in this heterogeneous cell population at the single cell level. We present a work for one-step controllable chemical extraction of whole nuclei from prostate cancer cells captured using geometrically enhanced differential immunocapture (GEDI) microdevices. We have successfully used copy number profile analysis to differentiate between two unique cancer cell line populations of metastatic origin (LNCaP and VCaP), and to analyze key mutations important in disease progression.

[3]Erica D. Pratt, Asya Stepansky, James Hicks, Brian J. Kirby. "Single-Cell Copy Number Analysis of Prostate Cancer Cells Captured with Geometrically Enhanced Differential Immunocapture Microdevices," *Analytical Chemistry*, 86(22):11013-11017[128].

EDP processed all samples. AS performed WGA and generated copy number variation data. JH & AS generated dendrogram using neighbors-joining tree algorithm. EDP processed copy number data to create profiles for each cell type. EDP wrote the manuscript. JH and BJ provided technical expertise and guidance on structure and formatting.

4.2 Introduction

Copy-number variation (CNV) is a major component of genetic heterogeneity, and has been measured in bulk tumor tissues to quantify large-scale genetic rearrangements on chromosomes [116]. Genetic variation has recently become a focus in prostate cancer, where the five-year survival rate drops precipitously upon dissemination, decreasing from near 100% survival for localized stages of the disease to 28.7% for metastatic cases [141]. Navin et al. used single-nucleus sequencing (SNS) of cells isolated from primary tumors and metastases to measure CNV in breast cancer patients [116], identifying four heterogeneous subpopulations within a single tumor [116]. The genetic profiles of these subpopulations were then compared to liver metastases to infer the clonal evolution of individual cases of breast cancer. However, these studies relied upon resected or biopsied tumor tissue, which is frequently unavailable, or unrepresentative of the current disease state.

Magbanua et al. measured CNV in pooled breast cancer CTC samples, providing the opportunity for real-time analysis of a disseminating tumor cell population. Averaged CTC copy-number profiles evolved as a function of time and patient treatment [100]. Yu et al. found that averaged CTC copy-number profile predicted prostate cancer biochemical relapse (defined by rate of PSA rise) with 81% accuracy, which was comparable to relapse predictions made using solid tumor tissue [180]. Additionally, Powell et al. performed single-cell transcriptional profiling for a panel of cancer-related genes, and reported that distinct genetic subpopulations exist within the same patient CTC sample [127], reflecting the heterogeneity often found in solid tumors. Ozkumur et al. used single-cell RNA analysis to look at a panel of transcripts implicated in cancer

progression [121], and also reported unique CTC subpopulations within a single sample. These studies demonstrated CTC utility for CNV and other genetic assays in patient populations, but also required multistep blood processing to circumvent low-purity CTC isolation.

This has motivated the design of multiple cancer cell isolation microdevices used to measure average CTC expression of cancer-specific biomarkers. There are several microdevices for bulk and single-cell cellomics, ranging from microfluidic flow cytometry to digital PCR lab-on-a-chip devices [4, 155] However, few investigate broadscale genetic rearrangements on single cells. Genetic characterization of CTCs has been limited by *in vivo* concentrations that can be as low as 1 CTC per 10^9 blood cells [129]. Proof-of-principle microdevices have shown on-chip cell lysis as confirmed by PCR detection of genetic material[183, 145]. Other microdevices have been used for on-chip detection of cancer biomarkers *HER2* [104, 131] and *TMPRSS2:ERG* gene fusion [146, 147] in CTCs by FISH. A broad range of cancer-specific mutations such as *Wnt2*, *EGFR*, *KRAS*, and others have been detected in both cancer cell lines [131, 145, 37, 10] and CTCs [101, 179] via downstream PCR. However, these studies used pooled cancer cell samples, preventing characterization of heterogeneous subpopulations.

Although researchers have measured CNV in resected tumor tissue and pooled CTC samples, no reported microfluidic technology has demonstrated reproducible CNV analysis at the single-cell level. To address the need for pure and efficient rare cell capture for downstream genome analyses, we have combined geometrically enhanced differential immunocapture (GEDI) with SNS (GEDI-SNS) to generate CNV profiles for individual cancer nuclei. Prior studies

have reported GEDI microdevices isolate prostate CTCs with 60% purity [46]. GEDI-isolated CTCs have been analyzed on-chip for chemosensitivity and gene fusions [76]. We now describe a microdevice and one-step protocol for controllable chemical extraction of intact nuclei from prostate cancer cells following microfluidic capture. We present experiments to show that GEDI microdevices can be used as a platform for rapid and straightforward individual cancer cell CNV analysis, with comparable resolution to standard techniques.

4.3 Materials and Methods

4.3.1 Device fabrication and functionalization

GEDI microdevices were fabricated and functionalized with antibody as previously described [46]. Briefly, devices were fabricated using standard photolithography followed by DRIE etching. Microdevices were then functionalized using standard (3-Mercaptopropyl)-trimethoxysilane (MPTMS)- N-[γ-maleimidobutyryloxy]succinimide (GMBS)-NeutrAvidin-Biotin linker chemistry terminating with high-avidity, prostate-specific, antibody J591.

4.3.2 Cell line preparation

LNCaP human prostate adenocarcinoma cell lines were used as model CTCs for cell capture and CNV analysis. Cells were maintained in standard cell culture conditions (37 °C, 5% CO_2) with complete media. For sample preparation, LNCaPs were fluorescently labeled using 2 μM Calcein AM in PBS, and resus-

pended at approximately 200 cells/mL in PBS. VCaP prostate cancer epithelial cell lines were used as controls for CNV analysis and hierarchical clustering, and were maintained under the conditions listed above. Prior to FACS separation, VCaP nuclei were fluorescently labeled by incubating cells with NST-DAPI buffer for 15 minutes on ice.

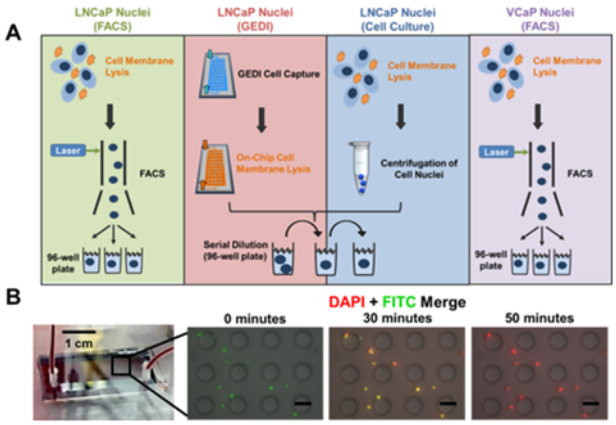

Figure 4.1: A)LNCaP nuclei were sorted via three methods 1) FACS only. 2) capture in GEDI microdevices, followed by serial dilution. 3) serial dilution only. VCaP controls underwent FACS. B) On-chip lysis of LNCaP cells in a GEDI microdevice via NST-DAPI buffer. Digestion of labeled cell membrane (green), and simultaneous nucleus labeling (red) is easily observed. Scale bars are 100 μm.

4.3.3 Isolation and nuclei extraction for single-cell SNS

1mL of LNCaP cell suspension was processed in GEDI devices at a volumetric flow rate of 1mL/hr. Immobilized LNCaPs were enumerated, and then the chip was perfused and incubated with a octylphenoxypolyethoxyethanol- 4',6-diamidino-2-phenylindole buffer solution (NST-DAPI buffer) for time periods ranging from 45 minutes to 24 hours to digest the cell membrane. Cell nu-

clei were eluted from the devices using low-shear fluid flow (<0.3 N/m^2) and stored at -80 °C (Figure 4.1). Control LNCaP cells were spiked in NST-DAPI buffer at comparable cell densities, and also stored at -80 °C.FACS-sorted nuclei were gated based on DNA content referenced to standardized diploid reference samples, and were deposited individually into a 96-well plate prepared with 10 μL of lysis solution per well (Figure 4.1). To measure copy-number, we used the SNS next-generation sequencing technique reported by Navin et al [117, 116]. Whole-genome amplification was used to amplify single-nucleus (or two-nuclei) genetic material to microgram levels. WGA-amplified libraries were randomly sequenced at 36 cycles with Illumina GA2 analyzers, sequencing reads were aligned, and copy-number was measured by read depth within fixed, 50-kb intervals in the genome [2, 22]. The read depths were normalized by a deep-sequenced reference sample.

4.4 Results and discussion

4.4.1 Repeatability and robustness of GEDI-SNS

To determine whether SNS of GEDI-isolated nuclei had sufficient resolution to discriminate between different cancer cell types, we compared CNV profiles of LNCaP and VCaP cell lines. Both lines are of PCa origin; however, LNCaPs were derived from a lymphatic metastasis [55], whereas VCaPs were derived from a vertebral metastasis [80]. GEDI-isolated LNCaP CNV profiles were compared to profiles from VCaP nuclei, which were sorted via FACS (Figure 4.1). Hypertetraploid LNCaP nuclei (base 4 chromosome copies) were easily distin-

guished from near-triploid VCaP nuclei (base 3 chromosome copies) [96] by simply comparing individual cell's CNV profiles (Figure 4.2A). Beyond DNA ploidy, cancer-specific mutations could be identified by comparing CNV profiles (Figure 4.22A). For example, the LNCaP genome contains a deletion of DNA repair gene *MSH2* [96], and a deletion of one allele of tumor suppressor gene *PTEN* [105] (Figure 4.2B). In contrast, the VCaP genome has neither mutation, but contains a deletion of candidate tumor suppressor *BNIP3L* [96], and overamplification of *E2F3*, which mediates DNA damage-induced apoptosis. VCaP also has overamplification of the androgen receptor (*AR*) relative to LNCaP cells (Figure 4.2B).

To assess the robustness of on-chip nuclei extraction and SNS, we compared CNV profiles from GEDI-isolated LNCaP nuclei to LNCaP nuclei sorted via FACS [116] and serial dilution, and VCaP sorted via FACS (Figure 4.3). CNVs from GEDI nuclei were highly repeatable, as single cell profiles from GEDI microdevices were in excellent agreement with one another (r^2 = 0.938) (Figure 4.3A). CNV profiles from microdevice-isolated nuclei were similar to nuclei sorted via FACS, an established method for sorting circulating tumor cell samples (r^2= 0.723) (Figure 4.3A). Additionally, profiles from GEDI nuclei also agreed with those using LNCaPs serially-diluted directly from culture (r^2= 0.607, supplementary information). In contrast, the correlation between LNCaP and VCaP CNV profiles was low (r^2 = 0.118).These data indicate that SNS is sensitive enough to detect the effects of active cell sorting and processing, although these are minimal relative to inter-cell line variation. Together, these data show that GEDI-SNS can be performed with excellent resolution, and with fewer steps and expense than conventional methods.

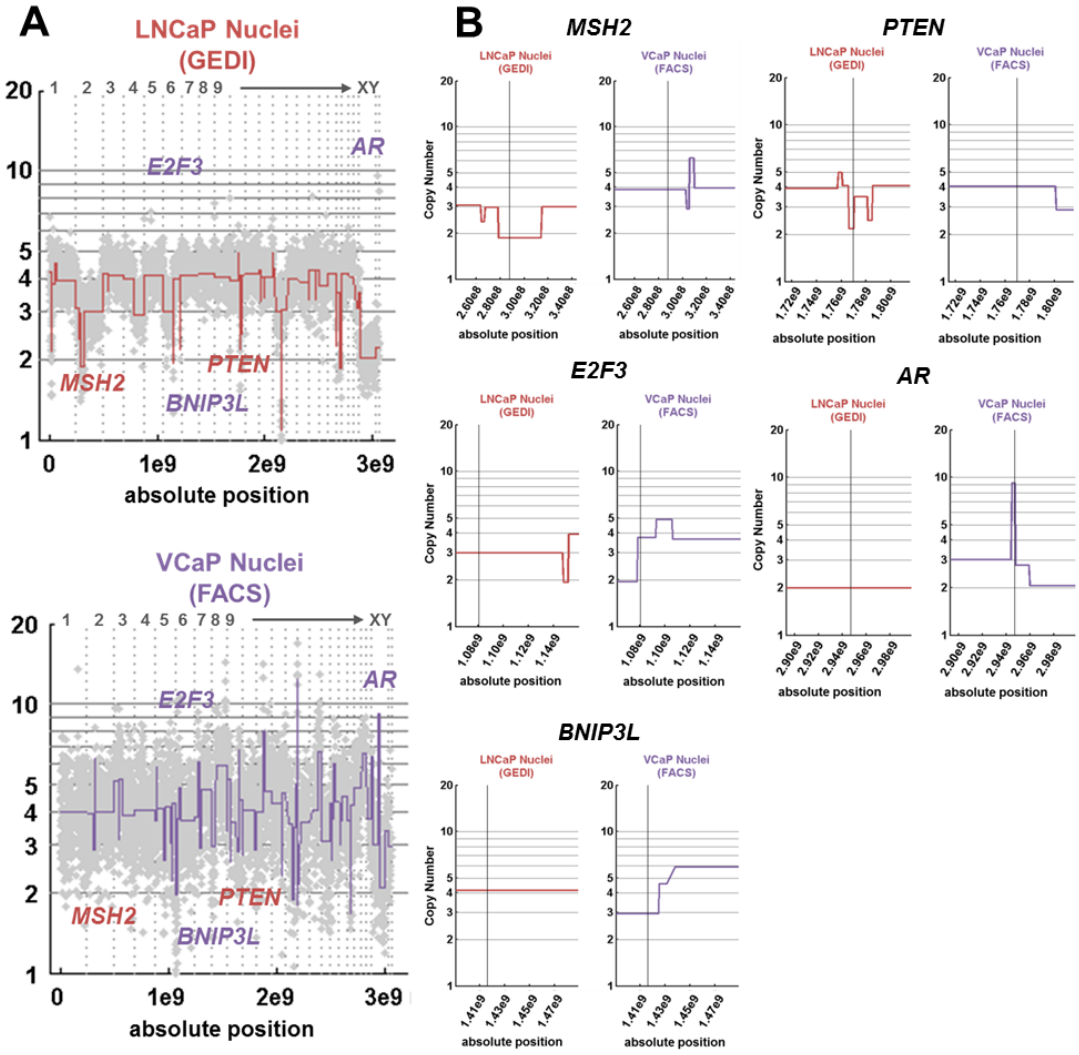

Figure 4.2: A) Copy-number profiles of individual LNCaP and VCaP nuclei after undergoing amplification followed by single-nucleus sequencing. B) By comparing copy-number profiles of the two different prostate cancer cell lines, one can contrast unique genetic amplifications and deletions across their respective genomes. CNVs of interest are marked by solid gray line.

4.4.2 CNV-based differentiation of prostate cells

We then pooled all CNV profiles and used a neighbors-joining tree to blindly cluster nuclei based on their genetic similarity (Figure 4.3B). The resulting phy-

logenetic tree shows that SNS easily distinguishes between metastatically derived prostate cancer cell populations, placing all 6 LNCaP profiles on a separate branch from the 2 VCaP profiles. LNCaPs CNV profiles were appropriately clustered together, and the sequencing resolution was high enough to further differentiate nuclei based on processing method (FACS vs serial dilution vs GEDI-isolation followed by serial dilution).

GEDI-SNS profiles were assigned to the same branch, whether it was from a single nuclei, or a profile averaged over two nuclei, further demonstrating the repeatability and robustness of the extraction and sequencing.

4.5 Summary

In summary, this work describes the use of a microdevice for cancer cell capture, followed by one-step chemical extraction of cancer nuclei and high-resolution CNV profile analysis of single-cell genomes. This work also demonstrates the depth of information achievable with GEDI-SNS analysis, which enables cell classification and identification of cancer-specific genomic alterations. For real-time patient monitoring of CTCs, GEDI-SNS can be combined with established methods for distinguishing circulating tumor DNA from benign: using matched leukocyte samples [140], deep sequencing that targets cancer-specific somatic mutations [118], measuring concordance of SNP genotype [140], among others.

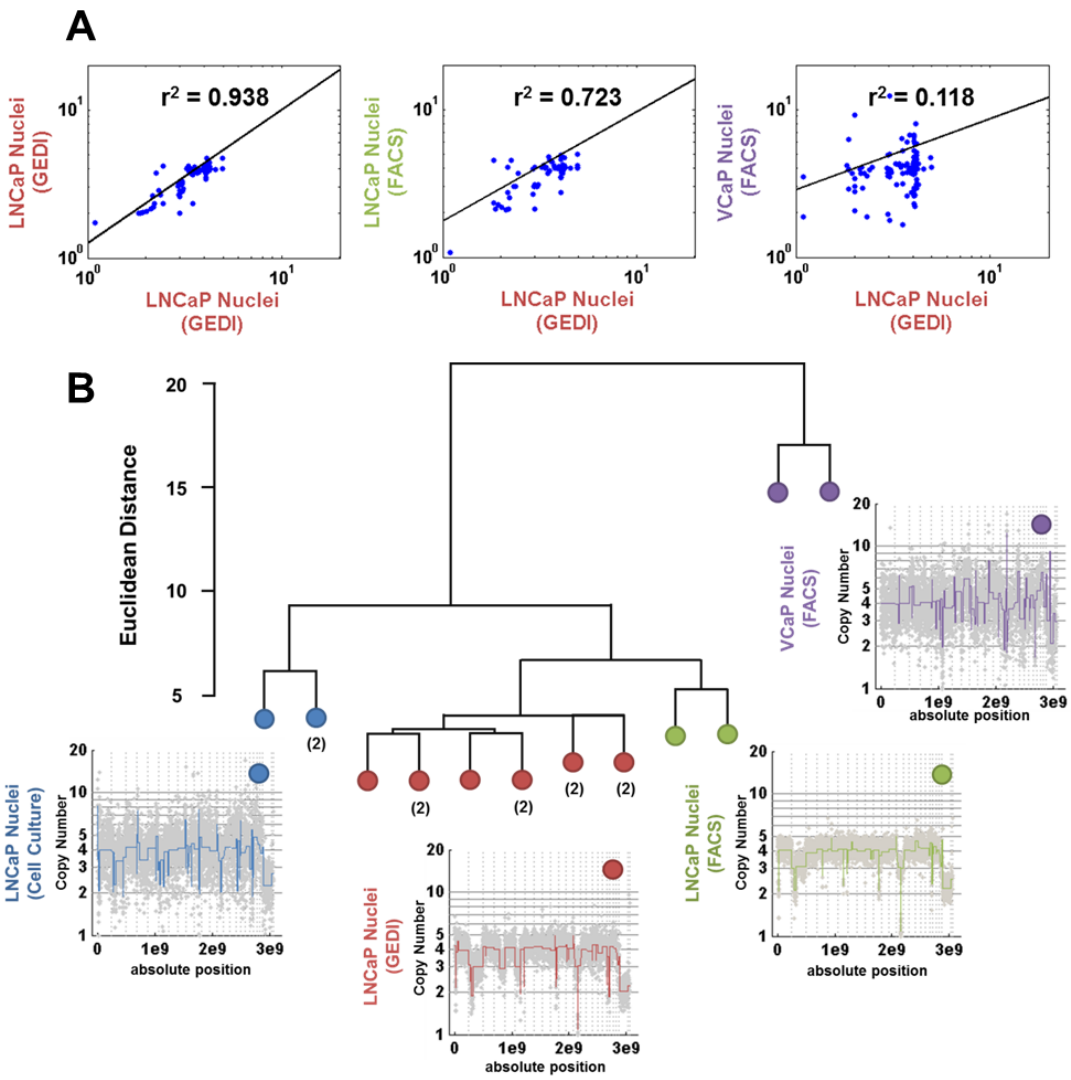

Figure 4.3: A) Simple linear regression was used to determine r^2 values for copy-number profile comparisons. B) Dendrogram showing level of genetic relationship between cell populations. (2) indicates profiles averaged over two nuclei, all others are from single cells.

4.6 Acknowledgment

This work was performed in part at the Cornell NanoScale Facility, a member of the National Nanotechnology Infrastructure Network, which is supported

by the National Science Foundation (Grant ECCS-0335765). Funding for these studies was provided by grant U54 CA143876 from the Cornell Center for the Microenvironment and Metastasis.

4.7 Supplementary Information

4.7.1 Single Nucleus Sequencing (SNS) experimental details

Samples were sorted using the BD Biosystems Aria II flow cytometer, and deposited into a 96-well plate containing 10 μL of lysis solution from the Sigma-Aldrich GenomePlex©WGA 4 kit. Single-read libraries were sequenced using the Illumina GA2 analyzer, and data was processed Illumina GA Pipeline bioinformatics software. Bowtie alignment software was used to align sequence reads to the human genome. S-Plus (Mathsoft, Inc.) software was used to calculate integer differences in copy-number using Gaussian kernel smoothed density plots. Generated copy-number profiles were then used to generate the neighbor-joining tree based on Euclidean distance metrics using Matlab (Mathworks).

4.7.2 LNCaP preparation via serial dilution

Frozen cell suspensions where thawed and seeded at either 0.5 nuclei per well (limiting dilution) or 1 nuclei per well (2x limiting dilution) in 96-well plates. Plated nuclei then underwent SNS as previously described. Poissons distribution dictates, at limiting dilution, that the probability of there being no cells

per well is 60%, the probability of a well containing a single cell is 30%, and the probability of two or more cells is 10%. These probabilities can be used to predict the number of wells that should successfully amplify for SNS (Table 4.1). 50.2%0.2% of predicted wells amplified using GEDI-isolated LNCaP nuclei, 44.2%0.4% amplified using nuclei from cell culture. 100% of amplified wells generated copy-number profiles. Amplification efficiencies are on the order of, but lower than, conventional FACS (90%). Conversion to copy-number profiles is equivalent.

	Limiting dilution	Expected # amplified cells	$2x$ Limiting dilution	Expected # amplified cells
$LNCaP_{GEDI}$	2/12	$4.52 \pm 1.80/12$	4/12	$7.42 \pm 1.86/12$
$LNCaP_{CellCulture}$	2/12	$6.05 \pm 2.32/12$	n/a	n/a

Table 4.1: Number of successfully amplified cell nuclei as compared to predicated values using Poissons distribution.

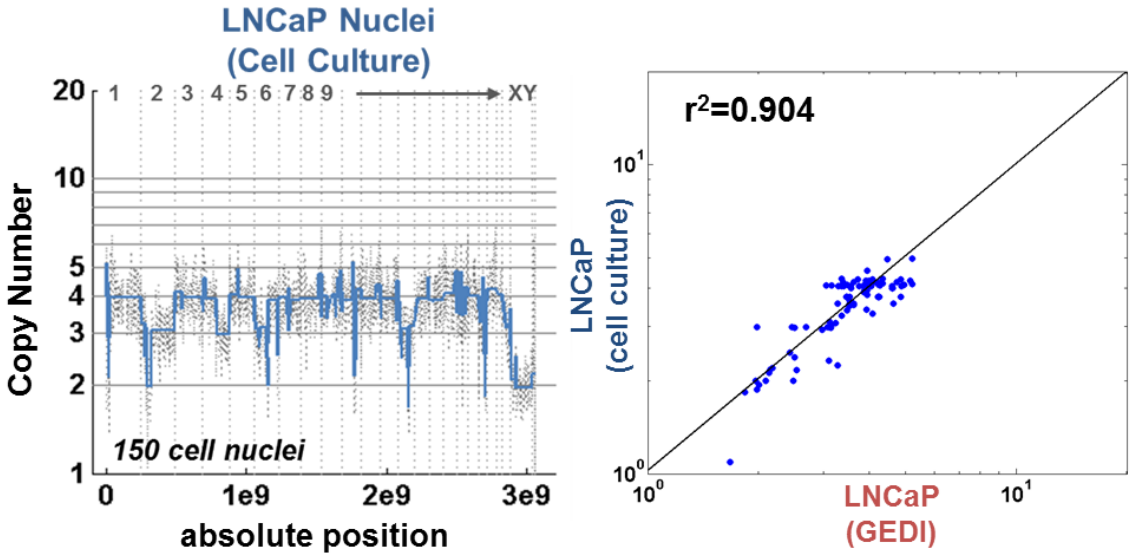

Figure 4.4: Simple linear regression for a bulk LNCaP sample from cell culture (150 cells). The averaged genetic profile agrees very well with copy-number profile generated form a single nuclei from a GEDI microdevice (r^2 = 0.904).

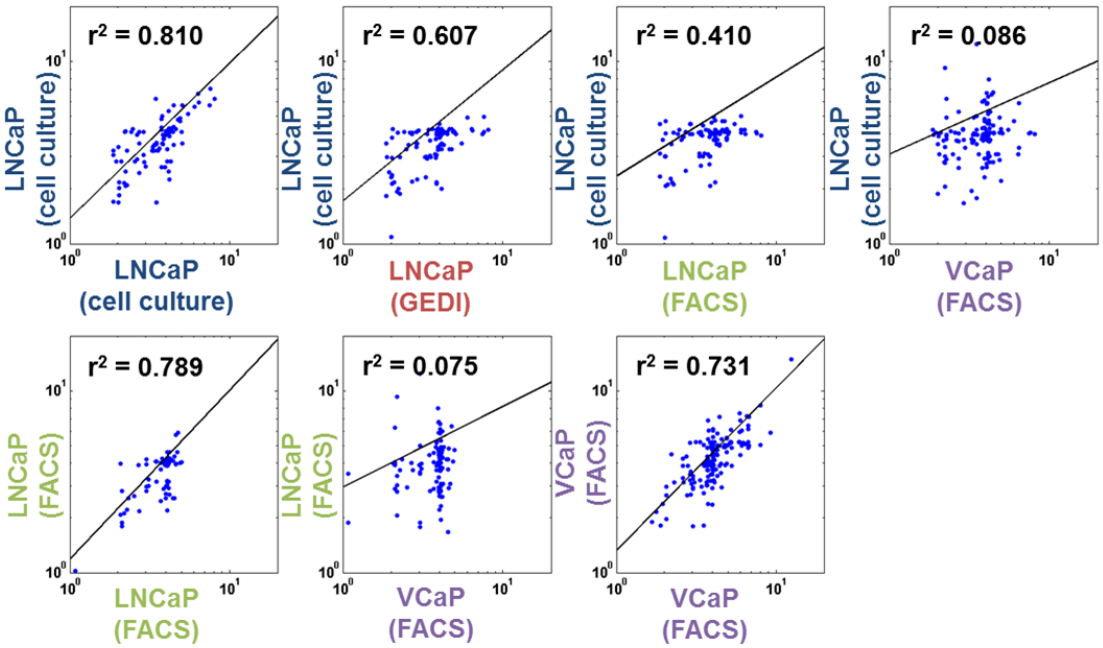

Figure 4.5: Pairwise comparisons of various SNS samples.

CHAPTER 5

IN-SITU MEASUREMENT OF CA^{2+}-FLUX TO ASSESS TAXANE TREATMENT EFFICACY

5.1 Abstract

Prostate cancer (PCa) is the second leading cause of cancer death for men in the US. Five-year survival rates for the disease drop precipitously upon onset of metastasis, decreasing from 100% survival for localized stages of the disease, to 28.7% for metastatic cases. Standard of care for advanced metastatic patients is taxane chemotherapy. However, nearly all PCa patients develop taxane resistance, though the mechanism is not well understood. Recent research has shown that taxane-resistant cancer cell lines have disregulated intracellular calcium homeostasis, which confers increased apoptotic resistance and development of an androgen-independent-like state. We present the development of an assay for *in-situ* imaging and measurement of differential calcium homeostasis in circulating tumor cells (CTCs) using geometrically enhanced differential immunocapture (GEDI) microdevices. This would be one of the few functional assessments of disseminating tumor cells informed by known mechanisms of cellular response to chemotherapy, and could allow real-time tracking of drug resistant CTC populations.

5.2 Introduction

Circulating tumor cells (CTCs) are increasingly studied as prognostic indicators of cancer progression. CTC counts have been correlated with tumor load, as well as metastatic site and location [3, 31]. Genetic analyses have shown there is wide intra- and inter-patient CTC genetic heterogeneity, reflecting the diversity often found in primary tumors [116, 127, 100]. These techniques have also been used to evaluate CTC genetic evolution from primary tumors and metastases [117, 116, 97], and in response to chemotherapeutic insult [100]. Using these methods, CTC phenotype can be characterized within the context of the metastatic niche from which it originated.

While assays have been developed to perform genetic and immunohistochemical analysis of CTCs based on their *in-vitro* morphological properties [78, 178], there are few tests measuring cell response via a known biological mechanism related to treatment efficacy. Recent work using GEDI microdevices performed *in-situ* imaging to measure taxane drug-target engagement in castrate-resistant prostate cancer patients CTCs [76]. The canonical mechanism of action is mitotic-arrest, but Darshan et al. have shown taxanes also prevent androgen-androgen receptor (A-AR) trafficking to the nucleus via microtubule arrest [32]. However, most prostate cancer patients develop taxane resistance and relapse[8], indicating that there are other cellular mechanisms for androgen sensitivity [99, 149].

Differential regulation of calcium homeostasis is an important route by which cancer cells acquire increasingly aggressive and chemotherapy-resistant phenotypes [47, 160, 12, 122, 48]. When non-excitable cells are stimulated, there

is typically a biphasic response: 1) an increase in cytosolic Ca^{2+} ($[Ca^{2+}]_c$) from intracellular stores, especially the endoplasmic reticulum (ER), and 2) when the intracellular stores drop to a threshold $[Ca^{2+}]$, dedicated ion channels in the plasma membrane allow Ca^{2+} from the extracellular space to enter the cytoplasm, where it is pumped back into the intracellular stores [9]. The second stage is called store-operated calcium entry (SOCE), and both processes are disregulated in malignant cells. Preventing ER store re-filling by using sarco/endoplasmic reticulum Ca^{2+}-ATPase (SERCA) pump inhibitor thapsigargin (TG) results in protein kinase C- and calmodulin-independent decrease of androgen receptor mRNA and protein synthesis in prostate cancer cell lines [47, 48]. TG exposure also sensitizes androgen-dependent cancer cells to taxanes, increasing cell death by 10- to 20-fold [171]. Prostate cancer cells modified to transition from an androgen-dependent to neuroendocrine phenotype were found to have reduced SERCA pump expression, and lowered ER store $[Ca^{2+}]$/SOCE, leading to increased apoptotic resistance [160, 12]. This response has also been recapitulated in taxane-resistant lung cancer cells, though basal $[Ca^{2+}]_c$ were the same [122]. Research in non-malignant cell types suggests SOCE suppression is also correlated with effective taxane stabilization [136]. There is compelling evidence that cancer cell manipulation of native Ca^{2+} receptors and stores is a critical component of acquired taxane resistance.

Using GEDI microdevices to capture CTCs for live-cell imaging would enable characterization of Ca^{2+} fluxes at the single-cell level. Genetic and morphological analyses have shown that CTCs have many subpopulations, which evolve as a function of time and patient treatment. Measuring the spatiotemporal Ca^{2+} dynamics of prostate CTCs could reveal the emergence of taxane-resistant phenotypes prior to clinical relapse. Cell response could also guide the

use of new, tumor-specific, Ca^{2+}-targeting therapies, such as PSMA-activated thapsigargin [35]. Combined with other functional analyses, such as imaging of CTC microtubule stablization post *ex-vivo* taxane exposure [76], CTCs could be screened for a variety of phenotypical changes associated with oncoming drug resistance. We describe the development of a Ca^{2+}-flux measurement assay that can be implemented in GEDI microdevices for real-time screening of patient samples.

5.3 Materials & Methods

5.3.1 Cell Culture

LNCaP (androgen-sensitive) human prostate adenocarcinoma cell-lines were purchased from American Type Culture Collection (ATCC) [Manassas, VA] and cultured in standard cell culture conditions (37 °C, 5% CO2) in cell culture flasks. Complete culture medium consisted of RPMI-1640 [Lonza, Walkersville, MD] supplemented with 10% fetal bovine serum [Gemini Bio-Products, W. Sacramento, CA] and 1% penicillin/streptomycin [Mediatech Inc.,Herndon, VA]. Upon reaching confluence, cells were passaged with trypsin at a subcultivation ratio of 1:5.

5.3.2 Cell Preparation and Labeling

Cells were seeded at a 1:5 ratio on 0.5% v/v gelatin-coated #1 borosilicate glass coverslides (22mm x 40mm) in complete media and imaged within 24-48 hrs.

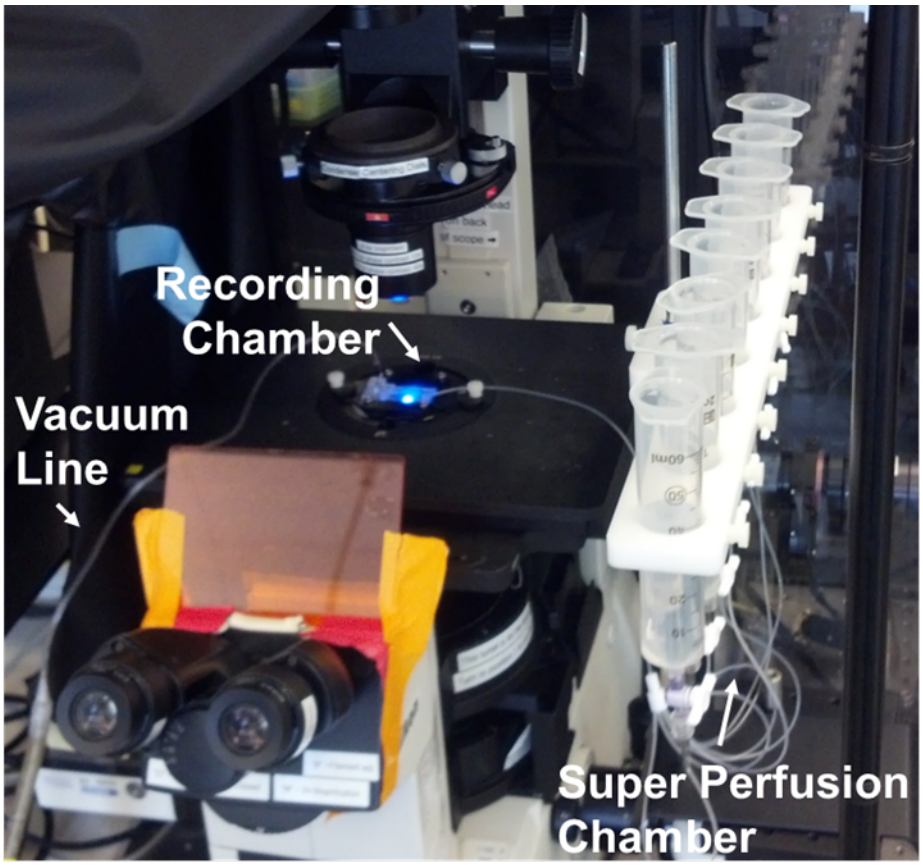

Figure 5.1: Imaging setup for continuous superperfusion of LNCaP cells with Ca^{2+} agonists.

Cells were rinsed with HBSS (5.33 mM KCl, 0.44 mM KH_2PO_4, 137.9 mM NaCl, 3.36 mM Na_2HPO_4-$7H_2O$, 5.5 mM d-glucose, 2.1 mM Ca^2, 2.1 mM $MgCL_2$, pH 7.43) and incubated with 10 μM Fluo-4AM for 30 min at 37 °C. Post-incubation, slides were rinsed with Ca^{2+}-free HBSS and left to de-esterify for 30 min at RT.

5.3.3 Intracellular Ca^{2+} Imaging

Coverslides were mounted in an open-bath perfusion chamber (RC-26GLP Recording Chamber, Harvard Apparatus) and immersed in Ca^{2+}-free HBSS. Cy-

tosolic Ca^{2+} levels were quantified using NIS-Elements imaging software and a CCD camera (Micropublisher 3.3) (Figure 5.1). Cells were exposed to mercury arc light every 5 s and fluorescent emissions were recorded for 100-200 ms per exposure. Cells were monitored using a Nikon TE2000U inverted microscope, and were continuously perfused at 2 mL/min with one of the following: HBSS, Ca^{2+}-free HBSS, 1-4 μM thapsigargin, 5 μM ionomycin (non-specific calcium ionophore) + 10 mM EGTA, or 5 μM ionomycin + 10 mM Ca^{2+}.

Individual cell Ca^{2+} events were measured manually using ImageJ software. Values were calculated as $\frac{F}{F_0}$, where F is the treatment-associated fluorescence and F_0 is the baseline fluorescence intensity. Responding cells were defined whose response to ionomycin controls were $\geq$ 140% of F_0. Measured values are reported as mean ± standard error of the mean (SEM). $[Ca^{2+}]$ was calculated using provided K_d values for Fluo-4AM dye.

5.4 Results & Discussion

5.4.1 LNCaP response to ER-stress via Thapsigargin

To determine cellular response to ER stress, we exposed LNCaPs to SERCA-pump inhibitor thapsigargin. Thapsigargin induced no measurable emptying of the Ca^{2+} store in responding cells at either concentration tried (1 μM and 4 μM) (Figure 5.2A). There was an expected flux of $[Ca^{2+}]$ across teh plasma membrane upon reintroduction of HBSS, resulting in a 76.0% ± 15.9% (SEM) increase in mean fluorescent intensity.

Ionomycin is an ionophore known to introduce large $[Ca^{2+}]_{cytosolic}$ transients, and often used to calibrate individual cell's maximum fluorescent intensity for quantitative $[Ca^{2+}]$ calculations. 5 μM Ionomycin in 10 mM Ca^{2+} did induce a large $[Ca^{2+}]_{cytosolic}$ flux, causing an average 146% ± 25.8% increase in cell fluorescence. Of the 85% of LNCaP cells which responded to ionomycin, 82% also experienced membrane flux when transitioning from Ca^{2+}-free to 2 mM Ca^{2+} HBSS (Figure 5.2 B).

These data suggest that the current setup can measure Ca^{2+} transients at resolutions compatible with GEDI microdevice imaging protocols, and can provide quantitative data on Ca^{2+} flux due to various insults. However, before moving forward, cell response to thapsigargin must be further investigated so as to avoid introducing cytotoxic levels of the agonist [122].

5.4.2 Summary

The underlying mechanisms of prostate turmorigenesis depend upon disrupting normal cellular processes, such as metabolism, growth and apoptosis. An integral factor for all these regulatory processes is calcium signaling. For this reason, observing the amplitude and spatio-temporal characteristics of calcium in a cell can inform how cell behavior is altered by tumorigenesis progression and outside stimuli. While there are several studies linking Ca^{2+} signaling with chemoresistance and acquisition of hormone-independent phenotypes, there is no study that conclusively shows if the two states disrupt the same calcium regulation pathways. I have successfully constructed a setup for live-cell imaging of Ca^{2+} flux in response to various chemical insults. When combined with our

previously demonstrated ability to image captured CTC *in-situ*, quantification of Ca^{2+} flux could be powerful assay in measuring the onset of prostate cancer taxane resistance or disease progression.

5.4.3 Future Work

Further work is needed to troubleshoot LNCaP unresponsiveness to thapsigargin. Previous work has shown LNCaPs to respond to TG at concentrations as low as 0.5μM, so different agonist formulations should be explored such as to induce response while staying below reported acute cytotoxic levels. Work should also be done characterizing the heterogeneity of SOCE as a function of both thapsigargin concentration and taxane exposure. While studies of shown taxane-mediated Ca^{2+} SOCE, most use taxane concentrations well above peak blood serum concentration levels [122, 136].

LNCaP cells can be induced to become androgen-independent through long-term passaging at low androgen concentrations [27]. The cell line is also an inherent resistance to docetaxel treatment, and through continuous exposure can be induced to become fully docetaxel-resistant [43]. This makes LNCaP cells an ideal testbed for Ca^{2+} measurements in combination with previously established taxane efficacy assays [76]. This would allow us to better understand the relationship between chemoresistance and hormone-refractory cell states, under controlled experimental conditions.

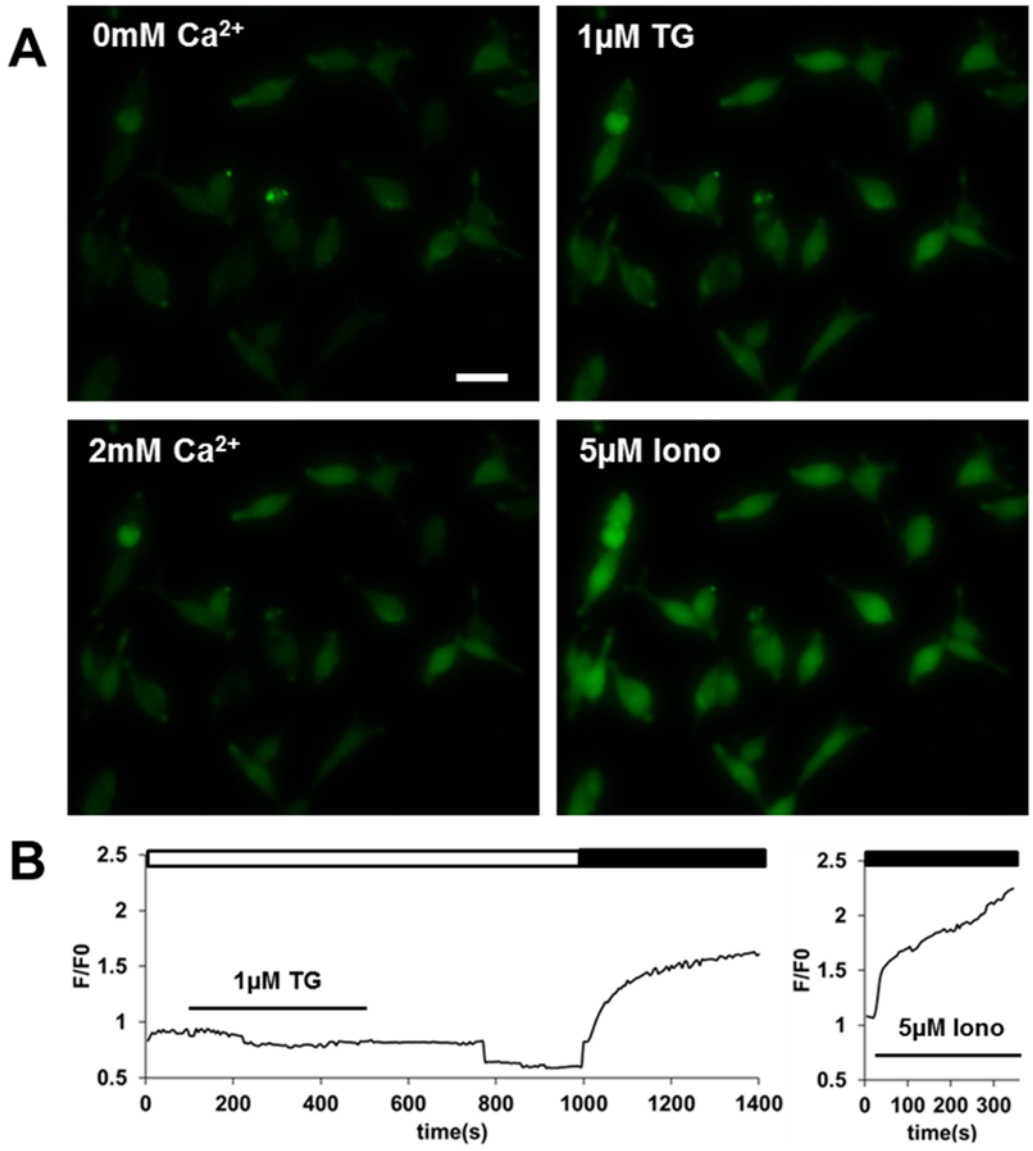

Figure 5.2: A) Fluorescent intensity images of cells loaded with Ca^{2+}-sensitive dye Fluo-4AM. Fluorescent intensity does not increase upon application of thapsigargin, but does when exposed to 2 mM Ca^{2+}, and also upon exposure to 5 μM of Ca^{2+} ionophore Ionomycin (Iono) in 10 mM Ca^{2+}-HBSS. Scale bar 50 μm. B) Traces of cell response to TG and ionomycin exposure. White bars indicate 0 mM [Ca^{2+}]. Data average of 23 cells across two experiments.

CHAPTER 6

CONCLUSION

In this work, I presented the development of techniques to characterize and chemically release circulating tumor cells (CTCs) from microfluidic devices. Each of these techniques could facilitate single-cell analyses for real-time identification of CTC subpopulations relevant to the metastatic cascade.

6.1 Summary of Accomplishments

I outlined electrokinetic and non-electrokinetic microfluidic techniques for the isolation, fractionation, or capture of rare cells from complex biological suspensions in chapter 2. I detailed major areas for technology improvement, primarily in whole cell release for viable cell culture and high-purity isolation methods for affordable single-cell analyses. In chapters 3 and 4, I presented two such methods for single-cell genetic analysis and whole cell release.

In chapter 3, I characterized whole cell release of CTCs from silicon GEDI microdevices using two reversible biotin analogues, desthiobiotin and photocleavable-biotin. I measured capture and release performance as a function of a variety surface chemistry parameters. Furthermore, I identified the differential capture performance of desthiobiotin (a low-affinity linker competitively displaced by biotin) and photocleavable-biotin (cleaved via exposure to UVA light). Specifically, I found that desthiobiotin was an efficient release method, but its bond to NeutrAvidin was too weak for cell isolation under the shear stress ranges in GEDI microdevices. Photocleavable-biotin was more robust and its immunocapture performance was indistinguishable from

standard biotin-avidin chemistry. I also fabricated GEDI microdevices using polystyrene, which transmits higher wavelength UV light, to further facilitate cell elution. My preliminary results showed we could release cancer cells using photocleavable-biotin while also maintaining high cell viability.

Next, in chapter 4, I reported the first microfluidic platform for robust and repeatable nuclei extraction, followed by single-nucleus sequencing (SNS). In collaboration with Cold Spring Harbor, I identified known, cancer-specific, CNVs in different prostate cell lines captured in geometrically enhanced differential immunocapture (GEDI) microdevices. GEDI-SNS had comparable resolution to SNS performed on cells sorted via FACS. This allowed us to distinguish between prostate cancer cells derived from different metastatic sites and separate LNCaP and VCaP copy-number profiles via unsupervised hierarchical clustering.

Finally, in chapter 5, I described the development of a Ca^{2+}-flux measurement assay that for real-time screening of patient samples. Cancer cells have been previously demonstrated to down-regulate, reorganize, or otherwise manipulate a number of native Ca^{2+} receptors and stores to turn normal cellular processes pathological. However, all of these characterization studies have used cell lines derived from PCa tissue(e.g. LNCaP, DU145, PC3). I proposed to ultimately use our high-efficiency, high-purity geometrically enhanced differential immunocapture (GEDI) microdevices to study the effects of androgen agonists, and androgen antagonists on Ca^{2+} in patient PCa cells, which has, to date, not been shown in the literature.

Many of the methods I have developed are generalizable across microfluidic immunocapture platforms, and have the potential to increase standardization and system integration of such platforms. These tools could greatly enhance

CTC recovery and assessment to inform cancer diagnosis and progression.

6.2 Future Work

Whole-cell release. Additional photocleavable-biotin characterization is recommended. My data showed that photocleavable-biotin release is unreliable, with no clear underpinning factors contributing to said variability. Further work is needed to assess successful linker immobilization, through HPLC and other analytical chemistry methods. These assays would clarify the conditions needed for effective linker photolysis and subsequent cell release. Implementation in UVA-transmissive materials, such as polystyrene, could further improve cell release. Successfully eluted cells must also be assessed for UV damage as a function of exposure and time, as well as plated for proliferation assays.

Single-cell CNV. Future work for CNV analysis of CTCs should include the design or integration of a microfluidic single-cell sorting platform. This would reduce the need for sample pre- or post-processing and increase the rate of CTC recovery. This is a critical step for reducing sequencing costs and would make GEDI-SNS a feasible option for patient-monitoring.

Taxane-mediated Ca^{2+} flux. Further work is needed to troubleshoot LNCaP unresponsiveness to thapsigargin. Previous work has shown LNCaPs to respond to TG at concentrations as low as 0.5 μM, so different agonist formulations should be explored such as to induce response while staying below reported acute cytotoxic levels. Work should be done characterizing the heterogeneity of SOCE as a function of both thapsigargin concentration and taxane exposure. While studies of shown taxane-mediated Ca^{2+} SOCE, most use taxane concen-

trations well above peak blood serum concentration levels [122, 136].

LNCaP cells can be induced to become androgen-independent through long-term passaging at low androgen concentrations [27]. The cell line is also an inherent resistance to docetaxel treatment, and through continuous exposure can be induced to become fully docetaxel-resistant [43]. This makes LNCaP cells an ideal testbed for Ca^{2+} measurements in combination with previously established taxane efficacy assays [77]. This would allow us to better understand the relationship between chemoresistance and hormone-refractory cell states, under controlled experimental conditions.

BIBLIOGRAPHY

[1] A. A. Adams, P. I. Okagbare, J. Feng, M. L. Hupert, D. Patterson, J. Gottert, R. L. McCarley, D. Nikitopoulos, M. C. Murphy, and S. A. Soper. Highly efficient circulating tumor cell isolation from whole blood and label-free enumeration using polymer-based microfluidics with an integrated conductivity sensor. *Journal of the American Chemical Society*, 130(27):10, 2008.

[2] C. Alkan, J. M. Kidd, T. Marques-Bonet, G. Aksay, F. Antonacci, F. Hormozdiari, J. O. Kitzman, C. Baker, M. Malig, O. Mutlu, S. C. Sahinalp, R. A. Gibbs, and E. E. Eichler. Personalized copy number and segmental duplication maps using next-generation sequencing. *Nature Genetics*, 41(10):1061–1067, 2009.

[3] W. J. Allard, J. Matera, M. C. Miller, M. Repollet, M. C. Connelly, C. Rao, A. G. T. J. W. Uhr, and L. W. M. M. Terstappen. Tumor cells circulate in the peripheral blood of all major carcinomas but not in healthy subjects or patients with nonmalignant diseases. *Clinical Cancer Research*, 10(20):6897–904, 2004.

[4] H. Andersson and A. van den Berg. Microfluidic devices for cellomics: a review. *Sensors and Actuators B*, 92:315–325, 2003.

[5] N. Bao, J. Wang, and C. Lu. Recent advances in electric analysis of cells in microfluidic systems. *Analytical and bioanalytical chemistry*, 391(3):933–42, 2008.

[6] Barrett, L. M, Skulan, A. J, Singh, A. K, Cummings, E. B, Fiechtner, and G. J. Dielectrophoretic manipulation of particles and cells using insulating ridges in faceted prism microchannels. *Analytical chemistry*, 77(21):6798–804, Nov. 2005.

[7] Becker, F. F, Gascoyne, P. R, Wang, X. B, Huang, Y, Pethig, R, Vykoukal, and J. Separation of human breast cancer cells from blood by differential dielectric affinity. *Proceedings of the National Academy of Sciences of the United States of America*, 92(3):860–4, Jan. 1995.

[8] M. F. Berger, M. S. Larence, F. Demichelis, Y. Drier, K. Cibulskis, A. Y. Sivachenko, A. Sboner, R. Esgueva, D. Pflueger, C. Sougnez, R. Onofrio, S. L. Carter, K. P. an dLukas Habegger, L. Ambrogio, T. Fennell, M. Parkin, G. Saksena, D. Voet, A. H. Ramos, T. J. Pugh, J. Wilkinson, S. Fisher, W. Winckler, S. Mahan, K. Ardlie, J. Bladwin, J. W. Simons, N. Kitabayashi,

T. Y. MacDonald, P. W. Kantoff, L. Chin, S. B. Gabriel, M. B. Gerstein, T. R. Golub, M. Meyerson, A. Tewari, E. S. Lander, G. Getz, M. A. Rubin, and L. A. Garaway. The genomic complexity of primary human prostate cancer. *Nature*, 470(7333):214–220, 2010.

[9] M. J. Berridge, M. D. Bootman, and H. L. Roderick. Calcium signalling: dynamics, homeostasis and remodelling. *Nature Reviews Molecular Cell Biology*, 4:517–529, 2003.

[10] M. Birkhahn, A. P. Mitra, A. J. Williams, N. J. Barr, E. C. Skinner, J. P. Stein, D. G. Skinner, Y.-C. Tai, R. H. Datar, and R. J. Cote. The genomic complexity of primary human prostate cancer. *Nature*, 470(7333):214–220, 2010.

[11] Braschler, Thomas, Demierre, Nicolas, Nascimento, Elisabete, Silva, Tiago, Oliva, A. G, Renaud, and Philippe. Continuous separation of cells by balanced dielectrophoretic forces at multiple frequencies. *Lab on a chip*, 8(2):280–6, 2008.

[12] T. Capiod, Y. Shuba, R. Skryma, and N. Prevarskaya. *Subcellular Biochemistry*, chapter Calcium signalling and cancer cell growth, pages 405–427. Springer, 2007.

[13] E. Cen, C. Dalton, Y. Li, S. Adamia, L. M. Pilarski, and K. V. I. S. Kaler. A combined dielectrophoresis and traveling wave dielectrophoresis and electrorotation microchip for the manipulation and characterization of human malignant cells. *Journal of microbiological methods*, 58(3):387–401, Sept. 2004.

[14] W. C. Chang, L. P. Lee, and D. Liepmann. Adhesion-based capture and separation of cells for microfluidic devices. *Materials Research Society Proceedings*, 79, 2002.

[15] C. X. Chen and Y. F. Zhang. Manipulation of single-wall carbon nanotubes into dispersively aligned arrays between metal electrodes. *Journal of Physics D-Applied Physics*, 39(1):172–176, Jan. 2006.

[16] D. F. Chen and H. Du. Simulation studies on electrothermal fluid flow induced in a dielectrophoretic microelectrode system. *Journal of Micromechanics and Microengineering*, 16(11):2411–2419, Nov. 2006.

[17] P. Chen, X. Feng, W. Du, and B. Liu. Microfluidic chips for cell sorting. *Frontiers in Bioscience*, 2008.

[18] Z. Chen, S. Zhang, Z. Tang, P. Xiao, X. Guo, and Z. Lu*. Pooldam structure based microfluidic devices for filtering tumor cells from blood mixtures. *Surface and Interface Analysis*, 2006.

[19] Cheng, I-Fang, Chang, Hsien-Chang, Hou, Diana, Chang, and Hsueh-Chia. An integrated dielectrophoretic chip for continuous bioparticle filtering and focusing and sorting and trapping and and detecting. *Biomicrofluidics*, 1(2):21503, 2007.

[20] Cheng, I-Fang, Froude, V. E, Zhu, Yingxi, Chang, Hsueh-Chia, Chang, and Hsien-Chang. A continuous high-throughput bioparticle sorter based on 3D traveling-wave dielectrophoresis. *Lab on a chip*, 9(22):3193–201, 2009.

[21] L. S. L. Cheung, X. Zheng, A. Stopa, J. C. Baygents, R. Guzman, J. A. Schroeder, R. L. Heimark, and Y. Zohar. Detachment of captured cancer cells under flow acceleration in a bio-functionalized microchannel. *Lab on a Chip*, 9:1721–1731, 2009.

[22] D. Y. Chiang, G. Getz, D. B. Jaffe, M. J. T. O'Kelly, X. Zhao, S. L. Carter, C. Russ, C. Nusbaum, M. Meyerson, and E. S. Lander. High-resolution mapping of copy-number alterations with massively parallel sequencing. *Nature Methods*, 6(1):99–103, 2009.

[23] Cho, Yoon-Kyoung, Kim, Suhyeon, Lee, Kyusang, Park, Chinsung, Lee, Jeong-Gun, Ko, and Christopher. Bacteria concentration using a membrane type insulator-based dielectrophoresis in a plastic chip. *Electrophoresis*, 30(18):3153–9, 2009.

[24] S. Choi, S. Song, C. Choi, and J.-K. Park. Microfludic self-sorting of mammalian cells to achieve cell cycle synchrony by hydrophoresis. *Analytical Chemistry*, 81:1964–1968, 2009.

[25] Chou, C, Tegenfeldt, J. O, Bakajin, O, Chan, S, Cox, E, Darnton, N, Duke, T, Austin, and R. Electrodeless Dielectrophoresis of Single- and Double-Stranded DNA. *Biophysical Journal*, 83(4):2170–2179, Oct. 2002.

[26] Church, Christopher, Zhu, Junjie, Wang, Gaoyan, Tzeng, T.-R. J., Xuan, and Xiangchun. Electrokinetic focusing and filtration of cells in a serpentine microchannel. *Biomicrofluidics*, 3(4):044109, 2009.

[27] C.-P. Chuu, J. M. Kokontis, R. A. Hiipakka, J. Fukuchi, H.-P. Lin, C.-Y. Lin, C. Huo, L.-C. Su, and S. Liao. Androgen suppresses proliferation of

castration-resistant lncap 104-r2 prostate cancer cells via androgen receptor, skp2, and c-myc. *Cancer Sci.*, 102(11):2022–2028, Aug. 2011.

[28] Cristofanilli, Massimo, Krishnamurthy, Savitri, Das, C. M, Reuben, J. M, Spohn, William, Noshari, Jamileh, Becker, Frederick, Gascoyne, and P. R. Dielectric cell separation of fine needle aspirates from tumor xenografts. *Journal of separation science*, 31(21):3732–9, 2008.

[29] Cui, L, Morgan, and H. Design and fabrication of travelling wave dielectrophoresis structures. *Journal of Micromechanics and Microengineering*, 10(1):72–79, Mar. 2000.

[30] Cummings, E. B., Singh, and A. K. Dielectrophoresis in Microchips Containing Arrays of Insulating Posts: Theoretical and Experimental Results. *Analytical Chemistry*, 75(18):4724–4731, Sept. 2003.

[31] D. Danila, G. Heller, G. Gignac, R. Gonzalez-Espinoza, A. Anand, E. Tanaka, H. Lilja, L. Schwartz, S. Larson, M. Fleisher, and H. Scher. Circulating tumor cell number and prognosis in progressive castration resistant prostate cancer. *Clinical Cancer Research*, 2007.

[32] M. S. Darshan, M. S. Loftus, M. Thadani-Mulero, B. P. Levy, D. Escuin, X. K. Zhou, A. Gjyrezi, C. Chanel-Vos, R. Shen, S. T. Tagawa, N. H. Bander, D. M. Nanus, and P. Giannnakakou. Taxane-induced blockade to nuclear accumulation of the androgen receptor predicts clinical responses in metastatic prostate cancer. *Cancer Research*, 71(18):6019–6029, 2011.

[33] J. Davis, D. Inglis, K. Morton, D. Lawrence, L. Huang, S. Chou, J. Sturm, and R. Austin. Deterministic hydrodynamics: Taking blood apart. *Proceedings of the National Academy of Sciences of the United States of America*, 103(40):14779–14784, 2006.

[34] Y. Deng, Y. Zhang, S. Sun, Z. Wang, M. Wang, B. Yu, D. M. Czajkowsky, B. Liu, Y. Li, W. Wei, and Q. Shi. An integrated microfluidic chip system for single-cell secretion profiling of rare circulating tumor cells. *Scientific Reports*, 4, 2014.

[35] S. R. Denmeade, A. M. Mhaka, D. M. Rosen, W. N. Brennen, S. Dalrymple, I. Dach, C. Olesen, B. Gurel, A. M. DeMazro, G. Wilding, M. A. Carducci, C. A. Dionne, J. V. Mller, P. Nissen, S. B. Christensen, and J. T. Issacs. Engineering a prostate-specific membrane antigenactivated tumor endothelial cell prodrug for cancer therapy. *Science Translational Medicine*, 4(10):140ra86, 2012.

[36] U. Dharmasiri, S. Balamurugan, A. A. Adams, P. I. Okagbare, A. Obubuafo, and S. A. Soper. Highly efficient capture and enumeriation of low abundance prostate cancer cells using prostate-specific membrane antigen aptamers immobilized to a polymeric microfluidic device. *Electrophresis*, 30:3289–3300, 2009.

[37] U. Dharmasiri, S. K. Njoroge, M. A. Witek, M. G. Adebiyi, J. W. Kamande, M. L. Hupert, F. Barany, and S. A. Soper. High-throughput selection and enumeration and electrokinetic manipulation and and molecular profiling of low-abundance circulating tumor cells using a microfluidic system. *Analytical Chemistry*, 83(6):2301–2309, 2011.

[38] Du, F, Baune, M, Thoming, and J. Insulator-based dielectrophoresis in viscous media - Simulation of particle and droplet velocity. *Journal of Electrostatics*, 65(7):452–458, June 2007.

[39] Z. Du, K. Cheng, M. Vaughn, N. Collie, and L. Gollahon. Recognition and capture of breast cancer cells using an antibody-based platform in a microelectromechanical systems device. *Biomedical Microdevices*, 9(1):35–42, 2007.

[40] Falokun, C. D, Mavituna, F, Markx, and G. H. AC electrokinetic characterisation and separation of cells with high and low embryogenic potential in suspension cultures of carrot (Daucus carota). *Plant Cell Tissue and Organ Culture*, 75(3):261–272, Dec. 2003.

[41] Fatoyinbo, H. O, Hughes, M. P, Martin, S. P, Pashby, Paul, Labeed, and F. H. Dielectrophoretic separation of Bacillus subtilis spores from environmental diesel particles. *Journal of environmental monitoring : JEM*, 9(1):87–90, 2007.

[42] Gadish, Nitzan, Voldman, and Joel. High-throughput positive-dielectrophoretic bioparticle microconcentrator. *Analytical chemistry*, 78(22):7870–6, Nov. 2006.

[43] L. Gan, J. Wang, H. Xu, and X. Yang. Resistance to docetaxel-induced apoptosis in prostate cancer cells by p38/p53/p21 signaling. *The Prostate*, 71(11):1158–1166, 2011.

[44] Gascoyne, P. R. C, Noshari, Jamileh, Anderson, T. J, Becker, and F. F. Isolation of rare cells from cell mixtures by dielectrophoresis. *Electrophoresis*, 30(8):1388–98, 2009.

[45] Gascoyne, Peter, Mahidol, Chulabhorn, Ruchirawat, Mahidol, Satayavivad, Jutamaad, Watcharasit, Piyajit, Becker, and F. F. Microsample preparation by dielectrophoresis: isolation of malaria. *Lab on a chip*, 2(2):70–5, 2002.

[46] J. P. Gleghorn, E. D. Pratt, D. Denning, H. Liu, N. H. Bander, S. T. Tagawa, D. M. Nanus, P. A. Giannakakou, and B. J. Kirby. Capture of circulating tumor cells from whole blood of prostate cancer patients using geometrically enhanced differential immunocapture (gedi) and a prostate-specific antibody. *Lab on a Chip*, 10:27–29, 2010.

[47] Y. Gong, L. Blok, J. Perry, J. Lindzey, and D. Tindall. Calcium regulation of androgen receptor expression in the human prostate cancer cell line lncap. *Endocrinology*, 136(5):2172–2178, 1995.

[48] D. J. V. Griend, L. Antony, S. L. Dalrymple, Y. Xu, S. B. Christensen, S. R. Denmeade, and J. T. Issacs. Amino acid containing thapsigargin analogues deplete androgen receptor protein via synthesis inhibition and induce the death of prostate cancer cells. *Molecular Cancer Therapeutics*, 8(5):1340–1349, 2009.

[49] U. A. Gurkan, T. Anand, H. Tas, D. Elkan, A. Akay, H. O. Keles, and U. Demirci. Controlled viable release of selectively captured label-free cells in microchannels. *Lab on a Chip*, 11:3979–3989, 2011.

[50] Hashimoto, Masahiko, Kaji, Hirokazu, Nishizawa, and Matsuhiko. Selective capture of a specific cell type from mixed leucocytes in an electrode-integrated microfluidic device. *Biosensors & bioelectronics*, 24(9):2892–7, 2009.

[51] Hawkins, B. G, Gleghorn, J. P, Kirby, and B. J. *Dielectrophoresis for Particle and Cell Manipulations*. Artech House, Boston and MA, 1st edition, 2009.

[52] Hawkins, B. G, Smith, A. Ezekiel, Syed, Y. A, Kirby, and B. J. Continuous-flow particle separation by 3D Insulative dielectrophoresis using coherently shaped and dc-biased and ac electric fields. *Analytical chemistry*, 79(19):7291–300, Oct. 2007.

[53] J. D. Hirsch, L. Eslamizar, B. J. Filanoski, N. Malekzadeh, R. P. Haugland, J. M. Beechem, and R. P. Haugland. Easily reversible desthiobiotin binding to streptavidin, avidin, and other biotin-binding proteins: uses for protein labeling, detection, and isolation. *Analytical Biochemistry*, 308(2):343–357, Sept. 2002.

[54] Ho, C. T, Lin, R. Z, Chang, W. Y, Chang, H. Y, Liu, and C. H. Rapid heterogeneous liver-cell on-chip patterning via the enhanced field-induced dielectrophoresis trap. *Lab on a Chip*, 6(6):724–734, June 2006.

[55] J. S. Hororszewicz, S. S. Leong, E. Kawinski, J. P. Karr, H. Rosenthal, T. M. Chu, E. A. Mirand, and G. P. Murthy. LNCaP model of human prostatic carcinoma. *Cancer Research*, 43(4):1809–1818, 1983.

[56] H. W. Hou, M. E. Warkiani, B. L. Khoo, Z. R. Li, R. A. Soo, D. S.-W. Tan, W.-T. Lim, J. Han, A. A. S. Bhagat, and C. T. Lim. Isolation and retrieval of circulating tumor cells using centrifugal forces. *Sci. Rep.*, 3:–, Feb. 2013.

[57] S. Hou, H. Zhao, L. Zhao, Q. Shen, K. S. Wei, D. Y. Suh, A. Nakao, M. A. Garcia, M. Song, T. Lee, B. Xiong, S.-C. Luo, H.-R. Tseng, and H. hua Yu. Capture and stimulated release of circulating on polymer-grafted silicon nanostructures. *Advanced Materials*, 25(11):1547–1551, 2012.

[58] Huang, Jung-Tang, Wang, Guo-Chen, Tseng, Kuang-Ming, Fang, and Shiuh-Bin. A chip for catching and separating and and transporting bioparticles with dielectrophoresis. *Journal of industrial microbiology & biotechnology*, 35(11):1551–7, 2008.

[59] Huang, Y, Wang, XB, Becker, FF, Gascoyne, and PR. Introducing dielectrophoresis as a new force field for field-flow fractionation. *Biophysical Journal*, 73(2):1118–1129, Aug. 1997.

[60] Huang, Y, Yang, J, Wang, X. B, Becker, F. F, Gascoyne, and P. R. The removal of human breast cancer cells from hematopoietic CD34+ stem cells by dielectrophoretic field-flow-fractionation. *Journal of hematotherapy & stem cell research*, 8(5):481–90, 1999.

[61] Huang, Y, Yang, J. M, Hopkins, P. J, Kassegne, S, Tirado, M, Forster, A. H, Reese, and H. Separation of simulants of biological warfare agents from blood by a miniaturized dielectrophoresis device. *Biomedical Microdevices*, 5(3):217–225, Sept. 2003.

[62] H.-L. Huang, H.-W. Hsing, T.-C. Lai, Y.-W. Chen, T.-R. Lee, P.-C. L. Hsin-Tsu Chan1, C.-L. Wu, Y.-C. Lu, S.-T. Lin, C.-W. Lin, C.-H. Lai, H.-T. Chang, H.-C. Chou, and H.-L. Chan. Trypsin-induced proteome alteration during cell subculture in mammalian cells. *Journal of Biomedical Science*, 17:36, 2010.

[63] R. Huang, T. Barber, M. Schmidt, R. G. Tompkins, M. Toner, D. Bianchi, R. Kapur, and W. Flejter. A microfluidics approach for the isolation of nucleated red blood cells (nrbcs) from perpiheral blood of pregnant women. *Prenatal Diagnostics*, 28:892–899, 2008.

[64] M. Hupert, J. Jackson, H. Wang, M. Witek, J. Kamande, M. Milowsky, Y. Whang, and S. Soper. Arrays of high-aspect ratio microchannels for high-throughput isolation of circulating tumor cells (ctcs). *Microsystem Technologies*, 20(10-11):1815–1825, 2014.

[65] D. Inglis, J. Davis, T. Zieziulewicz, D. Lawrence, R. Austin, and J. Sturm. Determining blood cell size using microfluidic hydrodynamics. *Journal of Immunological Methods*, 329(1-2):151–156, 2008.

[66] S. Jeon, J.-M. Moon, E. S. Lee, Y. H. Kim, and Y. Cho. An electroactive biotin-doped polypyrrole substrate that immobilizes and releases epcam-positive cancer cells**. *Angewandte Chemie International Edition*, 126:1–7, 2014.

[67] H. Ji, V. Samper, Y. Chen, C. Heng, T. Lim, and L. Yobas. Silicon-based microfilters for whole blood cell separation. *Biomedical Microdevices*, 10(2):251–257, 2008.

[68] Jones and T. B. *Electromechanics of Particles*. Cambridge University Press, New York and NY, 1995.

[69] Kang, Yuejun, Li, and Dongqing. Electrokinetic motion of particles and cells in microchannels. *Microfluidics and Nanofluidics*, 6(4):431–460, 2009.

[70] Kang, Yuejun, Li, Dongqing, Kalams, S. A, Eid, and J. E. DC-Dielectrophoretic separation of biological cells by size. *Biomedical microdevices*, 10(2):243–9, 2008.

[71] B. L. Khoo, M. E. Warkiani, D. S.-W. Tan, A. A. S. Bhagat, D. Irwin, D. P. Lau, A. S. T. Lim, K. H. Lim, S. S. Krisna, W.-T. Lim, Y. S. Yap, S. C. Lee, R. A. Soo, J. Han, and C. T. Lim. Clinical validation of an ultra high-throughput spiral microfluidics for the detection and enrichment of viable circulating tumor cells. *PLoS ONE*, 2014.

[72] Kim, Unyoung, Qian, Jiangrong, Kenrick, S. A, Daugherty, P. S, Soh, and H. Tom. Multitarget dielectrophoresis activated cell sorter. *Analytical chemistry*, 80(22):8656–61, 2008.

[73] Kim, Unyoung, Shu, Chih-Wen, Dane, K. Y, Daugherty, P. S, Wang, J. Y. J, Soh, and H. T. Selection of mammalian cells based on their cell-cycle phase using dielectrophoresis. *Proceedings of the National Academy of Sciences of the United States of America*, 104(52):20708–12, 2007.

[74] Kim, Unyoung, Soh, and H. Tom. Simultaneous sorting of multiple bacterial targets using integrated dielectrophoretic-magnetic activated cell sorter. *Lab on a chip*, 9(16):2313–8, 2009.

[75] Kirby and B. J. *Micro- and Nanoscale Fluid Mechanics: Transport in Microfluidic Devices*. Cambridge University Press, 2010.

[76] B. J. Kirby, M. Jodari, M. S. Loftus, G. Gakhar, E. D. Pratt, C. Chanel-Vos, J. P. Gleghorn, S. M. Santana, H. Liu, J. P. Smith, V. N. Navarro, S. T. Tagawa, N. H. Bander, D. M. Nanus, and P. Giannakakou. Functional characterization of circulating tumor cells with a prostate-cancer-specific microfluidic device. *PLOS ONE*, 7(4):e35976, Jan. 2012.

[77] B. J. Kirby, M. Jodari, M. S. Loftus, E. Pratt, G. Gakhar, J. P. Gleghorn, S. M. Santana, H. Liu, J. P. Smith, S. T. Tagawa, N. H. Bander, D. M. Nanus, and P. Giannakakou. Functional characterization of circulating tumor cells with a prostate-cancer-specific microfluidic device. *PLoS ONE*, 2011.

[78] K. Kolostova, M. Cegan, and V. Bobek. Circulating tumour cells in patients with urothelial tumours: Enrichment and in vitro culture. *Canadian Urological Assocation Journal*, 8(9-10):E715–E720, 2014.

[79] Koo, O. Kyung, Liu, Yishao, Shuaib, Salamat, Bhattacharya, Shantanu, Ladisch, M. R, Bashir, Rashid, Bhunia, and A. K. Targeted capture of pathogenic bacteria using a mammalian cell receptor coupled with dielectrophoresis on a biochip. *Analytical chemistry*, 81(8):3094–101, 2009.

[80] S. Korenchuk, J. Lehr, L. MClean, Y. Lee, S. Whitney, R. Vessella, D. Lin, and K. Pienta. VCaP and a cell-based model system of human prostate cancer. *In Vivo*, 15(2):163–168, 2001.

[81] C. M. Kraning-Rush, J. P. Califano, and C. A. Reinhart-King. Cellular traction stresses increase with increasing metastatic potential. *PLoS ONE*, 7(2):e32572–, Feb. 2012.

[82] Kremser, Leopold, Blaas, Dieter, Kenndler, and Ernst. Capillary electrophoresis of biological particles: viruses and bacteria and and eukaryotic cells. *Electrophoresis*, 25(14):2282–91, 2004.

[83] Kua, C. Hock, Lam, Y. Cheong, Rodriguez, Isabel, Yang, Chun, Youcef-Toumi, and Kamal. Dynamic cell fractionation and transportation using moving dielectrophoresis. *Analytical chemistry*, 79(18):6975–87, Sept. 2007.

[84] T. Kulrattanarak, R. van der Sman, C. Schron, and R. Boom. Classification and evaluation of microfluidic devices for continuous suspension fractionation. *Advances in Colloid and Interface Science*, 2008.

[85] S. Kuntaegowdanahalli, A. A. S. Bhagat, G. Kumar, and I. Papautsky. Inertial microfluidics for continuous particle separation in spiral microchannels. *Lab on a Chip*, 9:2973–2980, 2009.

[86] J.-M. Lai, H.-J. Shao, J.-C. Wu, S.-H. Lu, and Y.-C. Chang. Efficient elusion of viable adhesive cells from a microfluidic system by air foam. *Biomicrofluidics*, 8(5), 2014.

[87] Lapizco-Encinas, B. H, Davalos, R. V, Simmons, B. A, Cummings, E. B, Fintschenko, and Yolanda. An insulator-based (electrodeless) dielectrophoretic concentrator for microbes in water. *Journal of microbiological methods*, 62(3):317–26, Sept. 2005.

[88] Lapizco-Encinas, B. H, Simmons, B. A, Cummings, E. B, Fintschenko, and Yolanda. Dielectrophoretic concentration and separation of live and dead bacteria in an array of insulators. *Analytical chemistry*, 76(6):1571–9, Mar. 2004.

[89] Lapizco-Encinas, B. H, Simmons, B. A, Cummings, E. B, Fintschenko, and Yolanda. Insulator-based dielectrophoresis for the selective concentration and separation of live bacteria in water. *Electrophoresis*, 25(10-11):1695–704, June 2004.

[90] Lei, U, Huang, C. W, Chen, James, Yang, C. Y, Lo, Y. J, Wo, Andrew, Chen, C. F, Fung, and T. W. A travelling wave dielectrophoretic pump for blood delivery. *Lab on a chip*, 9(10):1349–56, 2009.

[91] Li, H, Bashir, and R. Dielectrophoretic separation and manipulation of live and heat-treated cells of Listeria on microfabricated devices with interdigitated electrodes. *Sensors and Actuators B: Chemical*, 86(2-3):215–221, Sept. 2002.

[92] L. S. Lim, M. Hu, M. C. Huang, W. C. Cheong, A. T. L. Gan, X. L. Looi, S. M. Leong, E. S.-C. Koay, and M.-H. Li. Microsieve lab-chip device for

rapid enumeration and fluorescence in situ hybridization of circulating tumor cells. *Lab Chip*, 12(21):4388–4396, 2012.

[93] C.-H. Lin, C.-Y. Lee, C.-H. Tsai, and L.-M. Fu. Novel continuous particle sorting in microfluidic chip utilizing cascaded squeeze effect. *Microfludics and Nanofluidics*, 7:499–508, 2009.

[94] Liu, C. X, Lagae, L, Borghs, and G. Manipulation of magnetic particles on chip by magnetophoretic actuation and dielectrophoretic levitation. *Applied Physics Letters*, 90(18):–, Apr. 2007.

[95] Liu, Yi-Shao, Walter, T. M, Chang, Woo-Jin, Lim, Kwan-Seop, Yang, Liju, Lee, S. W, Aronson, A, Bashir, and R. Electrical detection of germination of viable model Bacillus anthracis spores in microfluidic biochips. *Lab on a chip*, 7(5):603–10, 2007.

[96] W. Liu, C. C. Xie, Y. Zhu, T. Li, J. Sun, Y. Cheng, C. M. Ewing, S. Dalrymple, A. R. Turner, J. Sun, J. T. Isaacs, B.-L. Chang, S. L. Zheng, W. B. Isaacs, and J. Xu. Homozygous deletions and recurrent amplifications implicate new genes involved in prostate cancer. *Neoplasia*, 10(8):897–907, 2008.

[97] J. G. Lohr, V. A. Adalsteinsson, K. Cibulskis, A. D. Choudhury, M. Rosenberg, P. Cruz-Gordillo, J. Francis, C.-Z. Z. A. K. Shalek, R. Satija, J. T. Trombetta, D. Lu, N. Tallapragada, N. Tahirova, S. Kim, B. Blumenstiel, C. Sougnez, A. Lowe, B. Wong, D. Auclair, E. M. V. Allen, M. Nakabayashi, R. T. Lis, G.-S. M. Lee, T. Li, M. S. Chabot, A. Ly, M.-E. Taplin, T. E. Clancy, M. Loda, A. Regev, M. Meyerson, W. C. Hahn, P. W. Kantoff, T. R. Golub, G. Getz, J. S. Boehm, and J. C. Love. Whole exome sequencing of circulating tumor cells provides a window into metastatic prostate cancer. *Nature Biotechnology*, 32(5):479–484, 2014.

[98] Loire, S., Mezic, and I. *Separation of bioparticles using the travelling wave dielectrophoresis with multiple frequencies*, volume 6. IEEE, Maui and Hawaii and USA, 2003.

[99] F. Lyng, G. Jones, and F. Rommerts. Rapid androgen actions on calcium signaling in rat sertoli cells and two human prostatic cell lines: Similar biphasic responses between 1 picomolar and 100 nanomolar concentrations. *Biology of Reproduction*, 63(3):736–747, 2000.

[100] M. J. M. Magbanua, E. V. Sosa, R. Roy, L. E. Eisenbud, J. H. Scott, A. Olshen, D. Pinkel, H. Ruogo, and J. W. Park. Genomic profiling of isolated

circulating tumor cells from metastatic breast cancer patients. *Cancer Research*, 73(1):30–40, 2013.

[101] S. Maheswaran, L. V. Sequist, S. Nagrath, L. Ulkus, B. Brannigan, C. V. Collura, elizabeth Inserra, S. Diederichs, A. J. Iafrate, D. W. Bell, S. Digumarthy, A. Muzikansky, D. Irimia, J. Settleman, R. G. Tompkins, T. J. Lynch, M. Toner, and D. A. Haber. Detection of mutations in EGFR in circulating lung-cancer cells. *New England Journal of Medicine*, 359(4):366–377, 2008.

[102] Marks, G. H., Huang, Y., Zhou, X.-F., Pethig, and R. Dielectrophoretic characterization and separation of micro-organisms. *Microbiology*, 140(3):585–591, Mar. 1994.

[103] Markx, G. H, Pethig, and R. Dielectrophoretic separation of cells: Continuous separation. *Biotechnology and bioengineering*, 45(4):337–43, Feb. 1995.

[104] J. A. Mayer, T. Pham, K. L. Wong, J. Scoggin, E. V. Sales, T. Clarin, T. J. Pricher, S. D. Mikolajczyk, P. D. Cotter, and F. Z. Bischoff. Fish-based determination of HER2 status in circulating tumor cells isolated with the microfluidic CEE platform. *Caner Genetics*, 204(11):589–595, 2011.

[105] M. E. McMenamin, P. Soung, S. Perera, I. Kaplan, M. Loda, and W. R. Sellers. Loss of PTEN expression in paraffin-embedded primary prostate cancer correlates with high gleason score and advanced stage. *Cancer Research*, 59(17):4291–4296, 1999.

[106] Mehrishi, J. N., Bauer, and Johann. Electrophoresis of cells and the biological relevance of surface charge. *Electrophoresis*, 23(13):1984, 2002.

[107] Mela, Petra, van Den Berg, Albert, Fintschenko, Yolanda, Cummings, E. B, Simmons, B. A, Kirby, and B. J. The zeta potential of cyclo-olefin polymer microchannels and its effects on insulative (electrodeless) dielectrophoresis particle trapping devices. *Electrophoresis*, 26(9):1792–9, May 2005.

[108] D. T. Miyamoto, R. J. Lee, S. L. Stott, D. T. Ting, B. S. Wittner, M. Ulman, M. E. Smas, J. B. Lord, B. W. Brannigan, J. Trautwein, N. H. Bander, C.-L. Wu, L. V. Sequist, M. R. Smith, S. Ramaswamy, M. Toner, S. Maheswara, and D. A. Haber. Androgen receptor signaling in circulating tumor cells as a marker of hormonally responsive prostate cancer. *Cancer Discovery*, 2(11):995–1003, 2012.

[109] H. Mohamed, L. D. McCurdy, D. H. Szarowski, S. Duva, J. N. Turner, and M. Caggana. Development of a rare cell fractionation device: Application for cancer detection. *IEEE Transactions on Nanobioscience*, 3(4):251–256, 2004.

[110] H. Mohamed, J. N. Turner, and M. Caggana. Biochip for separating fetal cells from mathernal circulation. *Journal of Chromatography A*, 1162:187–192, 2007.

[111] H.-S. Moon, K. Kwon, K.-A. Hyun, T. S. Jim, J. C. Park, J.-G. Lee, and H.-I. Jung. Continual collection and re-separation of circulating tumor cells from blood using multi-stage multi-orifice flow fractionation. *Biomicro*, 7(1):014105, 2013.

[112] Morgan, Hywell, Green, and Nicholas. *AC Electrokinetics: Colloids and Nanoparticles*. Research Studies Press and Ltd., Baldock and Hertfordshire and England, 1 edition, 2002.

[113] V. T. Moy, E.-L. Florin, and H. E. Gaub. Intermolecular forces and energies between ligands and receptors. *Science*, 266(5183):257–259, 1994.

[114] S. K. Murthy, A. Sin, R. G. Tompkins, and M. Toner. Effect of flow and surface conditions on human lymphocyte isolation using microfluidic chambers. *Langmuir*, 20(26):8, 2004.

[115] S. Nagrath, L. V. Sequist, S. Maheswaran, D. W. Bell, D. Irimia, L. Ulkus, M. Smith, E. L. Kwak, S. Digurmarthy, A. Muzikansky, P. Ryan, U. Balis, R. G. Tompkins, D. A. Haber, and M. Toner. Isolation of rare circulating tumor cells in cancer patients by microchip technology. *Nature*, 450, 2007.

[116] N. Navin, J. Kendall, J. Troge, P. Andrews, L. Rodgers, J. McIndoo, K. Cook, A. Stepansky, D. Levy, D. Esposito, L. Muthuswamy, A. Krasnitz, W. R. McCombie, J. Hicks, and M. Wigler. Tumor evolution inferred by single-cell sequencing. *Nature*, 472(7341):90–94, 2011.

[117] N. Navin, A. Krasnitz, L. Rodgers, K. Cook, J. Meth, J. Kendall, M. Riggs, Y. Eberling, J. Troge, V. Grubor, D. Levy, P. Lundin, S. Maner, A. Zetterberg, J. Hicks, and M. Wigler. Inferring tumor progression from genomic heterogeneity. *Genome Research*, 20(1):68–80, 2009.

[118] A. M. Newman, S. V. Bratman, J. To, J. F. Wynne, N. C. W. Eclov, L. A. Modlin, C. L. Liu, J. W. Neal, H. A. Wakelee, R. E. Merritt, J. B. Shrager,

B. W. L. Jr, A. A. Alizadeh, and M. Diehn. An ultrasensitive method for quantitating circulating tumor DNA with broad patient coverage. *Nature Medicine*, 2014.

[119] K. Okahara, B. Sun, and J. ichi Kambayashi. Upregulation of prostacyclin synthesisrelated gene expression by shear stress in vascular endothelial cells. *Arteriosclerosis and Thrombosis and and Vascular Biology*, 1998.

[120] J. Olejnik, S. Sonar, E. Krzymañska-Olejnik, and K. J. Rothschild. Photocleavable biotin derivatives: A versatile approach for the isolation of biomolecules. *Proceedings of the National Academy of Sciences*, 92(16):7590–7594, 1995.

[121] E. Ozkumur, A. M. Shah, J. C. Ciciliano, B. L. Emmink, D. T. Miyamoto, E. Brachtel, M. Yu, P. i Chen, B. Morgan, J. Trautwein, A. Kimura, S. Sengupta, S. L. Stott, N. M. Karabacak, T. A. Barber, J. R. Walsh, K. Smith, P. S. Spuhler, J. P. Sullivan, R. J. Lee, D. T. Ting, X. Luo, A. T. Shaw, A. Bardia, L. V. Sequist, D. N. Louis, S. Maheswaran, R. Kapur, D. A. Haber, and M. Toner. Intertial focusing for tumor antigen-dependent and -independent sorting of rare circulating tumor cells. *Science Translational Medicine*, 5(179):179ra47, 2013.

[122] S. Padar, C. van Breeman, D. W. Thomas, J. A. Uchizono, J. C. Livesey, and R. Rahimian. Differential regulation of calcium homeostasis in adenocarcinoma cell line a549 and its taxol-resistant subclone. *British Journal of Pharmacology*, 142:305–316, 2004.

[123] Pappas, D, Wang, and K. Cellular separations: A review of new challenges in analytical chemistry. *Analytica Chimica Acta*, 601(1):26–35, Oct. 2007.

[124] B. D. Plouffe, D. N. Njoka, J. Harris, J. Liao, N. K. Horick, M. Radisic, and S. K. Murthy. Peptide-mediated selective adhesion of smooth muscle and endothelial cells in microfluidic shear flow. *Langmuir*, 23:7, 2007.

[125] B. D. Plouffe, M. Radisic, and S. K. Murthy. Microfluidic depletion of endothelial cells and smooth muscle cells and and fibroblasts from heterogeneous suspensions. *Lab on a Chip*, 8:11, 2008.

[126] Pommer, M. S, Zhang, Yanting, Keerthi, Nawarathna, Chen, Dong, Thomson, J. A, Meinhart, C. D, Soh, and H. T. Dielectrophoretic separation of platelets from diluted whole blood in microfluidic channels. *Electrophoresis*, 29(6):1213–8, 2008.

[127] A. A. Powell, A. A. H. Talasaz, H. Zhang, M. A. Coram, A. Reddy, G. Deng, M. L. Telli, R. H. Advani, R. W. Carolson, J. A. Mollick, S. Sheth, A. W. Kurian, J. M. Ford, F. E. Stockdale, S. R. Quake, R. F. Pease, M. N. Mindrinos, G. Bhanot, S. H. Dairkee, R. W. Davis, and S. S. Jeffrey. Single cell profiling of circulating tumor cells: Transcriptional heterogeneity and diversity from breast cancer cell lines. *PLoS ONE*, 8(10):1253–1256, 2012.

[128] E. D. Pratt, J. Hicks, A. Stepansky, and B. J. Kirby. Copy Number Analysis of Prostate Cancer Cells using GEDI Microdevice. *submitted*, 2014.

[129] E. D. Pratt, C. Huang, B. G. Hawkins, J. P. Gleghorn, and B. J. Kirby. Rare cell capture in microfluidic devices. *Chemical Engineering Science*, 66(7):1508–1522, 2011.

[130] Pui-ock, Sittisak, Ruchirawat, Mathuros, Gascoyne, and Peter. Dielectrophoretic field-flow fractionation system for detection of aquatic toxicants. *Analytical chemistry*, 80(20):7727–34, 2008.

[131] E. A. Punnoose, S. K. Atwal, J. M. Spoerke, H. Savage, A. Pandita, R.-F. Yeh, A. Pirzkall, B. M. Fine, L. C. Amler, D. S. Chen, and M. R. Lackner. Molecular biomarker analyses using circulating tumor cells. *PLoS ONE*, 5(9):e12517, 2010.

[132] Pysher, M. D, Hayes, and M. A. Electrophoretic and dielectrophoretic field gradient technique for separating bioparticles. *Analytical chemistry*, 79(12):4552–7, June 2007.

[133] E. Retegui, N. Aceto, E. J. Lim, J. P. Sullivan, A. E. Jensen, M. Zeinali, J. M. Martel, A. J. Aranyosi, W. Li, S. Castleberry, A. Bardia, L. V. Sequist, D. A. Haber, S. Maheswaran, P. T. Hammond, M. Toner, and S. L. Stott. Tunable nanostructured coating for the capture and selective release of viable circulating tumor cells. *Advanced Materials*, 27(9):1593–1599, 2015.

[134] Rhoades, E. R, Geisel, R. E, Butcher, B. A, McDonough, Sean, Russell, and D. G. Cell wall lipids from Mycobacterium bovis BCG are inflammatory when inoculated within a gel matrix: characterization of a new model of the granulomatous response to mycobacterial components. *Tuberculosis (Edinburgh and Scotland)*, 85(3):159–76, May 2005.

[135] Rousselet, J, Markx, GH, Pethig, and R. Separation of erythrocytes and latex beads by dielectrophoretic levitation and hyperlayer field-flow fractionation. *Colloids and Surfaces A: Physicochemical and Engineering Aspects*, 140(1-3):209–216, Sept. 1998.

[136] A. D. Russa, N. Ishikita, K. Masu, H. Akutsu, T. Saino, and Y. ichi Satoh. Calcium regulation of androgen receptor expression in the human prostate cancer cell line lncap. *Archives of Histology and Cytology*, 71(4):249–263, 2008.

[137] S. Santana, H. Liu, N. Bander, J. Gleghorn, and B. Kirby. Immunocapture of prostate cancer cells by use of anti-psma antibodies in microdevices. *Biomedical Microdevices*, 14(2):401–407, 2012.

[138] P. Sethu, A. Sin, and M. Toner. Microfluidic diffusive filter for apheresis (leukapheresis). *Lab on a Chip*, 6:83–89, 2005.

[139] Shafiee, Hadi, Sano, M. B, Henslee, E. A, Caldwell, J. L, Davalos, and R. V. Selective isolation of live/dead cells using contactless dielectrophoresis (cDEP). *Lab on a chip*, 10(4):438–45, 2010.

[140] J. A. Shaw, K. Page, K. Blighe, N. Hava, D. Guttery, B. Ward, J. Brown, C. Ruangpratheep, J. Stebbing, R. Payne, C. Palmieri, S. Cleator, R. A. Walker, and R. C. Coombes. Genomic analysis of circulating cell-free DNA infers breast cancer dormancy. *Genome Research*, 22(2):220–231, 2012.

[141] R. Siegel, E. Ward, O. Brawley, and A. Jemal. Cancer statistics 2011: The impact of eliminating socioeconomic and racial disparities on premature cancer deaths. *CA: A Cancer Journal for Clinicians*, 61(4):212–236, 2011.

[142] A. Sin, S. K. Murthy, A. Revzin, R. G. Tompkins, and M. Toner. Enrichment using antibody-coated microfluidic chambers in shear flow: model mixtures of human lymphocytes. *Bioengineering and Biotechnology*, 91(7):816–826, 2005.

[143] E. Sollier, D. E. Go, J. Che, D. R. Gossett, S. O'Bryne, W. M. Weaver, N. Kummer, M. Rettig, J. Goldman, N. Nickols, S. McCloskey, R. P. Kulkarni, and D. D. Carlo. Size-selective collection of circulating tumor cells using vortex technology. *Lab on a Chip*, 14(1):63–77, 2014.

[144] J. SooHoo and G. Walker. Microfluidic liquid filters for leukocyte isolation. *Proceedings of the 29th Annual International Conference of the IEEE EMBS*, 2007.

[145] T. Stakenborg, C. Liu, O. Henry, E. Borgen, N. Laddach, T. R. M. Ritzi-Lehnert, C. Fermer, S. Hauch, C. K. O'Sullivan, and L. Lagae. Automated genotyping of circulating tumor cells. *Expert Reviews in Molecular Diagnostics*, 10(6):723–729, 2010.

[146] S. L. Stott, C.-H. Hsu, D. I. Tsukrov, M. Yu, D. T. Miyamoto, B. A. Waltman, S. M. Rothenberg, A. M. Shah, M. E. Smas, G. K. Korir, F. P. Floyd, A. J. Gilman, J. B. Lord, D. Winokur, S. Springer, D. Irimia, S. Nagrath, L. V. Sequist, R. J. Lee, K. J. Isselbacher, S. Maheswaran, D. A. Haber, and Mehmet. Isolation of circulating tumor cells using a microvortex-generating herringbone-chip. *Proceedings of the National Academy of Sciences*, 107(43):18392–18397, 2010.

[147] S. L. Stott, R. J. Lee, S. Nagrath, M. Y. an dDavid T Miyamoto, L. Ulkus, E. J. Inserra, M. Ulman, S. Springer, Z. Nakamura, A. L. Moore, D. I. Tsukrov, M. E. Kempner, D. M. Dahl, C.-L. Wu, A. J. Iafrate, M. R. Smith, R. G. Tompkins, L. V. Sequist, M. Toner, D. A. Haber, and S. Maheswaran. Isolation and characterization of circulating tumor cells from patients with localized and metastatic prostate cancer. *Science Translational Medicine*, 2(25):25ra23, 2010.

[148] Sun, Tao, Morgan, Hywel, Green, and Nicolas. Analytical solutions of ac electrokinetics in interdigitated electrode arrays: Electric field and dielectrophoretic and traveling-wave dielectrophoretic forces. *Physical Review E*, 76(4), Oct. 2007.

[149] Y.-H. Sun, X. Gao, Y.-J. Tang, C.-L. Xu, and L.-H. Wang. Androgens induce increases in intracellular calcium via a g proteincoupled receptor in lncap prostate cancer cells. *Journal of Andrology*, 27(5):671–678, 2006.

[150] C. Tai, S. Hsiung, C. Chen, M. Tsai, and G. Lee. Automatic microfluidic platform for cell separation and nucleus collection. *Biomedical Microdevices*, 9(4):533–543, 2007.

[151] Talary, M. S, Burt, J. P. H, Tame, J. A, Pethig, and R. Electromanipulation and separation of cells using travelling electric fields. *Journal of Physics D-Applied Physics*, 29(8):2198–2203, Aug. 1996.

[152] T. Tanaka, T. Ishikawa, K. Numayama-Tsuruta, Y. Imai, K. Ueno, N. Matsuki, and T. Yamaguchi. Separation of cancer cells from a red blood cell suspension using inertial force. *Lab on a Chip*, 12(21):4336–4343, 2012.

[153] Y. Tang, J. Shi, S. Li, L. Wang, Y. E. Cayre, and Y. Chen. Microfluidic device with integrated microfilter of conical-shaped holes for high efficiency and high purity capture of circulating tumor cells. *Sci. Rep.*, 4:–, Aug. 2014.

[154] F. I. Thege, T. B. Lannin, T. N. Saha, S. Tsai, M. L. Kochman, M. A. Hollingsworth, A. D. Rhim, and B. J. Kirby. Microfluidic immunocap-

ture of circulating pancreatic cells using parallel epcam and muc1 capture: characterization, optimization and downstream analysis. *Lab Chip*, 14(10):1775–1784, 2014.

[155] A. M. Thompson, A. L. Paguirigan, J. E. Kreutz, J. P. Radich, and D. T. Chiu. Microfluidics for single-cell genetic analysis. *Lab on a Chip*, 2014.

[156] Turgeon, R. T, Bowser, and M. T. Micro free-flow electrophoresis: theory and applications. *Analytical and bioanalytical chemistry*, 394(1):187–98, 2009.

[157] Vahey, M. D, Voldman, and J. An equilibrium method for continuous-flow cell sorting using dielectrophoresis. *Analytical chemistry*, 80(9):3135–43, May 2008.

[158] V. VanDelinder and A. Groisman. Separation of plasma from whole human blood in a continuous cross-flow in a molded microfluidic device. *Analytical Chemistry*, 78(11):3765–3771, 2006.

[159] V. VanDelinder and A. Groisman. Perfusion in microfluidic cross-flow: Separation of white blood cells from whole blood and exchange of medium in a continuous flow. *Analytical Chemistry*, 79(5):2023–2030, 2007.

[160] K. Vanoverberghe, F. V. Abeele, P. Mariot, G. Lepage, M. Roudbaraki, J. L. Bonnal, B. Mauroy, Y. shuba, R. Skryma, and N. Prevarskaya. Ca2+ homeostasis and apoptotic resistance of neuroendocrine-differentiated prostate cancer cells. *Cell Death and Differentiation*, 11:321–330, 2004.

[161] Voldman and J. Electrical forces for microscale cell manipulation. *Annual Review of Biomedical Engineering*, 8:425–454, 2006.

[162] Vykoukal, Jody, Vykoukal, D. M, Freyberg, Susanne, Alt, E. U, Gascoyne, and P. R. C. Enrichment of putative stem cells from adipose tissue using dielectrophoretic field-flow fractionation. *Lab on a chip*, 8(8):1386–93, 2008.

[163] Wang, X. B, Huang, Y, Burt, J. P. H, Markx, G. H, Pethig, and R. Selective Dielectrophoretic Confinement of Bioparticles in Potential-Energy Wells. *Journal of Physics D-Applied Physics*, 26(8):1278–1285, Aug. 1993.

[164] Wang, X. J, Yang, J, Gascoyne, and P. R. C. Role of peroxide in AC electrical field exposure effects on Friend murine erythroleukemia cells during dielectrophoretic manipulations. *Biochimica Et Biophysica Acta-General Subjects*, 1426(1):53–68, Jan. 1999.

[165] Wang, Lisen, Lu, Jente, Marchenko, S. A, Monuki, E. S, Flanagan, L. A, Lee, and A. P. Dual frequency dielectrophoresis with interdigitated sidewall electrodes for microfluidic flow-through separation of beads and cells. *Electrophoresis*, 30(5):782–91, 2009.

[166] Wang, XB, Huang, Y, Wang, X, Becker, FF, Gascoyne, and PR. Dielectrophoretic manipulation of cells with spiral electrodes. *Biophysical Journal*, 72(4):1887–1899, Apr. 1997.

[167] Wang, Xiao-Bo, Yang, Jun, Huang, Ying, Vykoukal, Jody, Becker, F. F., Gascoyne, and P. R. C. Cell Separation by Dielectrophoretic Field-flow-fractionation. *Analytical Chemistry*, 72(4):832–839, 2000.

[168] Z. Wang, S. Y. Chin, C. D. Chin, J. Sarik, M. Harper, J. Justman, and S. K. Sia. Microfluidic cd4+ t-cell counting device using chemiluminescence-based detection. *Analytical Chemistry*, 82:39–40, 2010.

[169] F. Wernig, M. Mayr, and Q. Xu. Mechanical stretch-induced apoptosis in smooth muscle cells is mediated by 1-integrin signaling pathways. *Hypertension*, 2003.

[170] M. Wirkner, J. M. Alfonso, V. Maus, M. Salierno, T. T. Lee, A. J. Garcia, and A. del Campo. Triggered cell release from materials using bioadhesive photocleavable linkers. *Advanced Materials*, 23:3907–3910, 2011.

[171] Y. Wu, M. Fabritius, and C. Ip. Chemotherapeutic sensitization by endoplasmic reticulum stress: Increasing the efficacy of taxane against prostate cancer. *Cancer Biology and Therapy*, 8(2):146–152, 2009.

[172] Z. Wu, B. Willing, J. Bjerketorp, J. K. Jansson, and K. Hjort. Soft inertial microfluidics for high throughput separation of bacteria from human blood cells. *Lab on a Chip*, 9:1193–1199, 2009.

[173] Y. Xu, J. A. Philips, J. Yan, Q. Li, Z. H. Fan, and W. Tan. Aptamer-based microfluidic device for enrichment, sorting, and detection of multiple cancer cells. *Analytical Chemistry*, 81:7436–7442, 2009.

[174] P. Xue, K. Le, J. Gao, Y. Wu, J. Guo, K. M. Hai, and Y. Kang. Isolation and elution of hep3b circulating tumor cells using a dual-functional herringbone chip. *Microfluidics and Nanofluidics*, 16(3):605–612, 2013.

[175] Yang, J, Huang, Y, Wang, XB, Becker, FF, Gascoyne, and PRC. Differ-

ential Analysis of Human Leukocytes by Dielectrophoretic Field-Flow-Fractionation. *Biophysical Journal*, 78(5):2680–2689, 2000.

[176] Yang, Jun, Huang, Ying, Wang, Xiao-Bo, Becker, F. F., Gascoyne, and P. R. C. Cell Separation on Microfabricated Electrodes Using Dielectrophoretic/Gravitational Field-Flow Fractionation. *Analytical Chemistry*, 71(5):911–918, Mar. 1999.

[177] Yang, Liju, Banada, P. P, Chatni, M. R, Seop Lim, Kwan, Bhunia, A. K, Ladisch, Michael, Bashir, and Rashid. A multifunctional micro-fluidic system for dielectrophoretic concentration coupled with immuno-capture of low numbers of Listeria monocytogenes. *Lab on a chip*, 6(7):896–905, 2006.

[178] X. Yao, A. D. Choudhury, Y. J. Yamanaka, V. A. Adalsteinsson, T. M. Gierahn, C. A. Willamson, C. R. Lamb, M.-E. Taplin, M. Nakabayashi, M. S. Chabot, T. Li, G.-S. M. Lee, J. S. Goehm, P. W. Kantoff, W. C. Hahn, K. D. Wittrup, and J. C. Love. Functional analysis of single cells identifies a rare subset of circulating tumor cells with malignant traits. *Integrative Biology*, 6(4):375–478, 2014.

[179] M. Yu, D. T. Ting, S. L. Stott, B. S. Wittner, F. Ozsolak, S. Paul, J. C. Ciciliano, M. E. Smas, D. Winokur, A. J. Gilman, M. J. Ulman, K. Xega, G. Contino, B. Alagesan, B. W. Brannigan, P. M. Milos, D. P. Ryan, L. V. Sequist, N. Bardeesy, S. Ramaswamy, M. Toner, S. Maheswaran, and D. A. Haber. RNA sequencing of pancreatic circulating tumor cells implicates WNT signalling in metastasis. *Nature*, 487(7408):510–513, 2012.

[180] Y. P. Yu, C. Song, G. Tseng, B. G. Ren, W. LaFramboise, G. Michalopoulos, J. Nelson, and J.-H. Luo. Genome abnormalities precede prostate cancer and predict clinical relapse. *The American Journal of Pathology*, 180(6):2240–2248, 2012.

[181] Zhang, C, Khoshmanesh, K, Mitchell, A, Kalantar-Zadeh, and K. Dielectrophoresis for manipulation of micro/nano particles in microfluidic systems. *Analytical and bioanalytical chemistry*, 396(1):401–20, Jan. 2010.

[182] Zhang, Y. T, Bottausci, F, Rao, M. P, Parker, E. R, Mezic, I, MacDonald, and N. C. Titanium-based dielectrophoresis devices for microfluidic applications. *Biomedical Microdevices*, 10(4):509–517, Jan. 2008.

[183] S. Zheng, H. Lin, J.-Q. Liu, M. Balic, R. Datar, R. J. Cote, and Y.-C. Tai. Membrane microfilter device for selective capture and electrolysis and ge-

nomic analysis of human circulating tumor cells. *Journal of Chromatography A*, 1162(2):154–161, 2007.

[184] S. Zheng, J.-Q. Liu, and Y.-C. Tai. Streamline-based microfluidic devices for erythrocytes and leukocytes separation. *Journal of Microelectromechanical systems*, 17:1029–1038, 2008.